Mechanistic Study of the Adsorption and Desorption of Proteins on Silica

Flora Felsovalyi

Submitted in partial fulfillment of the
requirements for the degree
of Doctor of Philosophy
in the Graduate School of Arts and Sciences

COLUMBIA UNIVERSITY

2012

© 2012

Flora Felsovalyi

All Rights Reserved

ABSTRACT

Mechanistic Study of the Adsorption and Desorption of Proteins on Silica

Flora Felsovalyi

Proteins are complex biomacromolecules that are intrinsically surface-active. Through the process of protein adsorption, the surface can act as a catalyst to facilitate dramatic structural alteration and destabilization of the protein. Understanding the mechanisms governing protein adsorption to a solid/liquid interface is pertinent in the wide range of applications in which this ubiquitous phenomenon plays a key role. One particular application, in which the consequences of adsorption must be especially well-characterized is prefilled drug container systems for protein-based therapeutics. Here, high-value biologics are exposed to solid/liquid interfaces often for extended periods of time, and any surface-induced change in concentration or conformation of the protein is strictly regulated. The goal of this research is to further our understanding about the factors affecting protein adsorption and desorption and the global interplay between various adsorption-related subprocesses. Our strategy is to expand the traditional design space of protein adsorption studies to target a wider range of surface coverages, longer desorption time scales and proteins with unique characteristics.

We begin our investigation with a critical assessment of the impact of surface-induced structural

perturbations on protein desorption, where irreversible conformational changes might lead to various forms of protein destabilization. We study the adsorption of lysozyme on silica and find that not only is adsorption reversible, but also that desorption is predictable in a coverage-dependent manner. Because we see evidence of coverage-independent structural perturbation on the surface, we speculate that more local descriptors, such as the number of amino acids per chain that are physically adsorbed on the surface, likely control the desorption process.

To evaluate the effects of protein stability on interfacial behavior, we employ two naturally occurring stability variants from the aldo-keto reductase superfamily. We compare their adsorption, structural transitions and desorbability in the presence of silica nanoparticles. We find little correlation between a protein's thermostability, surface-affinity and susceptibility to surface-induced unfolding. Our results question the idea that thermal stability is an accurate predictor of adsorption behavior. In a similar effort to evaluate the effects of electrostatic interactions, we use supercharged GFP variants that have dramatically different surface charge distributions. Here, we find that protein/surface charge differences correlate more strongly with surface affinity and desorption kinetics. These results highlight the more dominant role of electrostatics, compared to intrinsic structural stability, in determining protein interfacial behavior on hydrophilic surfaces.

Finally, we question the widely accepted notion that due to the complex, multi-segment binding of proteins and surface-induced unfolding, protein adsorption is a thermodynamically irreversible process. We study the desorption of several proteins and find that all proteins exhibit reversible binding and structural refolding, albeit at very different time scales. To interpret our

protein desorption data, we take an interdisciplinary approach in applying models from polymer theory. In this way, we uncover new similarities between the two fields and gain interesting insight into the heterogeneity of the adsorbed protein layer. By showing reversibility of adsorption, we also analyze the role of the Langmuirian parameters, K and Γ_{max}, and combined with intrinsic protein parameters, we develop a framework for predicting protein desorption behavior.

TABLE OF CONTENTS

LIST OF FIGURES

LIST OF TABLES

TABLE OF ABBREVIATIONS

AdhD	Alcohol dehydrogenase
ANOVA	Analysis of variance
CD	Circular dichroism
Cyt	Cytochrome c
ELISA	Enzyme-linked immunosorbent assay
FTIR	Fourier transform infrared spectroscopy
GFP	Green fluorescent protein
hAR	Human aldose reductase
HSA	Human plasma albumin
IeP	Isoelectric point
LOD	Limit of detection
MW	Molecular weight
RNase	Ribonuclease A
PCA	Principal component analysis
SAMs	Self-assembled monolayers

ACKNOWLEDGEMENTS

I have been fortunate to have a dynamic group of advisors who provided me with the mentorship and intellectual momentum I needed to pursue this interesting project, and to develop as a scientist and critical thinker. Thank you very much to Drs. Scott Banta, Sanat Kumar and Paolo Mangiagalli. I am also grateful to the rest of my committee members: Drs. Koberstein and Leonard. I have been lucky enough to be a member of two great labs—thanks to all past and present members of the Banta and Kumar labs. Specifically, I am grateful those who helped me get started: Mark Blenner, Doris Glykys and Ian Wheeldon; and to those with whom I worked closely these past five years. You have helped me technically, intellectually, and have shared with me lots of fun times and endless cups of coffee: Elliot Campbell, Kevin Dooley, Tushar Patel, Asli Sahin, Oren Shur and Géza Szilvay. I also thank my undergraduates who worked diligently through their summers and busy semesters: Sara Chuang, Ohn Mar and Josh Steinberg.

I am extremely grateful to Becton Dickinson for funding my doctoral research, and especially to the leadership of BD Medical—Pharmaceutical Systems and Medical Surgical System. I have had the privilege to be surrounded by extremely supportive colleagues, both past and present. First and foremost, I thank Ramin Mojdeh and Jack Kelley who saw potential in me, persuaded me to take on this endeavor and set up this collaboration. I also owe many thanks to the following people who helped make my doctoral pursuit a reality: Rick Byrd, Mike Garrison, Christophe Bureau, Mitali Aon, Eric Schiller, E Guan, Justin Wright, Theresa Bankston and Masoud Samandi—thank you! And thanks to all my other friends and colleagues who have helped me throughout the years, both in Franklin Lakes and Pont de Claix.

Finally, I am very lucky and grateful to have such a supportive and loving family. I cannot thank enough parents, my sisters and my husband, who have provided me with motivation, encouragement and endless patience. Köszönöm szépen!

CHAPTER 1. INTRODUCTION

1.1. RECOMBINANT PROTEIN THERAPEUTICS

Presently, more than 130 biologically-active pharmaceuticals, also called biologics, founded on the principles of recombinant DNA protein production, are approved for clinical use by the FDA, and over 200 more are in Phase III clinical trials [1]. Ever since the first recombinant peptide was expressed in *E. coli* in 1977 and the first FDA-approved genetically engineered protein, insulin, was manufactured by Eli Lilly in 1982, biotechnology products have begun replacing small molecule drugs in the treatment of a wide variety of diseases. Currently, biologics account for over $50 billion in annual sales and make up the majority of parenteral drugs in clinical trials [2]. These biologics can be categorized as follows: monoclonal antibodies, recombinant proteins, viral agents, nucleic acids and bacterial vaccine therapies.

Biologics have several key advantages over small molecule drugs. First and foremost, small molecules simply cannot accomplish the same highly specific and complex set of functions that proteins can. Furthermore, due to the specific action of proteins, there is little chance of protein therapeutics interfering with other, non-related biological activity, causing unknown side-reactions. Because the body naturally produces many of the proteins used in therapeutics, these molecules are less likely to be recognized by the immune system as antigens, and thus have a decreased level of immunogenicity. Protein therapeutics are also attractive from a financial perspective in that the time required for clinical development and FDA approval is on average one year less for biologics than for small molecules [3]. In addition, companies are able to obtain

far-reaching patents for protein therapeutics, allowing for more protection from competition. These factors, as well as the recent advances in protein engineering, explain the increasing trend of biologically-active compounds replacing small molecule drugs.

While oral administration of medicines is the preferred and most widely used route of administration, this is not feasible for the delivery of biomacromolecules such as proteins, due to their instability in the gastro-intestinal tract and low permeability across the biological membranes lining the capillaries. Thus, parenteral administration, and more specifically intravenous injection, is the most common route of administration for delivering biologics to the systemic circulation [4]. A significant aspect of intravenous injection is that the medicine must be either formulated in the form of a suspension or aqueous solution, or in the case of lyophilized drugs, it must be reconstituted prior to administration. As such, a system arises in which a high-value protein therapeutic agent is exposed to a solid/liquid interface, for various amounts of time (up to 2 years) often under sub-optimal conditions.

1.2. COMPLEXITY OF PROTEIN STRUCTURE

Proteins are large, complex biomacromolecules containing functional groups of varying size, shape, charge and hydrogen binding capacity. This large variety of functional groups comes from the twenty different amino acid monomers which are linked together in a polypeptide chain to form the protein copolymer. Proteins are intrinsically surface-active because they have both amphiphilic and amphoteric characteristics from the presence and distribution of polar and non-polar and acidic and basic side chains, respectively, that form regions of various hydrophobicity and surface charge. Such chemical and electrical diversity of proteins, coupled to their marginal

conformational stability in aqueous environments, leads to their spontaneous adsorption in the presence of nearly all surfaces.

The secondary and tertiary structure of proteins, whose complexity is illustrated in Figure 1-1, is determined by a delicate balance of the following interactions occurring within the molecule and between the protein and solute: (i) Spontaneous dehydration of the hydrophobic residues driven by gain in entropy of the surrounding solute molecules and resulting in a compact structure with a hydrophobic core and a mainly hydrophilic exterior; (ii) Coulombic interactions between charged residues resulting in an uncharged interior and charged protein exterior; (iii) Hydrogen bonding of the backbone amide and carbonyl groups, as well as other polar side chains, resulting in the formation of secondary structures (on average, about 40-70% of the amino acid residues are part of secondary structures, which include α-helices, β-sheets, β-turns and random coils; (iv) Van der Waals interactions among adjacent atoms; and (v) Disulfide bridges which stabilize the three-dimensional structure. Additionally, the compact structure of folded proteins forms distorted bonds, causing stress and strain and increasing bond enthalpy. Due to the aforementioned forces which both drive and oppose the formation of a compact three-dimensional structure, native, folded protein structure is thermodynamically only marginally more stable than its unfolded counterpart. Notably, protein molecules can exist in several conformational states. The free energy change required to transition from one state to another is relatively small (several kcal/mol, equivalent to the dissociation of several hydrogen bonds). Due to the flexible and dynamic nature of these molecules, conformational change of proteins on surfaces is expected to be a natural response of adaptation to their microenvironment [5].

1.3. PROTEIN STABILITY CHALLENGES

In the production, formulation, storage and handling of biologics, a major challenge and criterion for success is maintaining the both physical and chemical stability of the protein throughout its entire lifecycle. This is especially important because the therapeutic activity of a protein is highly dependent on its conformation [6]. Protein structure is flexible and can assume a large number of possible conformations, the relative stabilities of which are sensitive to environmental conditions and external factors such as pH, temperature, ionic strength, presence of ligands, cosolutes or impurities, and surface interactions. Figure 1-2 illustrates possible conformational choices for a polypeptide chain.

Degradation pathways for proteins can be separated into chemical and physical instabilities. Chemical instabilities include deamidation, oxidation, proteolysis and racemization. Physical instabilities include denaturation, aggregation, precipitation, and surface adsorption. Denaturation refers to the alteration of the tertiary and sometimes secondary structure, of the protein that may result in an unfolded state. Between the native and unfolded states, partially unfolded intermediates can occur. Protein adsorption to surfaces can catalyze the structural denaturation of the protein and may create such partially unfolded intermediates [7]. These intermediates are believed to be the precursors for non-native aggregate formation, which is an irreversible process that can result in precipitate formation, inhibition of biological activity and may lead to enhanced immunogenicity. Although physical instabilities are rarely an issue for small molecule drugs; physical instability is of great concern for biologics [8] and will be the main focus of this research project.

1.4. PROTEIN ADSORPTION

The adsorption of numerous proteins onto various surfaces under diverse environmental conditions has been the subject of research for the past 40 years, resulting in over 4800 publications since 1970, with 500 manuscripts written on the topic in 2008 alone. Interest in the field first arose from studying the adsorption of blood proteins onto biomaterial surfaces. This critical work demonstrated that the initial protein adsorption step triggers an intrinsic coagulation cascade that can lead to thrombogenesis and implant rejection. Further interest in the field has developed due to the relevancy and applicability of protein adsorption to various systems, both synthetic and natural, as listed in Table 1-1. Germane examples include biofouling of ship hulls, protein deposition on food processing equipment, buildup of lysozyme on contact lenses, attachment of biofilm to implants and interaction between biopharmaceuticals with various surfaces used in their manufacture. An overview of protein adsorption topics studied in literature, associated experimental techniques and relative weight in terms of number of publications are illustrated in Figure 1-3.

1.4.1. System Components

The overall behavior of proteins at interfaces is the net result of interactions between various system components: protein, substrate, solvent, other low molecular weight electrolytes, and for pharmaceutical formulations, surfactants, excipients and other stabilizers [9]. The key properties of each of these components that affect adsorption behavior are outlined below:

Protein: Distribution of hydrophobic domains on the surface, overall protein hydrophobicity, surface charge distribution, effective surface area available for adsorption, number and types of

functional groups which can specifically associate with groups on the substrate, stability and rigidity of the native state and level of secondary structure are the key properties of the protein.

Substrate surface: Effective surface area, surface charge distribution, chemical and structural homogeneity, and surface hydrophobicity and roughness are critical parameters.

Solvent: Properties of the aqueous medium that should be considered are dielectric constant, electrostatic force and intermolecular forces. Environmental conditions such as pH, temperature, ion concentration, and concentration of protein in the solution are important parameters of the system.

Solutes: In pharmaceutical formulations, excipients, surfactant and stabilizers represent small, surface-active molecules, which often out-compete the protein for surface-binding sites, thereby reducing the amount of protein adsorption.

1.4.2. Kinetics of Protein Adsorption

The protein adsorption process can be divided into five basic steps as illustrated by Figure 1-4A:

1. *Transport to interface:* The rate of transport from solution to the interfacial region is driven by diffusion processes that depend on bulk protein concentration and the diffusion coefficient of the protein, in which case Fick's equation can be applied to obtain the rate of adsorption. Because the attachment of the protein to the surface is independent of bulk concentration, transport is usually the rate limiting step at low protein concentrations. Transport mechanisms to the surface other than diffusion include convective transport by laminar or turbulent flow or Brownian motion under quiescent conditions.

2. *Surface attachment*: The collision frequency and surface chemistry of both protein and surface dictate the residence time of the protein on the surface. Because proteins are not homogenous particles, not all collisions are equally effective in adsorption: they result in different interaction energies, and therefore varying tendencies for surface denaturation. As adsorption progresses, the number of free binding sites decreases, and a common finding is that once a closely packed monolayer forms, the rate of adsorption falls below the rate of diffusion [10].

3. *Structural rearrangement in adsorbed state*: Proteins are large, heterogeneous molecules that can interact with the surface through many points of contact and can change their conformation to optimize their surface interaction. The extent of structural change of an adsorbed protein layer is a function of surface coverage, rate of arrival and residence time.

4. *Detachment from interface*: Structural rearrangement on the surface has been linked to irreversible adsorption, and has been observed for numerous systems, especially for hydrophobic surfaces. Irreversibility refers to the fact that a molecule does not desorb spontaneously in the presence of a pure solvent. However, it has been shown that despite being irreversibly adsorbed, proteins can still desorb from the surface in the presence of macromolecules in solution by exchange mechanisms. This happens by the gradual replacement of an adsorbed molecule by a molecule in solution [11]. Both homomolecular [12] and heteromolecular [13] exchange processes, such as the Vroman effect, have been reported. The protein that is released from the surface may either retain the conformation of its adsorbed state, or refold into its original conformation [14, 15]. If the desorbed protein has altered structure, the sorbent can be thought of as a catalyst facilitating structural transition.

5. *Transport away from interface:* This is usually not the rate limiting step, as the kinetics of desorption are slower than that of adsorption. This step may be treated similarly to transport to the surface, except the diffusion coefficient may have a different value if structural perturbation of the protein has occurred.

1.4.3. Adsorption Isotherms

Adsorption data are often represented in terms of an adsorption isotherm, which relates the concentration of free protein in solution (C_{eq}) to the amount adsorbed to a given substrate surface (Γ) at constant temperature and pressure. Adsorption isotherms are typically obtained by ellipsometry or by the depletion method, in which the concentration of the supernatant is measured, following protein/particle incubation, and used to calculate the amount of protein adsorbed by mass balance. Adsorption is defined as reversible if the ascending and descending branches of the isotherm (shown schematically in Figure 1-5A) overlap, meaning that points on the isotherm are achieved in a path-independent manner. Only in the case of reversibility can the adsorption isotherm be used to derive the equilibrium binding constant, K.

Historically, the Langmuir equation (Eq. 1-1) has been used to model the adsorption isotherms of proteins, in spite of the fact that not all necessary assumptions are met (structural alteration and lateral interactions of adsorbed molecules can occur) [16]. It is important to note, however, that the system must be at thermodynamic equilibrium in order for the Langmuir equation to be applied. In situations where this criterion is met, Langmuirian parameters K and Γ_{max}, maximum surface coverage, can be use the characterize adsorption.

$$\Gamma = \frac{\Gamma_{max} \; C}{k + C}$$

Where Γ is surface coverage,
K is the apparent disassociation constant
Γ_{max} is the maximum surface coverage
C is bulk protein concentration

Eq. 1-1

1.4.4. Surface Unfolding

For reasons stated above, solid surfaces can act as catalysts to induce structural alteration, degradation and aggregation of proteins. Both immediate and time-dependent surface denaturation have been observed. However; adsorbed proteins rarely become fully unfolded; some degree of secondary structure is maintained. Several studies have been performed on adsorption-induced conformational change [17-23]. Pioneering work by Castillo showed evidence of the partial unfolding of human serum albumin (HSA) on different contact lens surfaces [24], while McMillin reported fibrinogen resistance to structural changes on quartz [25]. In contrast, using the same solvent and surface, McMillin showed a drastic, irreversible denaturation of blood clotting factor XII. Seminal work by Norde and Kondo followed, to understand the kinetics and extent of conformational changes of model proteins on ultrafine silica, polystyrene, and latex particles. Belfort [26] demonstrated that lysozyme adsorption onto self-assembled monolayers (SAMs) produces a perturbed conformation, with loss of α-helices and formation of β-sheets correlated to substrate hydrophobicity. Despite such studies, fairly little is understood about the general characteristics of surface-induced structural transitions.

1.4.5. Thermodynamic Driving Forces of Protein Adsorption

The overall Gibbs energy of adsorption, ΔG_{ads}, determines the feasibility of adsorption.

Adsorption will only occur if Eq. 1-2 holds true, at constant temperature and pressure. For simple, uncharged homopolymers, adsorption is mainly driven by enthalpic interactions and is opposed by conformational and translational entropy. However, the driving forces governing protein adsorption are more complex.

$$\Delta G_{ads} = \Delta H_{ads} - T\Delta S_{ads} < 0 \qquad \text{Eq. 1-2}$$

Entropic gain, ΔS_{ads}, drives partial dehydration of the apolar regions of the protein and substrate through adsorption. This phenomenon dominates in the presence of hydrophobic surfaces, and such adsorption has been reported to occur spontaneously [27]. Factors contributing to this entropic force include: (1) Gain of translational entropy by the solvent molecules bound to the sorbent and protein, which are released into solution. (2) Gain of conformational entropy by the protein during adsorption as the apolar residues in the protein core are able to relax, yet are still shielded from the aqueous environment by the hydrophilic shell and sorbent surface. (3) Gain of conformational entropy by the protein as secondary structure collapses when favorable attachments are formed with the surface. (4) Loss of translational entropy of the protein when it is bound to the surface.

Enthalpic driving forces affecting protein adsorption, ΔH_{ads}, include: (1) Disruption of sorbent-solvent and protein-solvent contacts, and concomitant formation of protein-sorbent and solvent-solvent contacts. (2) Change in protein-solvent interactions due to difference in polymer segment density between adsorbed and bulk layer. (3) Coulombic interaction between protein and sorbent and between adjacent adsorbed proteins. Both the protein and sorbent can carry a distribution of surface charge, and in solution, a layer of weakly associated counterions. In a thermodynamically

stable system, electroneutrality requires the charged surface to be balanced by a countercharge, forming an electrical double layer. The general trend regarding electrostatics is that this effect likely dominates in the presence of hydrophilic surfaces, while on hydrophobic surfaces, electrical interactions are overruled by hydrophobic interactions.

Intrinsic protein stability also plays an important role in protein adsorption. Because native structure is thermodynamically often only marginally more stable in solution than other conformations, structure can be altered due to even subtle changes in environmental conditions. Based on the seminal work of Norde, proteins are often classified into two major categories regarding stability: rigid (i.e. hard) and flexible (i.e. soft) proteins [28]. It is believed that hard proteins tend to adsorb to a lesser degree and are less prone to structural rearrangement upon adsorption. These proteins adsorb to hydrophobic surfaces under any charge, but only adsorb to hydrophilic surfaces in the presence of electrostatic attraction. Soft proteins, on the other hand, adsorb on both hydrophobic and hydrophilic surfaces, even under repulsive charge. In such cases, some other factor must outweigh the opposing contributions from hydrophilic dehydration and electrostatic repulsion. The hypothesis is that structural rearrangement upon adsorption provides this additional driving force.

1.4.6. Techniques for Evaluating Adsorption-Induced Structural Denaturation

Structural change of adsorbed proteins has been studied directly using *in situ* spectroscopic methods such as circular dichroism (CD) and Fourier transform infrared spectroscopy (FTIR), and indirect methods such as microcalorimetry, elutability and measurement of biological activity.

Direct Measurements. One of the most commonly used direct measurements of adsorbed protein conformation is CD spectroscopy, where spectra are obtained in the far-UV region, which is sensitive to detailed secondary conformation of proteins. CD, which has become a gold standard for analyzing protein structure in solution, can be adapted to measure the conformation of proteins in the adsorbed state. With the right choice of particles such measurements are possible. Several research groups have identified particles which minimize such effects. These particles include silica [19, 29-35], Teflon [36], polystyrene [15, 37-39] and silver iodide [15], ranging between 12 to 215 nm in diameter. The absence of light scattering effects and fast sedimentation render them CD-compatible. Using such techniques, Norde [28] reported a 10% reduction in the helical structure of adsorbed albumins on hydrophilic oxides. Vermeer [40] found a 17% increase in α-helix and a decrease in β-sheet content when studying the adsorption of mouse monoclonal immunoglobulin to Teflon particles. Zoungrana [41] found contradictory results: cutinase lost a large degree of helical structure upon adsorption to Teflon. Such differences in behavior are often explained by the subtle balance between energetically favorable enthalpic and unfavorable entropic interactions. These and various other studies on surface-induced conformation changes [42-45] illustrate the difficulty in predicting the structural behavior of proteins upon adsorption.

Indirect Measurements. The effect of the orientation and conformational state of the adsorbed protein on biological function has been used to make indirect observations about the adsorbed protein layer. Page [46] studied the adsorption of recombinant human Interleukin II to the walls of glass and polypropylene ampoules. An ELISA assay showed that all protein formulations experienced significant activity loss that was contributed to structural change upon adsorption. Tzannis [47] studied the adsorption of recombinant Interleukin II onto walls of silicone rubber

tubing, a commonly used catheter material. While adsorption resulted in a 7-20% reduction in protein concentration after 24 hours, loss of biological activity decreased by 90% as a direct consequence of surface-induced structural loss.

1.4.7. Desorption

Extensive studies have been done by Granick [48, 49] on the desorption behavior of simple homopolymers, but few studies have been reported for proteins. Contradictory opinion exists related to the similarity in homopolymer and protein interfacial behavior. Our own results, presented in Chapter 5, highlight similarities between the two fields. Protein adsorption is most often reported as irreversible [10, 11, 15, 28, 33, 50-54] or as quasi-reversible [55]. This phenomenon has often been studied on hydrophobic surfaces [10, 50] or at low surface coverages [28]. In most studies, exchange reactions [11, 15] or the presence of strong eluents [28, 51] are necessary to induce desorption, and simply replacing the bulk with pure solvent is not sufficient to drive surface detachment. Irreversible adsorption is often linked to conformational unfolding of the protein and the level of relaxation to the energetics of overcoming multi-segment protein/substrate detachment. Only a handful of studies report the presence of both reversibly and irreversibly bound molecules, and these studies often report that desorption follows first order kinetics [56-58]. In the relatively few studies that have isolated and characterized the desorbed protein, loss of secondary structure, increase in surface hydrophobicity and unaltered levels of thermostability have been reported [14, 15, 28].

1.5. PROBLEM STATEMENT

The use of pre-filled container systems for the storage and delivery of biologically-active, parenteral drugs is a quickly growing field in which protein adsorption plays a vital role [59, 60]. In such systems, the aqueous formulation is stored in the same device from which it is delivered, providing numerous benefits over conventional vial-based administration [1, 3]. Besides the well-known challenges of protecting biologics against chemical degradation and physical instabilities, such a device can introduce additional instabilities stemming from adsorption induced by delivery device surfaces [7, 61]. Although surface adsorption is not traditionally considered among the most common causes for physical instability, this phenomenon has been documented as a catalyst for denaturation [47]. Surface-induced structural changes are of concern: a perturbed, adsorbed state may interact with protein in bulk, or detach from the surface and maintain its surface-induced perturbations. Similarly, desorption and potential exchange between adsorbed and dissolved proteins may also present a concern, as this would make more surface sites available, allowing a larger fraction of bulk protein to interact with the surface. Therefore, we aim to better understand and attempt to predict desorption and surface-induced conformational changes of proteins. Moreover, this research also has broader implications in furthering our fundamental understanding about the global interplay and interdependencies of the various adsorption subprocesses.

This research aims to elucidate our fundamental understanding of the following questions: Is surface attachment and related structural change reversible? Does desorption occur in a predictable manner? What structural states do desorbed proteins populate?

1.6. MODEL SYSTEM AND EXPERIMENTAL APPROACH

Our criteria in system development include the ability to (i) induce and measure adsorption and desorption in a repeatable, robust manner, (ii) measure, *in situ*, structural transitions during the adsorption lifecycle and (iii) assess the effect of a wide range of surface coverages to expand the current experimental space to a broader portion of the adsorption isotherm. This last criterium allows us to better simulate our system of interest: relatively high concentration of proteins exposed to a delivery device surface. Typically, the concentrations of biologics range over several orders of magnitude (0.001-100 mg/mL) [62] and the surface area available for adsorption of containers is relatively low (c.a. 0.1 m^2/mL). In terms of surface coverage, these values represent a wide range, mostly along the plateau region of the adsorption isotherm (Region I, Figure 1-5B). In contrast, historically, most adsorption and desorption studies have been performed along the rising and early plateau regions of the isotherm (Region II and III, Figure 1-5B), where the ratio of protein/surface area is high.

The ability to assess the effect of coverage on adsorption is also important because past results indicate that surface-induced structural changes occur in a coverage-dependent manner [28, 34, 41, 63]. Researchers have hypothesized that the mechanisms of surface-induced unfolding are different at low coverages (high level of available surface area promotes unfolding) than at high coverages (crowding effects and steric hindrances prevent unfolding). However, a major limitation of these studies is that the structure of the adsorbed protein was not measured in isolation, but was confounded by signals from native or non-adsorbed protein. Or, in most cases, studies have been limited to low coverages where the majority of the protein is adsorbed to avoid this issue of confounding the CD signal. Few studies have been conducted at higher coverages.

An advantage of the model system we have developed is that it provides a way to isolate the secondary structure of adsorbed protein only, allowing the assessment of adsorbed structure over a wide range of surface coverages.

Our model system will allow us to evaluate the parameters associated with adsorption and desorption, structural transitions in the adsorbed state, as well as isolation and characterization of the desorbed protein. Our approach is illustrated in more detail in Figure 1-6.

Our criteria for particle selection are size (small enough to minimize light scattering effects), absorptive behavior (minimal light absorption in the far-UV region), refractive index (ideally close to that of water, 1.33) and chirality (minimal chirality reduces a secondary structure-like signal). We selected silicon dioxide nanoparticles, which fit the described criteria. Specifically, we use fumed silica, Cab-O-Sil M5 particles, manufactured by Cabot Corp, which have a specific surface area of 100 m^2/g, based on N_2 adsorption. The point of zero charge of these particles is at pH=2-3. These untreated, fumed particles are hydrophilic and have an average particle diameter of 250 nm.

1.7. RESEARCH AIMS

We first apply our robust system design to critically assess the impact of structural perturbations on desorption behavior. To this end, in Chapter 2, we evaluate the adsorption, desorption and structural transitions of lysozyme on silica. Our goal is to assess the degree of adsorption reversibility and the impact of structural transitions and surface coverage on desorption. We find that despite significant levels of structural unfolding on the surface, the adsorption of lysozyme

is reversible. Furthermore, we are able to use Langmuirian parameters to predict desorbed amounts. We find evidence of a two-state adsorption model, which involves exchange between a native-like, dissolved state and a highly perturbed, adsorbed state.

We hypothesize that our lysozyme results are strongly influenced by two key system parameters: the high intrinsic stability of the protein and the highly favorable protein/surface electrostatic interactions. To better understand the impact of these parameters, we designed systems to study their effects in isolation. In Chapter 3, we explore the relationship between stability and adsorption using naturally evolved homologs with very similar 3-D structure, yet vastly different intrinsic stabilities. Using the same surfaces and system conditions allows us to evaluate stability while keeping electrostatic effects constant. In Chapter 4, we assess the interfacial behavior of supercharged GFP variants with drastically different surface charge, yet very similar structural stabilities. We find that overall adsorption behavior correlates poorly with thermostability; however, protein/surface charge differences correlate strongly with surface affinity and desorption kinetics. These results highlight the more dominant role of electrostatics, compared to intrinsic structural stability, in determining protein interfacial behavior.

In Chapter 5, we evaluate the adsorption lifecycle of various proteins with diverse charges, stabilities and conformations. Surprisingly, we find that all proteins exhibit reversible binding and structural refolding, albeit at very different time scales. To interpret our protein desorption data, we take an interdisciplinary approach in applying models from polymer theory. In this way, we uncover new similarities between these two fields and gain interesting insight into the heterogeneity of the adsorbed protein layer. By showing reversibility of adsorption, we also

analyze the role of the Langmuirian parameters, K and Γ_{max}, and combined with intrinsic protein parameters, we develop a framework for predicting protein desorption behavior. Such new insight can be invaluable when designing systems where interfacial behavior must be strictly regulated.

1.8. TABLES AND FIGURES

Desirable outcomes of protein adsorption

Event
Adsorption chromatography
Emulsifiers, stabilizers in cosmetic, pharmaceutical and food industry
Bioorganic reactors and immobilized enzyme assays—immobilized enzymes
Liposomes for drug delivery
Active enzymes on biosensors/chips
Developing biocompatible hard and soft implant materials
Developing blood-compatible materials

Undesirable outcomes of protein adsorption

Event
Biofouling: Clogging of artificial dialysis membranes and ultrafiltration membranes Ship hulls Contact lenses Food processing equipment
Plaque on teeth
First step of thrombus development on implant surfaces, which can lead to rejection and failure of implant
Adsorption of protein therapeutic to various surfaces (filters, tubes, pumps, primary packaging material)

Table 1-1 Relevance of protein adsorption in various industries/fields

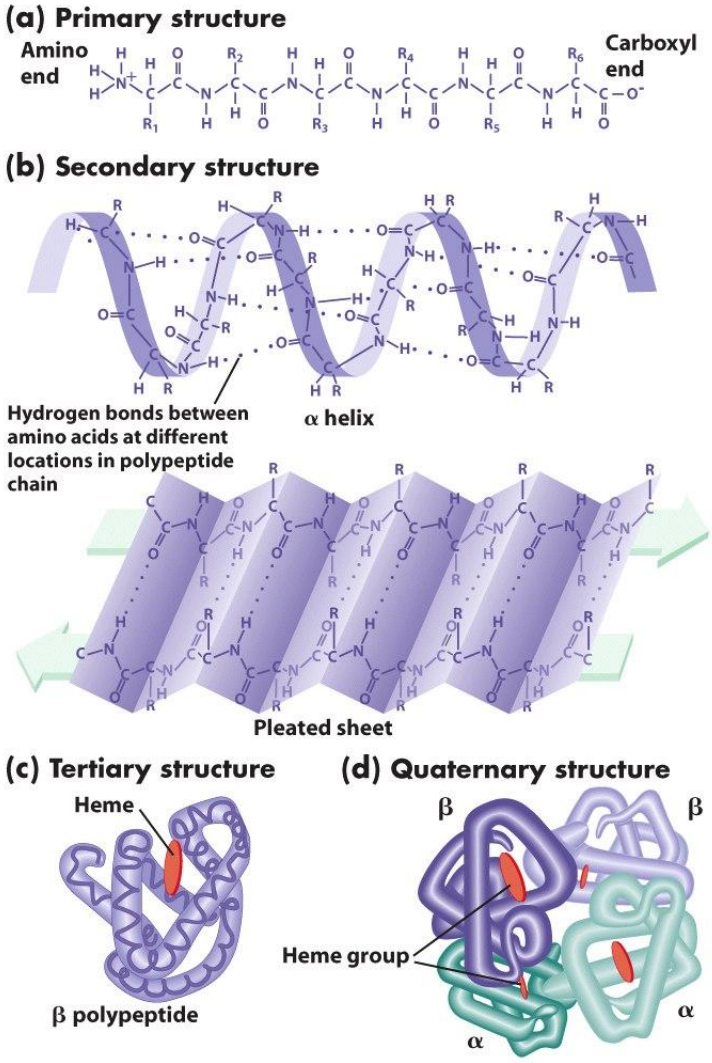

Figure 1-1 Depiction of the four levels of protein structure

Source for figure: [64]

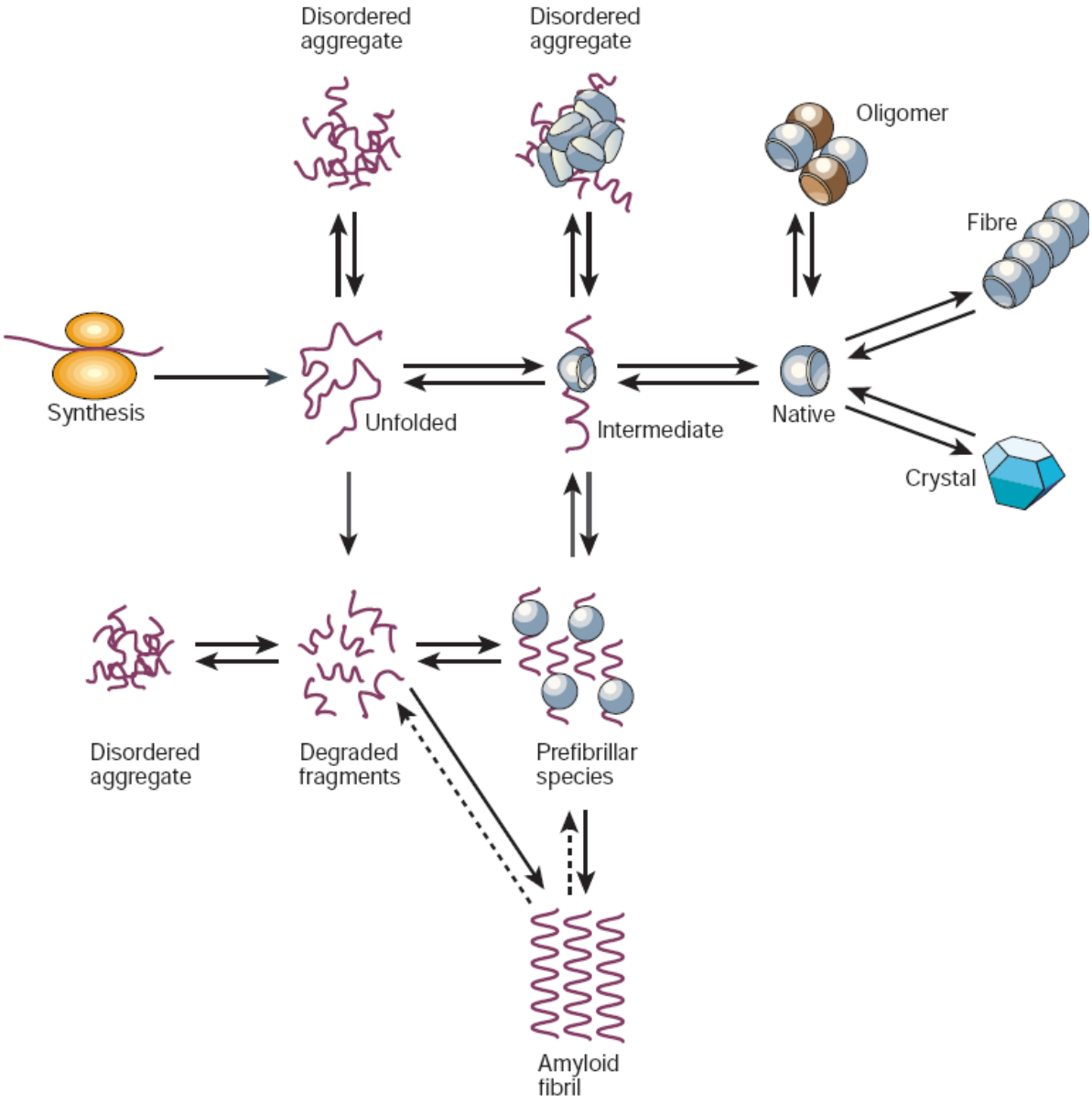

Figure 1-2 Possible conformational choices for a polypeptide chain

Source for figure: [65]

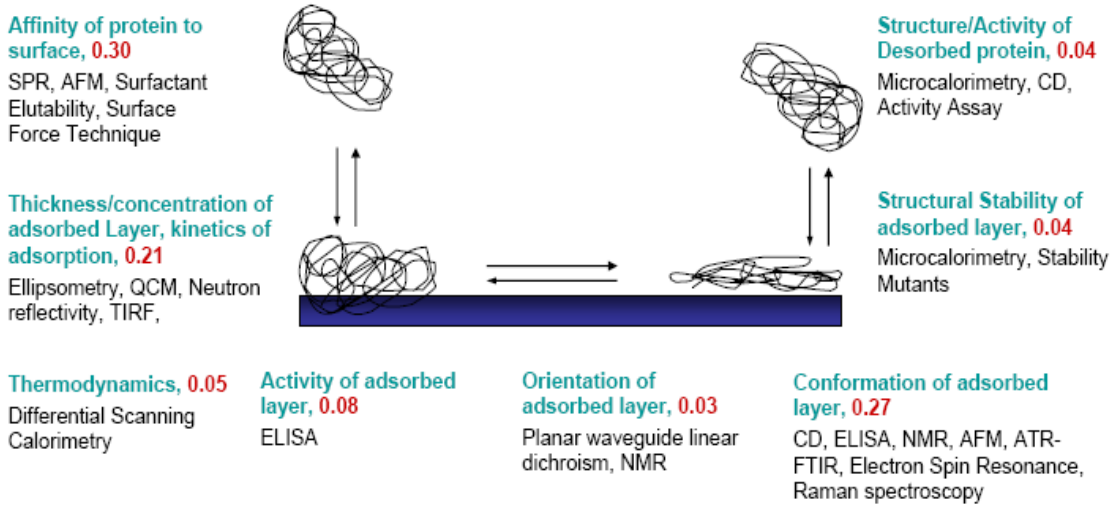

Figure 1-3 Overview of literature on protein adsorption

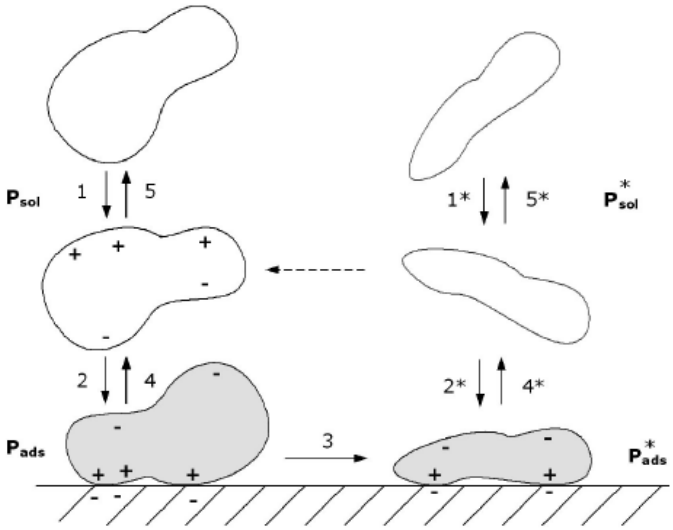

(A)

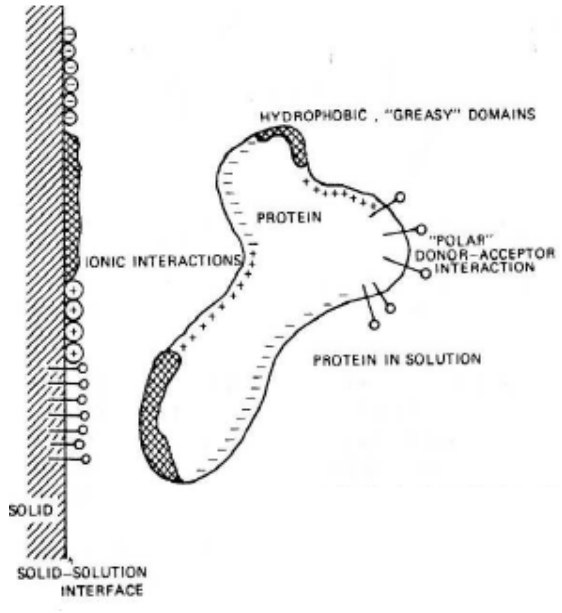

(B)

Figure 1-4 Schematic view of a protein interacting with a solid surface

(A) Kinetic overview of adsorption, Source for figure: [66], (B) Representation of the various types of interactions governing the driving forces of protein adsorption, Source for figure: [27]

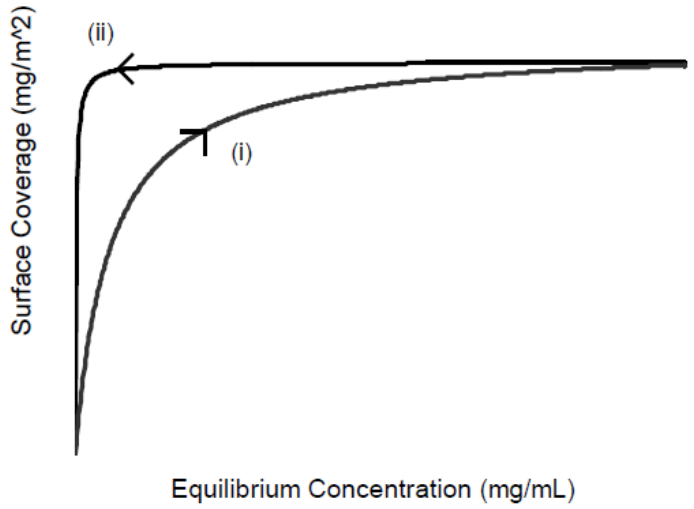

A

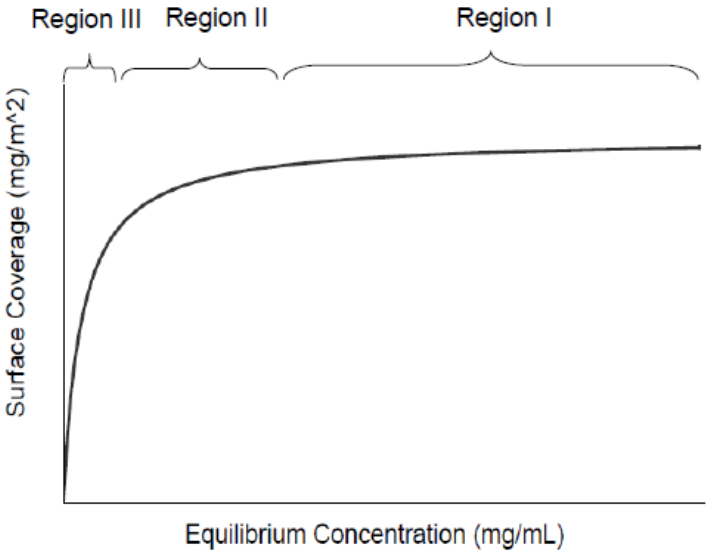

B

Figure 1-5 Typical high-affinity adsorption isotherm schematics

(A) Overlays the adsorption (i) and desorption (ii) pathways. Reversibility is defined as the overlap of these two pathways. (B) Represents three distinct regions of a high-affinity isotherm: the plateau value where full surface coverage has been achieved (I), the transition region (II) and the high affinity region, where the protein/surface area ratio is the lowest (III)

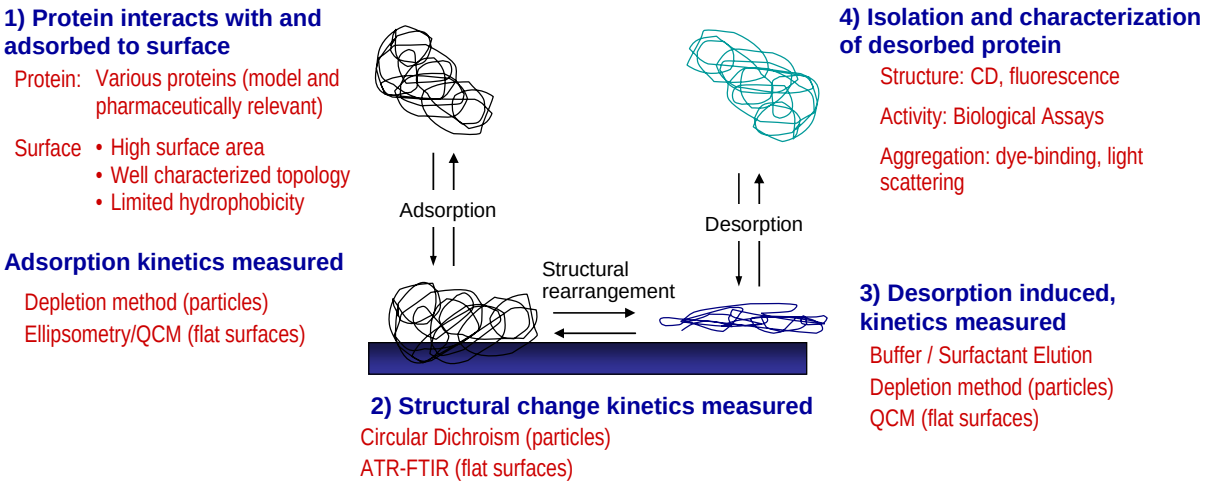

Figure 1-6 Characteristics and associated experimental techniques

CHAPTER 2. REVERSIBILITY OF THE ADSORPTION OF LYSOZYME ON SILICA [†]

2.1. ABSTRACT

A central paradigm that underpins our understanding of the interaction of proteins with solid surfaces is that protein adsorption leads to changes in secondary structure. The bound proteins tend to denature, and these non-native, adsorbed structures are likely stabilized through the loss of α-helices with the concomitant formation of intermolecular β-sheets. The goal of this work is to critically assess the impact this behavior has on protein desorption, where irreversible conformational changes might lead to protein aggregation or result in other forms of instability. The adsorption, desorption and structural transitions of lysozyme is examined on fumed silica nanoparticles as a function of the amount of protein adsorbed. Surprisingly, not only does the data indicate that adsorption is reversible, but that protein desorption is predictable in a coverage-dependent manner. Additionally, there is evidence of a two-state model, which involves exchange between a native-like dissolved state and a highly perturbed adsorbed state. Since the *in situ* circular dichroism (CD) derived secondary structure of the adsorbed proteins are

---

[†] A version of this chapter is published in Langmuir (2011), 27:19, 11873-82, with co-authors Paolo Mangiagalli, Christophe Bureau, Sanat K. Kumar, and Scott Banta. FF designed the experiments, performed the experiments, analyzed data, and wrote the manuscript.

essentially unaffected by changes in surface coverage, these results are not consistent with previous claims that surface-induced denaturation is coverage-dependent. Inspired by results from homopolymer adsorption experiments, we speculate that more local descriptors, such as the number of amino acids per chain that are physically adsorbed on the surface, likely control the desorption process.

2.2. INTRODUCTION

Gaining insight into the intricate interplay between proteins and interfaces has motivated a vast amount of research and many excellent reviews have been written which attest to the richness of the field and its role in a wide range of industries [27, 67-69]. A wide range of systems have been exploited to study the reversibility of protein adsorption. Reported behavior is diverse: adsorption in most systems is irreversible [24, 25, 70-72], but partial reversibility upon dilution is also found [66, 73]. Rarely, reversible binding is reported [58] and in such cases, a key question arises: How much similarity exists between the adsorption behavior of proteins and simple homopolymers? Surface denaturation plays a major role in adsorption reversibility. Although they are not mutually exclusive, the concept of reversibility and reconformation are closely related in protein adsorption, where the surface acts analogous to a heterogeneous catalyst to facilitate dramatic structural alteration of the protein [21, 25] resulting in an energetically favorable state.

Various techniques are available to monitor adsorbed protein structure, including CD [18, 21, 22, 74, 75], FTIR [20, 76, 77], total internal reflectance fluorescence [78], antibody-binding [79] and isotope exchange experiments [80, 81]. Of these methods, CD and FTIR have been used in the

most diverse applications to monitor surface denaturation. CD, when combined with a careful choice of nanoparticles [15, 19, 30, 32, 82], can be used to monitor the adsorbed state *in situ.* In FTIR, a flat plate is immersed into a protein solution and the refractive index of the adsorbed layer is used to infer information about its secondary structure. However, due to the low surface area/protein ratio that can be achieved in this setup, only a limited range of surface coverages can be targeted.

While both immediate and time-dependent surface denaturation behaviors have been observed, adsorbed proteins rarely become fully unfolded: some degree of secondary structure is maintained. In an influential study, Sethuraman [26] showed the secondary structure of adsorbed lysozyme, characterized by α-helix to β-sheet transition, correlated to surface hydrophobicity, indicating the extent of protein denaturation depends on surface properties. Comparatively, Norde [28] found that adsorption and surface unfolding depend on intrinsic protein properties, namely structural stability.

The previous approaches have several limitations: (1) Few systems, to date, have methodically and simultaneously monitored the entire lifecycle of an adsorbing protein. Although distinct legs of the kinetic diagram in Figure 2-1A have been assessed rigorously, rarely are all kinetic steps evaluated together to uncover the interdependencies of the various states. (2) The aforementioned CD-based method has known inaccuracies with respect to deconvolution, and the presence of the particles is only assumed to have negligible effect on the observed signal. Steps taken to mitigate these issues and a comparison of adsorbed structure measured by orthogonal methods are discussed later. (3) The design space of previous CD studies is limited

with respect to surface coverage. Although various results indicate coverage plays a key role in surface denaturation [28, 34, 41, 63], the inability to isolate the signal of the adsorbed state limits the studies to regimes where the majority protein is adsorbed. A related weakness is that in such cases only an approximation of adsorbed structure is provided.

To overcome previous limitations, we have employed a robust study design by expanding a model system presented in the pioneering work of Norde [28]. Lysozyme was adsorbed at various surface loadings onto hydrophilic silica particles and the desorbed amount upon buffer elution was examined. CD was used to monitor structural transitions on the surface *in situ* and upon desorption. By isolating the CD signal of the adsorbed protein, it is possible to assess the interplay between surface-related events and subsequent desorption behavior over a broad range of coverages.

By harnessing existing tools in a new way to rigorously investigate the entire lifecycle of a protein at a solid/liquid interface, we have broadened the experimental space for monitoring adsorption reversibility and surface-induced unfolding. Surprisingly, not only do the results indicate that lysozyme adsorption is reversible onto fumed silica surfaces, but also that protein desorption is predictable in a coverage-dependent manner. Additionally, as opposed to the traditional four-state model, these results offer evidence of a two-state model, which involves exchange between a native-like dissolved state and a highly perturbed adsorbed state, as shown in Figure 2-1B. Because there is essentially no coverage-dependence in the adsorbed protein secondary structure, we conclude that factors beyond the extent of such structural perturbations govern protein desorption behavior. Our results offer a new perspective into the arrangement and

structure of the adsorbed protein and their subsequent impact on desorption.

2.3. EXPERIMENTAL SECTION

2.3.1. Study Protocol Overview

Chicken egg white lysozyme, a highly-helical, intrinsically stable globular protein [83], was the focus of our adsorption and desorption studies. CD was used as the principle method to explore secondary structure, and so we desired a surface that was small enough to minimize light scattered while having a refractive index close to water. Fumed silica particles meet these criteria [19, 28, 32]. The physiochemical characteristics of the components of the model system are summarized in Table 2-1. For the adsorption studies, the silica particles are mixed with a solution of known protein concentration. After equilibration, solutions are centrifuged to separate the free solution and particle phases, enabling us to determine the concentration of unbound protein and examine its secondary structure by CD. The corresponding quantities for the adsorbed protein are determined through mass balance. Similar procedures are followed for the desorption experiments, except that the particles are resuspended in fresh buffer.

2.3.2. Materials

Lysozyme (from chicken egg white, purity ≥98%, Ref: L4919), bicinchoninic acid (BCA), the QuantiPro BCA Assay Kit, guanidine hydrochloride, sodium phosphate, monobasic and dibasic, and all other chemicals were obtained from Sigma (St. Louis, MO). Untreated, fumed, colloidal silicon dioxide (Cab-O-Sil, M5, purity >99.8) was obtained from Cabot Corp (Boston, MA). All water was purified using a Millipore water filtering system.

2.3.3. Protein Concentration Measurements

To minimize errors in concentration measurements, two orthogonal techniques were used to determine protein concentration: UV absorbance at 280nm and the BCA assay. Protein solutions were diluted with 6M guanidine hydrochloride prior to UV absorbance assays to ensure all chromophores contribute equally to light absorbance. A molar extinction coefficient 35.3 mM^{-1} cm^{-1} was used for lysozyme. Internal lysozyme standards were prepared for the BCA assay, and the error in accuracy was 3.6% for BCA and 3.2% for UV absorbance, and reproducibility was 5% between the assays. For concentrations below 0.05 mg/ml, the MicroBCA kit was used, with an error below 10%. BCA assays were performed according to the manufacturer's protocol. A SpectraMax M2 Spectrophotometer (Molecular Devices, Sunnyvale, CA) was used for all measurements. The limit of detection (LOD) of the concentration measurements was calculated as the baseline measurement (intercept) of the calibration curve plus three times the standard deviation of the buffer signal, converted into units of concentration [84].

2.3.4. Adsorption of Lysozyme onto Nanoparticles

Lyophilized lysozyme was reconstituted in 10mM sodium phosphate buffer (pH 7.0), and filtered through a 0.22μm membrane. Stock solutions of 12 mg/mL silica nanoparticles were prepared by reconstituting powdered silica in the same buffer. Solutions were vortexed immediately before use to ensure homogenous distribution of the colloidal suspension. Equal volumes of silica and protein solutions were added to 2mL Eppendorf tubes. The final volume in the tubes was 0.9 mL, resulting in a volume: container surface area ratio similar to that used by Norde [28]. The silica concentration was fixed at 6 mg/mL, while protein concentrations varied between 0.1 and 4.0 mg/mL. Samples were rotated end-on-end for 16 hr using a standard laboratory rotator. Previous

kinetic studies have shown this time period is sufficient to achieve equilibrium adsorption in this system. The depletion method was used to measure adsorbed protein concentration: following incubation solutions were centrifuged at 13,000 RPM for 1 min and the supernatant was collected. Three more rinse cycles followed to ensure all silica nanoparticles were removed. The protein concentration in the supernatant was determined using the BCA Assay. The concentration of protein adsorbed to the particles was calculated by mass balance.

2.3.5. Desorption and Resuspension

Fresh buffer (0.8 ml) was added to the pellet obtained in the previous step. The protein-particle mixture was gently resuspended by pipetting. Weights of the empty Eppendorf tubes, pellets and resuspensions were measured to accurately calculate protein concentration. A density of 1.02 g/mL, measured previously, was used to convert weight to volume for the resuspensions. The CD signal was measured immediately following resuspension of the pellet. Desorbed protein was obtained by repeating this cycle several times, and the supernatant after the fourth cycle was assumed to contain only protein which had interacted with the surface.

2.3.6. CD Measurements

All measurements were performed with a Jasco J-815 CD spectrometer (Jasco, Inc, Easton, MD) equipped with a Peltier junction temperature control. Quartz cuvettes with pathlengths of 0.01, 0.02 or 0.05 cm were used. Pure protein solution and protein-particle mixtures were examined, using buffer or silica blanks, respectively, for baselining. Far-UV spectra were collected between 185 and 240 nm in 0.1nm intervals, using a 1nm bandwidth, 8 sec response time and 50nm/min scanning speed. Temperature was held at 25°C. Three accumulations were averaged during each

run. Raw CD signal, θ, was converted to mean residue ellipticity using the equation: $[\theta]_{MRW} = \Theta/(10 \times C_r \times l)$, where C_r represents concentration (units = M*residue number) and l is the cuvette pathlength.

2.3.7. Deconvolution

CD spectra were deconvolved using the *CDPro* software package [85]. Each spectrum was analyzed by three different algorithms: *Continll*, *Selcon3* and *Cdstr*, and within each algorithm, 4 different reference sets (SP37, SDP42, CLSTR, SMP50) were used. The average across 3 algorithms and 4 reference sets is reported. Additionally, α-helix and β-sheet content is reported as the sum of the distorted and regular classes.

2.3.8. Dynamic Light Scattering and Electrophoretic Mobility

A Malvern Zetasizer Nano-ZS was used to measure particle size distribution and zeta potential of the silicon dioxide suspension in 10mM sodium phosphate (pH 7.0). A 50mW laser operating at a wavelength of 532nm was used. Scattering intensities were recorded at a 90° angle. A low volume (12uL) glass cuvette was used for the particle size measurements, and a clear, disposable zeta cell was used for zeta potential measurements. All measurements were performed at 25°C.

2.3.9. Statistical Analyses

The Minitab 15 Software Package was used to run an ANOVA General Linear Model to assess differences in the deconvoluted CD spectra.

2.4. RESULTS

2.4.1. Adsorption Isotherm

The amount adsorbed plotted as a function of free protein in solution (an adsorption isotherm), is shown in Figure 2-2A. An important point to note here is that we have used different pathways in these experiments but found essentially the same, path-independent results in all cases; for example, we exposed the particles to a high protein concentration (4 mg/mL), separated the particle phase from solution phase, and then exposed the particles to a lower concentration solution (0.5 mg/mL). This protocol was compared to a case where the experiment was performed in one step. The apparent path independence of our adsorption isotherm suggests that these proteins are not irreversibly bound (see also desorption studies below). The resulting adsorption isotherm has two important characteristics: (1) The initial portion of the isotherm is steep, indicating a high protein-surface affinity, (2) A well-defined plateau value, corresponding to roughly a protein monolayer. These data are well described by the Langmuir adsorption isotherm (Eq 1-1), where Γ_{max} (= 1.104 mg/m^2) represents the maximum surface coverage, C_{eq} the equilibrium supernatant concentration, and K (= 0.0061 mg/ml) the apparent dissociation constant. The standard deviations of the Γ_{max} and K parameters are 0.051 mg/m^2 and 0.0022 mg/mL, respectively. We note that there is a slight disagreement at intermediate concentrations between the model predictions and the experiments probably due to the assumptions made in the Langmuir model which are not appropriate for protein adsorption (see Section 2.5).

To allow for comparisons with the literature we define two different regimes with respect to surface coverage. Region A represents the low protein-to-surface area ratio used in most previous adsorption and desorption-related studies, where structural changes in the adsorbed and desorbed states were assessed. This region extends to only the initial part of the plateau region.

As a rough estimate (generalizing across the aforementioned subset of literature) this corresponds to surface coverages where 85% or more of the protein in the system is in the adsorbed state. Here, however, we have expanded the range of surface coverage to Region B as well. This region is more relevant to our specific therapeutic application, where the ratio of protein/surface area is higher than traditionally studied systems.

2.4.2. Desorption

Desorption experiments were performed in which fresh buffer was used as an eluent. This is in contrast to most previous reports where surfactants were needed to induce desorption [28, 35, 70, 86]. After a 16 hr incubation of the protein-silica mixture, the particles were separated from the solution via centrifugation, rinsed and resuspended in fresh buffer. This procedure was repeated for 10 consecutive cycles. Figure 2-2B shows the concentration of lysozyme in the resulting supernatant solutions following each buffer resuspension step. An additional way to represent the data is shown in Figure 2-2C, in which the total fraction desorbed is plotted against the original amount adsorbed to the beads after the incubation period. Five different points (Figure 2-2A, Points I-V) along the adsorption isotherm were examined in this fashion to assess the coverage-dependence of desorption. The results indicate that Points I-III, all on the plateau region, have similar desorption behavior. Although the concentration of the supernatant decreases relative to the initial protein concentration for the first 3-4 desorption cycles, after cycle 5 the amount of protein that desorbs is consistent from cycle to cycle and is of similar order of magnitude between points. For points I and II, 0.04 mg/mL protein desorbs for the last 5 cycles, while 0.02 mg/mL desorbs for Point III. For comparison, these desorbed amounts correspond to 8.5 and 3.2% of the adsorbed protein, indicating the surface strongly binds a large fraction of adsorbed

protein, and only a small population desorbs. In contrast, desorbed protein concentration for the last 5 rinse cycles for Points IV and V, both on the ascending regions of the isotherm, are more than an order of magnitude lower than the values for Points I-III. The values for Points IV and V are 0.0011 and 0.0018 mg/mL, respectively. These desorbed protein concentrations, for all rinse cycles, are at the LOD - shown as solid line in Figure 2-2 - of the assay indicating that their values are essentially undetectable. The lack of desorbed protein in the rising part of the isotherm is consistent with the work of Norde and coworkers [28].

To understand the cause of the apparent coverage-dependence of desorption behavior, surface coverage of adsorbed protein remaining attached to the beads is calculated after each rinse cycle. In this way, 5 separate desorption curves on generated, based on Points I-V of the desorption study described above. Figure 2-3 depicts the desorption curves of all five data sets overlaid with the Langmuir fit of the adsorption data. It is apparent that these desorption curves align very closely with the adsorption curve, indicating that because the attachment and detachment are path-independent, the adsorption is reversible. As a further examination of the desorption data, the desorbed amount for each cycle is predicted with the Langmuir isotherm equation (Eq. 1-1) based on the parameters obtained previously, as well as the measured equilibrium concentration left in solution after each rinse cycle. The predicted values for surface coverage value match the measured values remarkably well for Points I-III. The % error between predicted and measured is 4.0, 2.6, 11.3 for curves I, II, and III, respectively. The higher error for Curve III was mainly due to the contribution from a few points in the transition region of the desorption curve. We will discuss later the reason behind slight discrepancies in modeling this region. For curves IV and V, which reside solely within the high affinity region of the adsorption and desorption curves, the

error between predicted and measured desorption values are significantly higher, however, most concentration values in this region are at or below the LOD of our measurement system. Therefore predictability by the Langmuir equation, which relies on accurate equilibrium concentration values, is no longer applicable.

2.4.3. CD Spectra of Various Populations Present in the Protein-Particle System

Figure 2-9 shows a comparison between the CD spectra of the native protein and the supernatant obtained using two different methods: from a single rinse cycle at various coverages (A) and at various rinse cycles at a single surface coverage (B). In each case, the supernatant spectra are comparable to that of the native protein. Combined with the previously presented evidence that the adsorption process is reversible, this strongly suggest that the desorbed protein refolds to a native-like conformation

It is not possible to directly measure the CD spectra of the protein adsorbed on the silica particles in the absence of buffer, and resuspension of the pellets may lead to protein desorption (as previously observed). Therefore an indirect technique is used to deduce the CD spectrum of the adsorbed protein. Using the CD spectra of the supernatant, the spectra of the mixtures (i.e., a combination of the proteins adsorbed on particles and free in solution), and the fraction adsorbed ($1-\chi_{SN}$), the CD spectra of the adsorbed protein (assuming additivity) can be determined by the following equation:

$$[\theta]_{ADS} = \frac{[\theta]_{MIX} - \chi_{SN}[\theta]_{SN}}{1-\chi_{SN}} \qquad \text{Eq. 2-1}$$

where [θ] represents the mean residue ellipticity of different populations. It is possible that some dissolved protein may be entrained in the particle phase during centrifugation leading to an under-estimation of χ_{SN}. However, as we shall discuss below, we do not believe that this effect plays an important role here. See Section 2.8.1 for a further discussion of the validation of this indirect technique to assess adsorbed protein structure. Figure 2-4 shows the CD spectra of the different adsorbed populations, from 6 different points along the adsorption curve (A-C along the plateau; D-E in the transition region, and F in the high affinity region). We were unable to measure the CD spectra of the supernatant at points E and F because the protein concentration in these samples was too low to yield reliable spectra. However, based on the spectra of the other four points, nothing suggests that the desorbed protein at these points has non-native-like structure.

To better understand subtle differences between the calculated CD spectra of the adsorbed protein, the spectra were deconvoluted and the fraction of secondary structure (helix, sheet, turn and random structures) plotted as a function of surface coverage (Figure 2-5). The data show that the structure of the proteins are perturbed significantly on adsorption, but the change in structure correlates poorly with surface coverage. A significant decrease in helical structure (20% loss) is observed upon protein adsorption, which is accompanied by an increase in β-sheet content (14% gain). What is lost in helical structure and is not converted to sheets is converted into unordered structure (6% gain). The fraction of turns in the spectra remain relatively constant. (Numeric details for secondary structure fraction at various coverages are shown in Table 2-2). To assess whether there is any statistical significance between adsorbed protein spectra at different coverages, an ANOVA General Linear Model was used to compare the deconvolution results.

The output of the model indicates no significant differences between the fraction of any secondary structure and surface coverage. Therefore, CD shows a strong perturbation of protein structure on adsorption, but the level of secondary structural perturbation is coverage-independent.

2.5. DISCUSSION

The use of pre-filled systems for the storage and delivery of biologically-active parenteral drug is a quickly growing field in which protein adsorption plays a vital role [2, 59, 60] . Besides the well-known challenges of protecting biologics against chemical degradation and physical instabilities, such a device can introduce additional instabilities stemming from adsorption induced by delivery device surface [7, 61]. As illustrated in Figure 2-2A, the region which best represents our system of interest (based on the ratio of typical drug concentrations to the surface area of a device) falls to the far right of the adsorption isotherm. As a result, mere loss of active drug substance to the container due to monolayer adsorption would typically not represent a significant loss of concentration. Rather, surface-induced structural changes are of greater concern: a structurally perturbed, adsorbed state may interact with protein in bulk, or detach from the surface and maintain its surface-induced perturbations. Similarly, desorption and potential exchange between adsorbed and dissolved proteins may also present a concern, as this would free up surface sites allowing a larger fraction of bulk protein to interact with the surface.

Based on the above motivations, our criteria in system selection includes the ability to induce and measure adsorption and desorption in a repeatable manner, to measure structural transitions during the protein adsorption lifecycle and to assess the effect of a wide range of surface

coverages. To this end, we chose nanoparticles, as opposed to flat surfaces, to have great flexibility with respect to the range of surface area: protein concentration ratios targeted. We also choose particles which are compatible with CD, a widely-accepted tool to study changes in protein conformation in aqueous environments. Inspired by the work of Norde as well as other prominent groups,[22, 28, 87-90], we use fumed silica particles, a highly hydrophilic surface.

The high affinity adsorption isotherm in Figure 2-2A is typical for globular, structurally stable proteins such as lysozyme. The initial portion of the isotherm "merges" with the y-axis, indicating a high surface affinity, followed by a sharp transition from partial adsorption to full coverage. This behavior is likely caused by the dominant role of attractive electrostatic interactions between the protein and surface. In this system (pH=7) lysozyme is positively charged (IeP = 11.7) while the silica is negatively charged (pzc = 3). The theoretical surface coverage for a full monolayer, based on the molecular dimension of lysozyme (Table 2-1), is 1.3 mg/m^2. Since the plateau value of the Langmuir fit is 1.1 mg/m^2, we conclude that the adsorption limit is not inconsistent with a monolayer.

The Langmuir adsorption model (Eq. 1-1) accurately describes the system in the plateau and ascending regions. However, there is a slight discrepancy between the model and data in the transition between these regions. Two assumptions in the Langmuir model that may be violated here are: (1) the absence of conformational change on adsorption and (2) lateral interactions during adsorption. Our CD experiments demonstrate that conformational changes do occur during adsorption, and we also cannot rule out the second effect since adsorption-induced

conformational changes can easily enhance protein-protein contacts between neighboring proteins due to, for example, the exposure of hydrophobic domains.

To the best of our knowledge, the coverage-dependence of desorption has not been previously reported across the entire extent of the adsorption isotherm. Here, we examine the effect of buffer elution on inducing protein desorption in systems ranging from the dilution limit of solubilized protein to fully saturated system conditions. Unexpectedly, due to the large number of systems reporting irreversible adsorption in the absence of surfactants, our results indicate evidence of desorption along the entire plateau region as well as the transition region of the adsorption isotherm. We find that the desorption isotherm bears remarkable resemblance to the adsorption isotherm in these regions, indicating that attachment and detachment are path-independent, and thus adsorption is reversible. When we apply the Langmuir equation to predict desorption behavior, we find excellent agreement between measured and predicted values of desorbed amount and surface coverage across all desorption cycles. The implication of this is noteworthy in that up to a certain threshold value (which occurs at coverages below the transition region), the Langmuirian parameters, which can be fairly easily established, provide an accurate descriptor of desorption behavior in this system. The possibility of generalizing this behavior to other systems will be discussed below. But this finding holds great promise to the specific drug-container interaction cited above, since the experimental space resides solely in the plateau region of the adsorption isotherm.

Building upon our previous findings, we also observe that the desorbed protein populations exhibit native-like CD spectra at every surface coverage investigated. Since we have shown the

adsorbed state is highly perturbed, the protein must refold once it desorbs from the surface. Thus, we propose that the traditional four-state model in Figure 2-1A, which indicates that proteins can populate an adsorbed, desorbed, native or surface-induced unfolded state, can be simplified in this case, as our data are not inconsistent with a simpler two-state model, Figure 2-1B, involving only a highly-perturbed, adsorbed state and a native-like dissolved population.

Another interesting finding is the lack or correlation between surface coverage and surface-induced structural denaturation. Various past studies have indicated that adsorption-induced structural changes occur in a surface-dependent manner [28, 34, 41, 63]. The working hypothesis has been that the mechanisms of surface denaturation is different at low coverages (high level of available surface area promotes unfolding) than at high coverages (crowing effects and steric hindrances prevent unfolding). However, a major limitation of these studies is that the signal obtained for the entire protein-particle system (which also includes desorbed and non-adsorbed protein) is assigned to represent adsorbed protein structure. At low coverages, where the majority of protein is adsorbed, this approximation is relatively accurate, and these previous studies were therefore limited to low coverage regimes. In our system, we are able to replicate this coverage-dependence, when measuring the CD signal elicited by the entire protein-surface system (this effect can be seen when tracking the CD spectra of the mixture across Figure 2-4A-F). However, when we isolate the contribution of only the adsorbed protein, we find no significant differences between adsorbed protein structures at different coverages. Both the similarity in the CD spectra of the adsorbed protein in Figure 2-4A-F, as well as the deconvolution of the CD spectra shown in Figure 2-5 attest to this coverage-independence of adsorbed protein structure.

Two potential limitations to using CD to measure the structure of adsorbed protein is discussed here: (1) It is well documented that deconvolution algorithms have inherent limitations in quantifying the secondary structure of CD spectra[91]. A specific issue in this case may be that none of the reference bases used includes adsorbed or denatured protein, and that structural alterations specific to adsorption may not be captured. (2) In this, and numerous previous studies [18, 21, 22, 74, 75], is assumed that the difference in CD spectra with and without particles is due to the restructuring of proteins when they adsorb to the surface. However, it is possible that the difference in CD spectra could partly be due to a difference in environment sensed by the adsorbed protein compared to the protein in solution. Regarding these potential limitations, two important points must be made. First, we are fully aware of the potential inaccuracies with respect to deconvolution. This is part of the reason why the CD spectra are shown for 6 different coverages in Figure 2-4. These graphs show that adsorbed protein spectra are substantially different from the native (namely almost complete loss of peaks at 206 and 22s nm); and that the adsorbed CD spectra at various coverages are very similar. The key messages from the deconvolution results in Figure 2-5 (substantially loss of native-like structure upon adsorption and no coverage dependence on adsorbed protein spectra) are completely in line with these previous observations regarding CD spectra. So, even with potential inaccuracies due to deconvolution, this key messaging does not change. Secondly, to support both the deconvolution data as well as the use of particles with CD, results obtained by Sethuraman [26] via another technique, FTIR, for lysozyme adsorption, show similar results at saturation coverages: ~25% loss of helix, ~10% gain in sheet and 15% in turns and unordered structure. The respective numbers in this study are -20%, + 14% and +6%. So, even if the deconvolution and/or particles

impose an error, the number obtained by these two orthogonal methods are comparable.

One obvious means to explain the observed desorption behavior of the proteins is to postulate variations in the adsorbed protein's structure. In the proposed models of Morrisey [92] and Iverson [93], proteins adsorbed at lower coverages are more highly unfolded (pancake-like in the model) and have more surface attachments. At increased coverage, higher packing densities result in less unfolding (more spherical or native-like in the model), resulting in fewer surface attachments. Another model which must be mentioned was proposed by Schmidt [94] in which distinct populations with both fast and slow desorption times are identified. The former is attributed to the formation of multilayers, and the latter to surface-induced unfolding of the protein. In our study, we find that the adsorbed proteins exhibit equal levels of structural perturbation regardless of surface coverage, as measured by CD. This suggests that surface-induced denaturation occurs on a molecule-by-molecule basis, which is in contrast to the previous models where denaturation is affected by the surrounding environment. Additionally, we do not have any indication of multilayer adsorption, due to the consistently flat plateau region. In an effort to schematically interpret our findings, we suggest an alternate model (Figure 2-6), which is inspired by results obtained in the synthetic polymer community [95, 96]. One key feature of this model is that secondary structure of the adsorbed protein is similar at all coverages. We thus conjecture that differences in desorption behavior may be better correlated with local descriptors such as the number of surface contacts. At low and intermediate coverages (Regions I and II in Figure 2-6) there is ample room for all absorbed proteins to maximize surface contacts, therefore the number of attachment sites is fairly constant. At higher coverages (Region III), the number of proteins competing for surface contacts grows. Once proteins contact

the surface, unfolding occurs, but to maximize number of adsorbed proteins, not all proteins have equal number of attachments. These molecules, which have fewer attachment sites, are the ones which are more likely to desorb when a favorable chemical potential presents itself. This arrangement would not lead to an increased number of layers. Subsequent follow-up experiments to gain more information about the orientation, exact layer thickness and specific attachments of individual molecules will be required to validate this proposed model. Additionally, more insight gained from the results of systems will provide further insight into this proposed model.

It is possible that some of the observed desorption and surface-related results are directly related to specific characteristics of lysozyme. This model protein is involved in the hydrolysis of β-glycosidic linkages of carbohydrates in Gram positive bacteria cell walls [83]. Lysozyme is a highly helical, intrinsically stable, globular protein, which been evolutionary designed to withstand the relatively harsh extracellular environment, and has 4 disulfide bridges which adds to its high intrinsic stability [97]. Previous results indicate that both its high structural stability [28] as well as the favorable charge interactions between the protein and surface [58] play an important role in lysozyme's reversible adsorption behavior and in its tendency to regain native-like structure upon desorption.

2.6. CONCLUSIONS

The motivation for this work is to increase our understanding of the impact of various aspects of protein/surface interactions on protein stability. The ideas presented here suggest that expanding the traditional design space to include surface coverages representative of the entire adsorption isotherm yields unexpected results with respect to desorption behavior and its relationship to

surface-induced denaturations. Namely, both the attachment to as well as structural transitions on the surface appear to be reversible at saturation levels of surface coverage. Moreover, the amount desorbed is found to be predicted by simple Langmuirian parameters, and there is evidence of only 2-states in the traditional 4-state kinetic model. Although it is possible that some of the observed behavior is directly correlated to the specific components of the system used here, the results of this research offer new insight into the adsorption reversibility and its predictability, as well as consequences of surface-induced structural transitions.

2.7. FIGURES

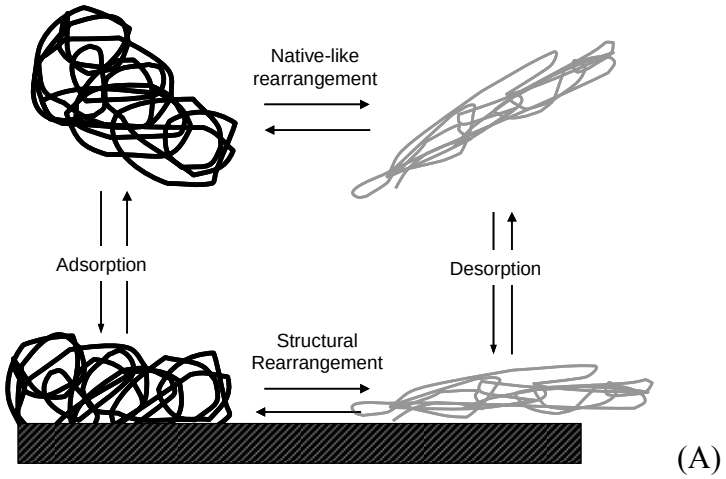

(A)

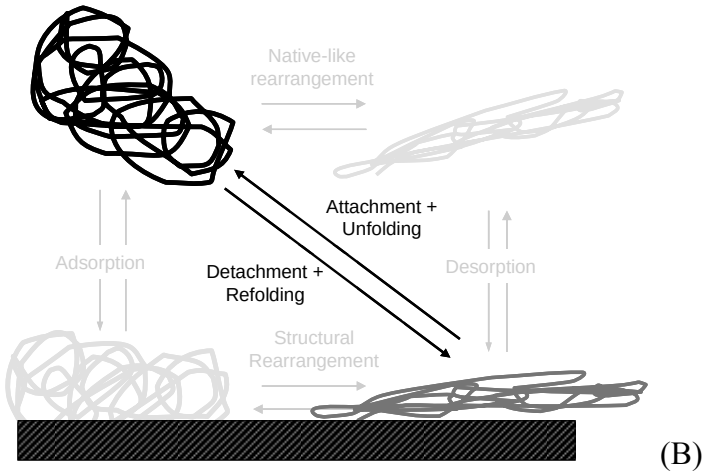

(B)

Figure 2-1 Kinetic model of protein adsorption

(A) Classical 4-State kinetic model, representing the native state in bulk before adsorption, the adsorbed state before unfolding, followed by structural rearrangement while on the surface, and by desorption into bulk, and refolding into native-like state. (B) Two states which have been observed in this current study with the tools described in the methods section.

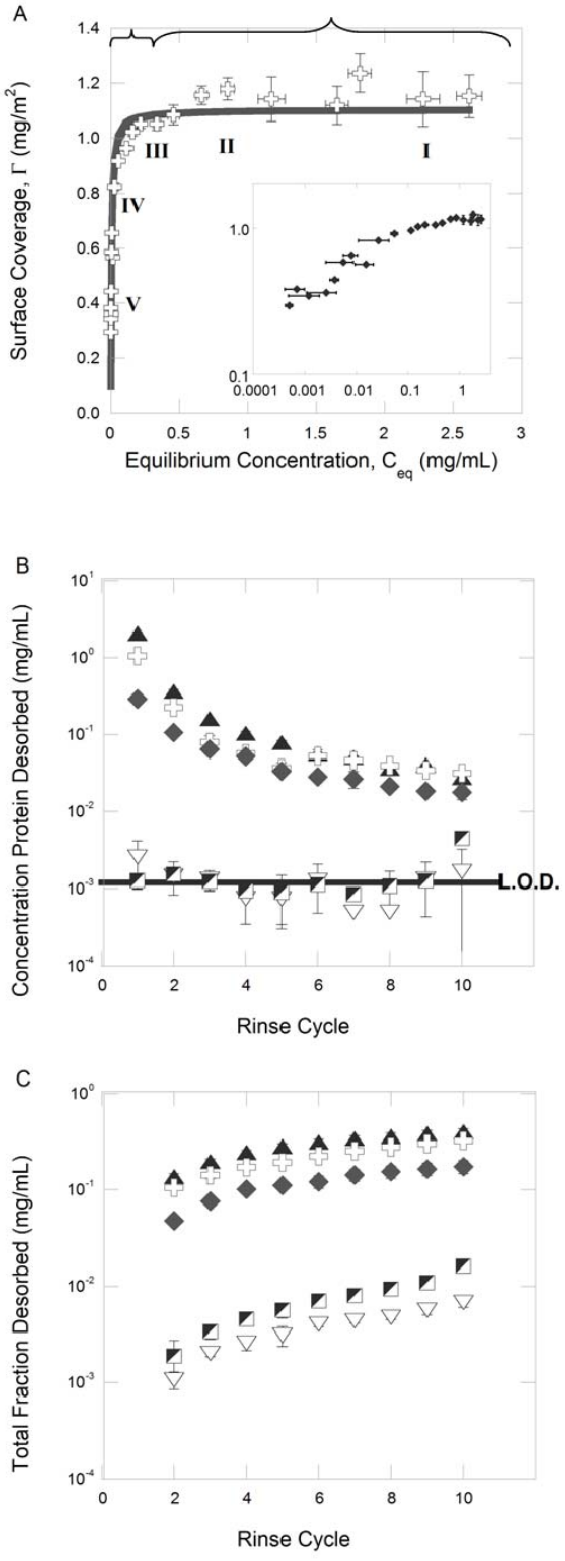

Figure 2-2 Adsorption and desorption curves of lysozyme on silica

(A) Adsorption isotherm for lysozyme onto silicon dioxide nanoparticles after 16 hr incubation at 25ºC in 10mM sodium phosphate (pH 7.0). Each diamond represents the average of three distinct replicates and error bars represent their standard deviation; the solid line represents a least squares fit of the Langmuir Equation. The parameters associated with this fit are: Γ_{max} = 1.104 mg/m^2 (st.dev. = 0.051).; K = 0.0061 mg/mL (st.dev. = 0.0022). The labeled points (I-V) along the adsorption isotherm refers to the desorption points represented in Figure B, The labels "Region A" and "Region B" refer to: A: the most common region within which conformational studies on adsorbed protein have been done in previous studies, and B: the additional region which is the focus of this paper, and which is more relevant to pre-filled drug delivery device systems. Inset: Same adsorption isotherm data plotted on a log-log basis in order to better depict the low surface coverage data points. (B) Desorbed protein concentration (based on lysozyme remaining in the supernatant after resuspension of silica particles in fresh 10mM sodium phosphate buffer) as a function of rinse cycle. Data shown rinse cycles 2-10. Protein/particle ratios corresponding to five different regions along the adsorption isotherm (as labeled I-V in Figure A) were used (surface coverage, C_{eq}, and fraction adsorbed follow each sample) ▲ Sample I: 1.29 mg m^{-2}, 2.06 mg mL^{-1}, 0.44; ✙ Sample II: 1.08 mg m^{-2}, 1.06 mg mL^{-1}, 0.55; ◆ Sample III: 1.18 mg m^{-2}, 0.29 mg mL^{-1}, 0.83; ▽ Sample IV: 0.72 mg m^{-2}, 0.003 mg mL^{-1}, 0.98; ◩ Sample V: 0.37 mg m^{-2}, 0.001 mg mL^{-1}, 0.99. Each point is the average of three distinct replicates and error bars represent their standard deviation. The solid, horizontal black line depicts the limit of detection of the concentration assay used for lysozyme measurement in the supernatant. (C) Total fraction desorbed (compared to original adsorbed amount) plotted as a function of rinse cycle.

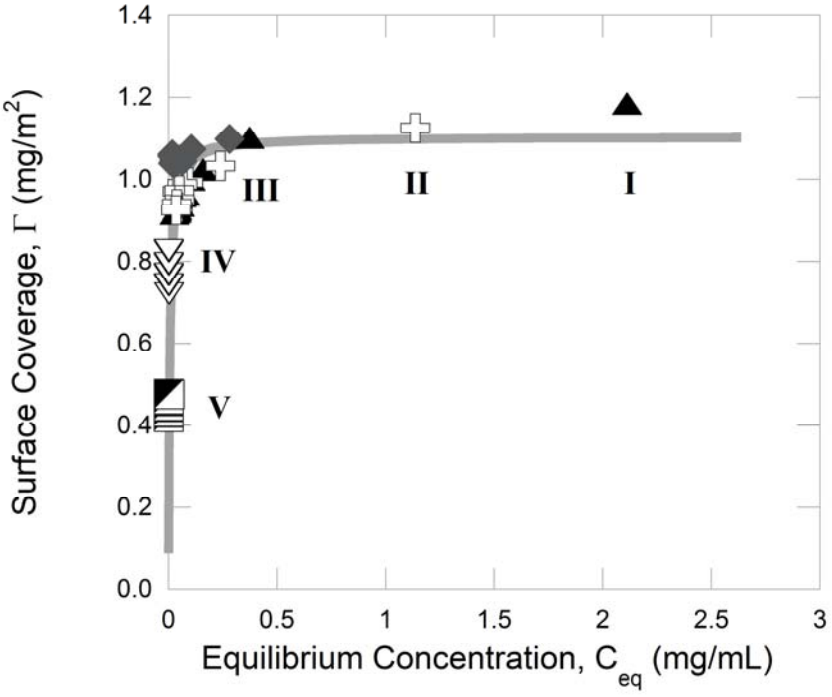

Figure 2-3 Desorption isotherm or lysozyme on silica

Isotherm calculated from data collected for desorption curves in Figure 2-2. Data for all 10 cycles are depicted. The same coverages were targeted for I-V as in Figure 2-2A The solid grey line represents the adsorption isotherm data.

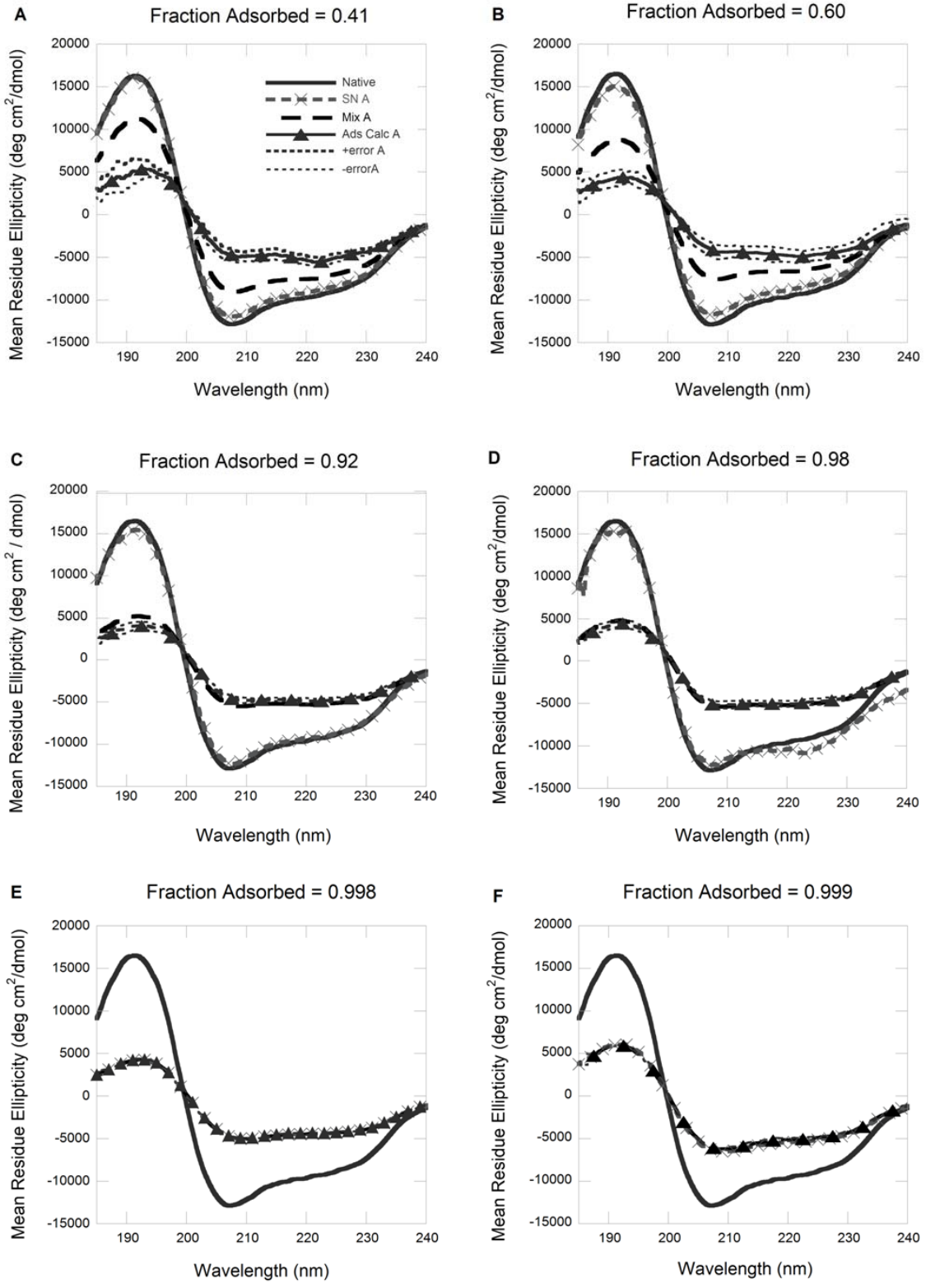

Figure 2-4 CD spectra of adsorbed protein populations of lysozyme

Spectra shown: ——Native protein; – –×– –Supernatant; —··—Mixture of particles and proteins; ··▲···Adsorbed, calculated; – – –Error bands associated with adsorbed calculation. Each graph (A-F) corresponds to the following fraction of protein adsorbed; supernatant concentration; and surface coverage, respectively: (A) 0.41; 2.55 mg mL^{-1}; 1.11 mg m^{-2} (B) 0.60; 1.65 mg mL^{-1}; 1.05 mg m^{-2}; (C) 0.92; 0.41 mg mL^{-1}; 1.03 mg m^{-2}, (D) 0.98; 0.19 mg mL^{-1}; 0.91 mg m^{-2}, (E) 0.998; 0.03 mg mL^{-1}; 0.78 mg m^{-2}, (F) 0.999; 0.007 mg mL^{-1}; 0.43 mg m^{-2}.

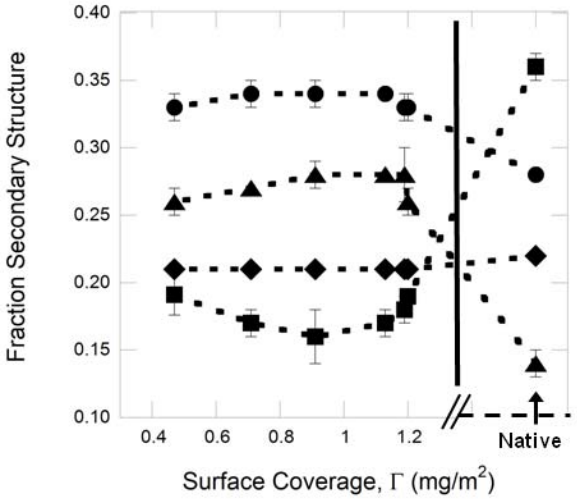

Figure 2-5 Deconvolution of adsorbed CD spectra at various surface coverages

The fraction of each secondary structure (■Helix, ▲Sheet, ◆Turn and ● Unordered structure) is plotted as a function of the surface coverage of lysozyme. Deconvolution was performed using CDPro, as detailed in the Methods section. Error bars represent the deconvolution of three separate replicates.

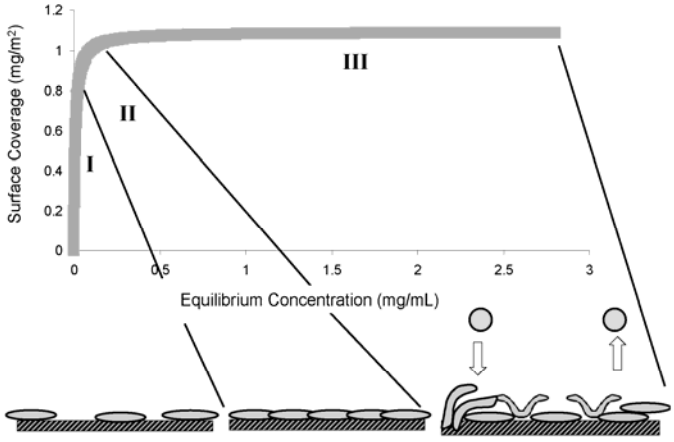

Figure 2-6 Proposed adsorption model

Regions I, II, III represent the ascending portion, transition region and plateau, respectively, of the adsorption isotherm. The "elongated" structures represent unfolded protein adsorbed to the surface. In all three regions, this level of perturbation of the adsorbed state remains the same—the difference comes from surface attachment sites. In Regions I and II, there is ample surface available to all protein to maximize protein-surface contacts. However, in Region III, in order to maximize the number of proteins that can adsorb, the number of surface attachment sites for each individual protein varies. The proteins with fewer attachments are most likely to desorb and refold into the native-like conformation

2.8. SUPPLEMENTAL INFOMRATION

2.8.1. Further Experimental Detail

Comparison of previously reported adsorption isotherms with current study. Various groups have reported adsorption isotherms of lysozyme on hydrophilic silica and other hydrophilic surfaces. However, there is a striking level of variation between reported isotherms. Comparison with the 1992 Norde study [28] is most appropriate, as the same type of particles, buffer system and mixing parameters were used. There is good agreement between Γ_{max}, while the K value differs by an order of magnitude. Possible explanations include: difference in properties of the model system (lysozyme, particles, environmental conditions), varying degree of sensitivity of techniques employed, and a difference in the range of coverages targeted. In comparison of this isotherm to other previous works, the basic qualitative characteristics of the lysozyme-silica adsorption isotherm are all similar (well-defined plateau values, high affinity behavior, and a distinct transition region), and less emphasis should be placed on quantitative comparison.

Validation of indirect approach to measuring adsorbed protein structure. To validate the accuracy of the indirect approach for calculating adsorbed protein structure, an experimental measurement was also taken. Following 16hr incubation, and removal of supernatant from the pellet, the pellet was resuspended in fresh buffer and the CD spectra was measured. Here, we assume that all protein molecules in the resuspended mixture are from the protein-particle complexes. Therefore, the CD spectra is of adsorbed protein only. This assumption is tested below. This experiment was carried out at both high (46% adsorption) and low (99% adsorption) levels of surface coverage. The comparison between the resuspended spectra (grey graph with

crosses) and the calculated spectra (solid line) are shown in Figure 2-7. In the top graph (on plateau level of adsorption isotherm), there is a distinct discrepancy between the direct and indirect methods of finding adsorbed protein structure, whereas in the bottom graph (rising portion of the adsorption isotherm) the two spectra are very similar. One explanation is that in regions where the crowing effect is high and the chances of protein desorbing is high, the resuspended solution also contains protein with fast desorption kinetics which regains native-like structure. This desorption can occur between the time the resuspension is mixed and the CD measurement is taken. Another possible explanation is that proteins with native-like structure remains loosely bound to the monolayer of protein directly adsorbed to the surface. At low levels of surface coverage, where desorption is less likely, this issue does not exist. To test which hypothesis regarding the high surface coverage scenario makes sense, a calculation was done to correct for the amount of protein desorbing from the protein surface and returning to the supernatant. This calculation was done by first measuring the concentration of protein in the supernatant by completing another cycle of rinsing, then assuming all protein found in the supernatant regains native-like structure, and subtracting the effect of this additional native-like protein from the resuspended spectra. Similar to equation (2):

$$[\theta]_{\mathrm{Re}\,suspension}^{Corrected} = \frac{[\theta]_{\mathrm{Re}\,suspension} - \chi_{resuspeded}[\theta]_{SN}}{1-\chi_{resusepnded}} \qquad (3)$$

Where $\chi_{\mathrm{resuspended}}$ is the ratio between the protein remaining in the second supernatant cycle and that in the resuspension. As shown in Figure 2-7, the result of this theoretical calculation gives back the calculated adsorbed protein structure (dashed line). Because this is the case, the inference is made that the first hypothesis is more likely: that desorbed protein which regains

native-like structure is responsible for the difference between the two graphs. To further test whether loosely bound or entangled native-like proteins are not present, the resuspension was repeated several times. Hypothetically, if such loosely bound molecules are present, then the spectra of the resuspension would lose structure as the number of resuspensions cycles increases and the loosely bound proteins are “washed off”.

To test this assumption and obtain an indication of the reversibility of structural transition in the adsorbed state, the CD spectra of the protein-particle system was measured immediately following several resuspension cycles. Figure 2-8 shows very consistent resuspension spectra over 10 cycles. This results indicates little evidence of loosely bound protein following each resuspension.

2.8.2. Supplementary Tables and Figures

Physical—Chemical Properties of Silicon Dioxide Beads		Physical—Chemical Properties of Lysozyme	
Density (g cm^{-3})	2.2	Molar Mass (g mol-1)	14331.2
B.E.T Surface Area (m^2 g^{-1})	200	Partial Spec. Volume (cm^3 g^{-1})	0.688
Particle Size (nm)	263 ± 13	Dimensions (nm^3)	4.5 x 3 x 3
Zeta Potential (mV) Medium: 10mM sodium phosphate buffer, pH=7	-25.3	Isoelectric Point	11.1
Point of zero charge of silica	2-3	Secondary Structure (X-ray crystallography data *	% Helix: 40 % Sheet: 10

Table 2-1 Physical—chemical properties of silica and lysozyme

Γ (mg m^{-2})	Helix	Sheet	Turn	Random Coil
Native	**0.36** (0.01)	**0.14** (0.01)	**0.22** (0.01)	**0.28** (0.01)
1.2	**0.19** (0.01)	**0.26** (0.01)	**0.21** (0.01)	**0.33** (0.01)
1.19	**0.18** (0.01)	**0.28** (0.02)	**0.21** (0.01)	**0.33** (0.01)
1.13	**0.17** (0.01)	**0.28** (0.01)	**0.21** (0.01)	**0.34** (0.01)
0.91	**0.16** (0.02)	**0.28** (0.01)	**0.21** (0.01)	**0.34** (0.01)
0.71	**0.17** (0.01)	**0.27** (0.01)	**0.21** (0.01)	**0.34** (0.01)
0.47	**0.19** (0.02)	**0.26** (0.01)	**0.21** (0.01)	**0.33** (0.01)

Table 2-2 Fraction of secondary structures of adsorbed protein spectra upon deconvolution

Data shown for CD data, average (standard deviation). This is a numerical representation of the data graphed in Figure 2-5.

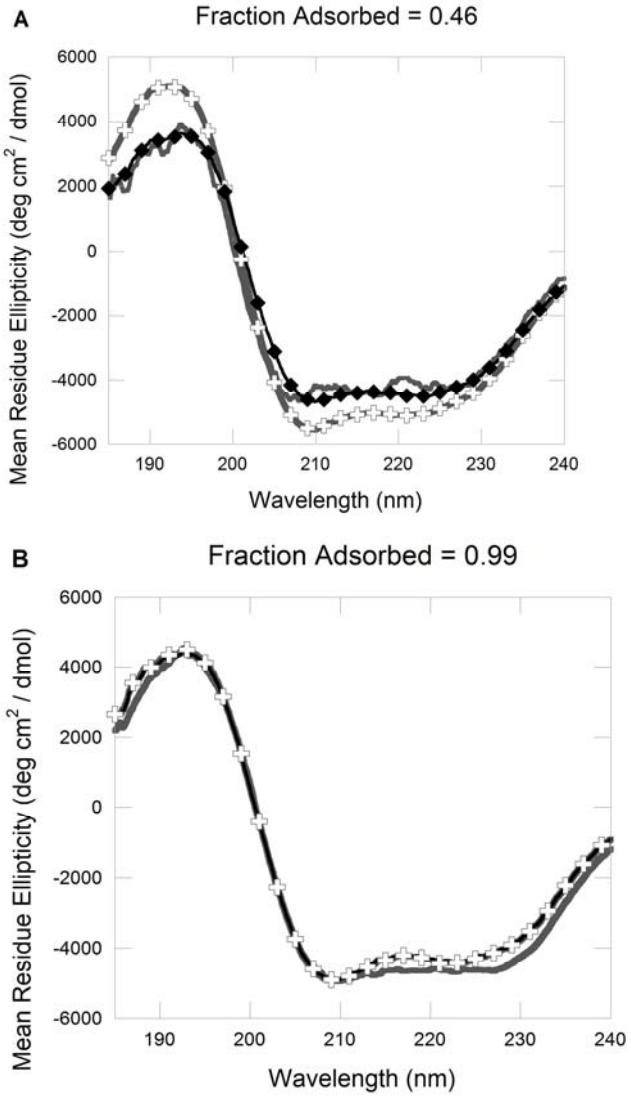

Figure 2-7 CD spectra comparison between measured and calculated adsorbed lysozyme

Data shown for protein structure indirectly calculated (——), and a measured CD spectra immediately following reconstitution of the pellet after centrifugation (····✙····). As discussed in the results section, a correction factor must be applied to the resuspended spectra, to account for protein desorbing with very fast kinetics into the resuspension buffer. Once this is applied, agreement between the direct and indirect approach of calculating adsorbed protein structure is achieved (—◆—). Figure (A) represent a point along the plateau level of the adsorption isotherm (fraction adsorbed = 0.46, C_{eq} = 1.65 mg mL^{-1}, Γ = 1.18 mg m^{-2}); and Figure B represent a points along the rising part of the adsorption isotherm,, when nearly all lysozyme is adsorbed to the surface (fraction adsorbed = 0.99, C_{eq} = 0.049 mg mL^{-1} , Γ = 0.83 mg m^{-2}).

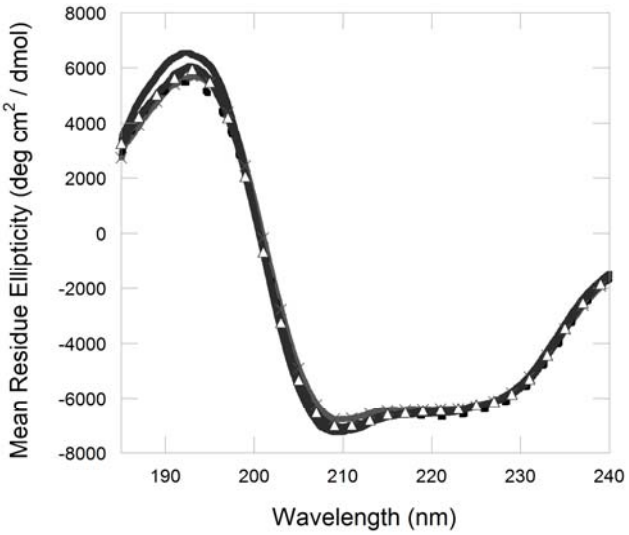

Figure 2-8 CD spectra of protein-particle system showing effect of resuspensions

Spectra of protein-[article mixture immediately following resuspension. The original protein/particle ratio chosen is from the plateau region of the adsorption isotherm (Fraction adsorbed = 0.45, C_{eq} = 2.01 mg mL^{-1}, Γ = 1.22 mg m^{-2}). The resuspension cycles shown are: —— Cycle 1, –×– Cycle 3, - - - Cycle 5, –△– Cycle 8, ____ Cycle 10.

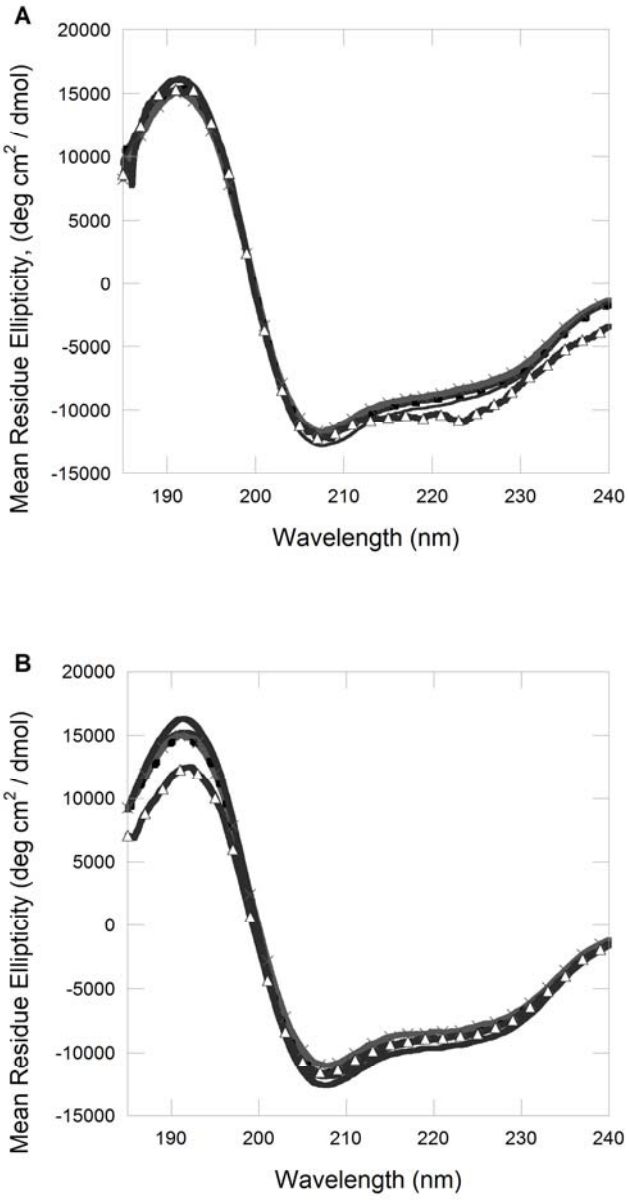

Figure 2-9 Comparison of supernatant and native lysozyme CD spectra

Data shown for: A) following a single rinse/resuspension cycle at various surface coverages, Coverage, equilibrium supernatant concentration, and fraction adsorbed, respectively: —— 1.13 mg m^{-2}, 1.96 mg mL^{-1}, 0.41; –×– 1.15 mg m^{-2}, 0.96 mg mL^{-1}, 0.60; - - - 1.00 mg m^{-2}, 0.13 mg mL^{-1}, 0.92; –△– 0.86 mg m^{-2}, 0.08 mg mL^{-1}, 0.98; ____ Native. B) at single surface coverage (Γ=1.2 mg/m^2), following ——1, –×–2, - - -3, and –△–4 rinse cycles, ____Native.

CHAPTER 3. EFFECT OF THERMAL STABILITY ON PROTEIN ADSORPTION TO SILICA USING HOMOLOGOUS ALDO-KETO REDUCTASES ‡

3.1. ABSTRACT

Gaining more insight into the mechanisms governing the behavior of proteins at solid/liquid interfaces is particularly relevant in the interaction of high-value biologics with storage and delivery device surfaces, where adsorption-induced conformational changes may dramatically affect biocompatibility. The impact of structural stability on interfacial behavior has been previously investigated by engineering non-wild-type stability mutants. Potential shortcomings of such approaches include only modest changes in thermostability, and the introduction of changes in the topology of the proteins when disulfide bonds are incorporated. Here we employ two members of the aldo-keto reductase superfamily (alcohol dehydrogenase, AdhD and human aldose reductase, hAR) to gain a new perspective on the role of naturally occurring thermostability on adsorbed protein arrangement and its subsequent impact on desorption. Unexpectedly, we find that during initial adsorption events, both proteins have similar affinity to

---

‡ A version of this chapter is in press in Protein Science (2012), 27:19, 11873-82, with co-authors Paolo Mangiagalli, Tushar Patel, Sanat K. Kumar, and Scott Banta. FF designed the experiments, performed the experiments, analyzed data, and wrote the manuscript.

the substrate and undergo nearly identical levels of structural perturbation. Interesting differences between AdhD and hAR occur during desorption and both proteins exhibit some level of activity loss and irreversible conformational change upon desorption. Although such surface-induced denaturation is expected for the less stable hAR, it is remarkable that the extremely thermostable AdhD is similarly affected by adsorption-induced events. These results question the role of thermal stability as a predictor of protein adsorption/desorption behavior.

3.2. INTRODUCTION

Over the past few decades, extensive focus has been applied to understanding the mechanisms governing the behavior of proteins at solid/liquid interfaces. Due to wide-spread implications of this phenomenon in numerous applications, a large number of systems have been studied. To gain more insight into how protein structure affects interfacial behavior, the importance of surface charge [51, 98], hydrophobicity [99], and structural stability [82, 100] have been investigated.

Approaches to study the effects of these parameters can be categorized as follows: the study of well-defined model proteins [27, 101-104], genetic variants [17, 105], mutants of single proteins [106-108], and most recently, synthetic polypeptides [87, 109, 110]. Significant effort in the two former categories has pioneered our overall understanding of the mechanisms governing protein adsorption; however, it is the latter groups in which the effect of subtle molecular effects can be assessed. Thus, ideal studies could be envisioned in which a single parameter, such as stability or surface charge, are studied in isolation.

Many of these studies have explored the structural consequences of adsorption. Elbaum [111] used stability variants of hemoglobin to hypothesize a strong structural basis for observed differences in adsorption kinetics and protein unfolding at the air/water interface. Kato [112] strengthened this correlation between conformational stability and interfacial affinity and level of surface-induced perturbation using tryptophan synthase mutants. More recently, bacteriophage T4 lysozyme has been the protein of choice for similar studies because it is extremely well characterized and synthesis of stability mutants is well documented. McGuire [107] created T4

variants with enhanced stability by introducing cysteine residues to form additional intra-molecular disulfide linkages. Following the kinetics of adsorption and elutability, they postulated a correlation between protein stability and time-scale of attachment and binding strength. CD spectroscopy revealed that both the rate and extent of unfolding (characterized by α-helical loss) upon adsorption to silica nanoparticles was most pronounced for the least stable mutants [82].

The general hypothesis emerging from these studies is a strong correlation between thermostability and affinity of surface attachment, structural perturbation and desorbability. However, there are two potential shortcomings with the application of stability mutants to evaluate surface activity. First, only incremental changes in stability can be assessed. The range of stabilities is limited by the number of residue substitutions which alter stability without impacting secondary structure. Second, stability is artificially optimized in these systems. For example, common approaches involve strategically placed disulfide bonds or the insertion of residues with side chains that cause steric disruptions in critical locations. However, these approaches change the topology of the peptide chain and it is difficult to decouple the effect of the stability-altering mutations from the effect on protein-surface interactions.

The goal of our investigation is to explore the relationship between stability and adsorption behavior using naturally evolved homologs with very similar 3-D structures yet vastly different intrinsic stabilities. We have chosen two members of the aldo-keto reductase (AKR) superfamily [113] which share high structural homology with low primary sequence homology (Figure 3-1). The members of the AKR superfamily are monomeric, do not contain disulfide bonds, and fold into well-known 8 stranded, TIM-like, α/β barrels. The first enzyme, alcohol dehydrogenase D (AdhD) from the hyperthermophilic archaea *Pyrococcus furiosus*, is highly thermostable [114,

115] while the second enzyme, human aldose reductase (hAR), is mesostable [116]. We believe this is the first time that homologous stability variants have been used to explore the effects of protein stability on interfacial behavior. Adsorption and desorption were investigated using a hydrophilic silica surface which has been used previously in adsorption studies [28-30].

Based on previous results, we hypothesized that AdhD and hAR would exhibit different adsorption behavior due to their drastically different thermostabilities. Unexpectedly, our results indicate that both proteins have similar affinities to the substrate and undergo nearly identical levels of structural perturbation. Interesting differences between AdhD and hAR are observed during desorption, with respect to elutability, refolding pathways and distribution of desorbed structural states. Both proteins exhibit some level of activity loss and irreversible conformational change upon desorption. Although surface-induced denaturation and activity loss is expected for the less stable hAR, it is remarkable that AdhD, which retains native-like structure and activity at even at 100°C, is significantly affected by adsorption-induced events. Therefore, our results suggest that intrinsic structural stability may not be the most accurate predictor of adsorption behavior, and that other predictors, such as electrostatics, may have a greater impact on the extent of surface affinity and unfolding. These results may call into question the commonly held belief that increasing thermostability should reduce surface activity.

3.3. EXPERIMENTAL SECTION

3.3.1. Materials

DNA oligonucleotides were synthesized by Integrated DNA Technology (IDT; Coralville, IA).

Isopropyl β-D-1-thiogalactopyranoside (IPTG) was obtained from Promega (Madison, WI). Fumed colloidal silica particles (Cab-o-sil M-5, <99.8% purity) were purchased from Cabot Corp. (Boston, MA) and used without further treatment. Bicinchoninic acid (BCA) and QuantiPro BCA Assay kits were purchased from Thermo Fisher Scientific (Rockford, IL). Restriction enzymes *Nco*I and *Hind*III, T4 DNA Ligase, and Phusion DNA Polymerase were purchased from New England Biolabs (Ipswich, MA). All other chemicals were obtained from Sigma-Aldrich (St. Louis, MO).

3.3.2. Cloning

The hAR gene was amplified from human placental cDNA (Clontech, Mountain View, CA) using overlap extension PCR to eliminate an internal *Nco*I restriction site present in the hAR gene. Detailed information about the primers can be found in the SI. The purified PCR fragment was doubly digested and ligated into a similarly digested pET-24d (Novagen, Gibbstown, NJ) vector containing a poly-His tag. Ligated plasmids were electroporated into BLR *E. coli* cells (Novagen) and selected on LB agar plates supplemented with 50 ng uL^{-1} kanamycin. Colonies were grown in terrific broth (TB) with 50 ng uL^{-1} kanamycin and stored as glycerol stocks at -80^{o}C. The correct insertion of the hAR gene was verified by DNA sequencing.

3.3.3. Protein Purification

AdhD from the hyperthermophilic archaea *Pyrococcus furiosus* was expressed and purified as previously described [22]. hAR was expressed and purified as follows. Following transformation and expression as described above, the cells were induced with 0.2mM IPTG at OD_{600} of 0.6. After incubating 18 hours at 37^{o}C with agitation, the cells were harvested by centrifugation. The

pelleted cells were resuspended in one-tenth of the expression volume in 20 mM Tris-HCl, 150 mM NaCl, and 40 mM imidazole (pH 7.5) and supplemented with 1x HALT protease inhibitor cocktail (Thermo-Fisher). The cells were lysed by sonication with an 8 minute run time with pulses of 5 seconds with a 5 second rest between each pulse. The cell debris was pelleted by centrifugation at 15,000xg for 30 minutes. The hAR was purified from the clarified lysate using a HisTrap column (GE Healthcare) on a GE ÄKTA FPLC. The fractions containing hAR, (verified by SDS-PAGE) were pooled and concentrated using Amicon (EMD Millipore) centrifugal filters with a 30 kDa MWCO. Protein stocks were stored at 4^{o}C.

3.3.4. Protein Concentration Measurements

Concentrations were determined by UV absorbance at 280 nm and the BCA total protein assay (Macro assay: 1-0.025 mg mL^{-1} and Micro assay: 0.05-0.0005 mg mL^{-1}). Absorbance measurements were conducted on a SpectraMax M2 spectrophotometer (Molecular Devices, Sunnyvale, CA). Extinction coefficients for AdhD (ε_{280} = 1.97 mL mg^{-1} cm^{-1}) and hAR (ε_{280} = 1.1 mL mg^{-1} cm^{-1}) were measured experimentally. Preparation of standards for the BCA assays and protein samples for extinction coefficient measurements are described in Section 3.8.1.

3.3.5. Activity Assay

The 2,3-butanediol oxidation activity of AdhD and DL-glyceraldehyde reduction activity of hAR were measured using spectrophotometric assays under saturation conditions. NAD^{+} and NADPH were used as cofactors for AdhD and hAR, respectively. For AdhD, the absorbance at 340 nm (tracking NAD^{+} reduction) was measured at 45^{o}C with final concentrations of reaction buffer (glycine, pH 8.8), substrate and cofactor of 50 mM, 100 mM, and 1 mM, respectively. For hAR,

the absorbance at 340 nm (tracking NADPH oxidation) was followed for reactions at 25^{o}C with concentrations of reaction buffer (sodium phosphate, pH 7.0), substrate and cofactor of 100 mM, 100 mM, and 0.5 mM, respectively. Raw absorbance change was converted to specific activity using enzyme concentration and cofactor extinction coefficient ($\varepsilon_{340nm} = 6.22x10^{3}$ cm^{-1} M^{-1}).

3.3.6. Adsorption Isotherms

Silica particles were suspended in 20 mM sodium cacodylate buffer pH 5.0 (AdhD) or pH 6.9 (hAR) to achieve a concentration of 12 mg mL^{-1}. Equal parts of protein solution and silica suspension were mixed. Protein concentrations of 0.1-6 mg mL^{-1}were achieved by diluting with 20 mM Tris pH 7.5. Final pH resulted in 5.7 for AdhD and 7.2 for hAR. The samples were rotated on a rotisserie shaker for 16 hours at room temperature.

3.3.7. Desorption

After removal of the supernatant, the particle pellet was resuspended in 0.8 mL of 10 mM sodium cacodylate buffer pH 5.0 (AdhD) or pH 6.9 (hAR). Samples were weighed to determine the particle loss over time. A solution density of 1.02 g cm^{-3} was used to determine the resuspension volume. After resuspension, the samples were incubated on a rotisserie shaker for 30 minutes. Then, supernatant was collected in the same as in the adsorption experiments. Resuspension was repeated for a total of 10 supernatants, from which a desorption curve was obtained. It was assumed that by the third resuspension cycle all of the protein had interacted with the particles, and these samples were used for CD and kinetic activity evaluation.

3.3.8. Circular Dichroism

A Jasco J-815 CD spectrometer (Jasco, Inc., Easton, MA) equipped with a Peltier junction temperature control was calibrated with 0.06% d-10-camphorsulfonate solution and used for far-UV CD measurements. Quartz cuvettes with path lengths of 0.01, 0.02, 0.05, or 0.1 cm were used. Protein solutions and protein-particle mixtures were measured using buffer or silica blanks, respectively, for subtraction of the baseline signal. Measurements were taken from 185 to 240 nm with a 0.1 nm interval, 1 nm bandwidth, 8 second response time, and scanning speed of 50 nm min^{-1}. For desorbed protein structure, the 0.1 cm cuvette was used, and the scan was cut off at 200 nm due to buffer interference. For each sample, 3 accumulations were measured and averaged. Raw CD signal, Θ, was converted to Mean Residue Ellipticity (MRE) using the equation $[\Theta]_{MRE} = \Theta/(10*C_r*l)$ where C_r is the protein concentration (M*residue number) and l is the cuvette path length (cm).

3.3.9. Measurement of Adsorbed Protein Structure

The pellets from the adsorption isotherm were resuspended with gentle pipetting using a 1:1 mixture of 20 mM Tris-HCl pH 7.5 and 20 mM sodium cacodylate pH 5.0 (AdhD) or pH 6.9 (hAR). An aliquot was removed for CD assessment, and the rest of the solution was pelleted through centrifugation (as described above) and supernatant concentration measured. The CD spectra of the supernatant were also recorded. Using the known amount of adsorbed protein, concentration in the resuspended pellet was determined. Using the MRE signal of the resuspended pellet, $[\Theta]_{pell}$, and of the supernatant $[\Theta]_{SN}$, and the fraction of total protein concentration in the supernatant, χ_{SN}, the adsorbed protein structure was calculated using Eq. 3-1:

$[\Theta]_{Ads} = ([\Theta]_{pell} - \chi_{SN}*[\Theta]_{SN})/(1 - \chi_{SN})$. (Eq. 3-1)

3.3.10. Deconvolution

The CD spectra were deconvoluted using the CD Pro software package [85]. With each deconvolution algorithm (Continll, Selcon3, and Cdstr), 3 different reference sets were applied: SP37, SPD42, and SMP50. The average across all 3 algorithms and 3 bases are used to estimate the helical, sheet, and disordered content of each sample. The α-helix and β-sheet content is reported as the sum of the distorted and regular classes.

3.3.11. Electrophoretic Mobility

A Malvern Zetasizer Nano-ZS was used to measure particle size distribution and zeta potential of the silica particle suspensions in the pH=5.7 and pH=7.2 Tris/cacodylate buffers, or protein—silica mixtures. A 50 mW laser operating at a wavelength of 532 nm was used. Scattering intensities were recorded at a 90°angle. A clear, disposable zeta cell was used for zeta potential measurements. All measurements were performed at 25°C.

3.4. RESULTS

3.4.1. Structural Characterization of Model System

Two homologous AKR superfamily members, AdhD and hAR, were chosen due to their similar secondary structures and different intrinsic structural stabilities. The sequence alignment (ClustalW2, EBI; A) and ribbon structures (Figure 3-1) show that while there is low sequence homology (<30%) between the proteins, the tertiary structures are very comparable. Overlaying the CD spectra for both proteins more clearly demonstrates these similarities (Figure 3-1C). The

high degree of spectral overlap indicates similar proportions of α-helical and β-sheet content. The fraction of secondary structure assigned to various domains from primary sequence predictions, the homology model (AdhD) or crystal structure (hAR; PDB: 2ACQ), and deconvolution of CD spectra are tabulated in Table 3-1. For both proteins, the fractions of secondary structure assigned to the helix and sheet domains are similar between the sequence prediction and homology model, but there is a discrepancy compared to experimental deconvolution values. This discrepancy is explained further in Section 3.5. However, the similarity in each secondary structure domain of the two proteins, with all three enumeration methods, is obvious from the table. The CD-based method was used as the principle experimental tool to assess relative changes in secondary structure. While the CD data demonstrate the similar structures of the proteins, the significant difference in structural stability is demonstrated by the melting curve shown in Figure 3-9, where the CD signal at 222nm (indicative of helical content) is measured over a thermal excursion from 25 to 95°C. The curve shows that hAR loses a considerable amount of helical structure, while AdhD is minimally affected and no noticeable unfolding occurs below 95°C.

3.4.2. Adsorption Behavior

The surface coverage of protein molecules adsorbed to the nanoparticles following a 16 hour isothermal incubation period is plotted against the equilibrium (supernatant) concentration (Figure 3-2). For both proteins, there are three well-defined regions: a rising linear portion, a transition region, and a maximum coverage plateau. At least one point from each of these regions is represented in subsequent data sets (letters in Figure 3-2 indicate these coverages). The adsorption data are described using the Langmuir adsorption isotherm defined in Eq. 1-1.

Although assumptions underlying the Langmuirian model are not all necessarily appropriate for the adsorption of complex biomacromolecules (absence of conformational change and lateral interaction on the surface), the model describes this high-affinity protein-surface interaction well. The maximum surface coverage and affinity obtained from this fit are 1.68 mg m^{-2} and 0.50 mg mL^{-1} for AdhD, and 2.40 mg m^{-2} and 0.35 mg mL^{-1} for hAR, respectively. The lower affinity coefficient and higher maximum surface coverage of hAR, as compared to AdhD, indicate an increased affinity and adsorbed amount. Based on the molecular volume of each protein, theoretical surface coverages of 2.20 and 2.26 mg m^{-2} for AdhD and hAR, respectively, were obtained. In order to account for the packing of molecules on the surface, the Random Sequential Adsorption (RSA) [117] packing density (Θ=0.547) was multiplied by the total surface area of the particles to obtain the available surface area [118]. Since these calculations only account for size and not intermolecular interactions, the variance from experimental values is not concerning.

3.4.3. Adsorbed Protein Structure

Figure 3-10 shows the CD spectra of the different populations of proteins following surface interaction. A combination of these spectra was used to calculate adsorbed protein spectra. Figure 3-3 shows the adsorbed spectra for 5 different coverages for AdhD (Figure 3-3A) and hAR (Figure 3-3B). Two important conclusions emerge from these plots: first, for both proteins, the adsorption induces a significant level of unfolding compared to native; and second, the adsorbed spectra do not vary significantly as a function of surface coverage. To further compare the level of unfolding that occurs upon adsorption, all spectra were deconvoluted and the results plotted in Figure 3-3C. The tabulation of results can be found in Table 3-2. The results show that both surface-bound proteins converge on similar α-helical (~0.06) and β-sheet (~0.35) content.

3.4.4. Desorption Behavior

The pellets obtained from the protein-particle mixtures were resuspended in fresh buffer to induce desorption. Previously, eluents such as morpholine [28] or dodeclytrimethylammonium bromide [51] were used to desorb bound proteins. In this study, we relied on the protein concentration gradient between the surface and bulk as the driving force for desorption. Introducing fresh buffer creates a transient difference in chemical potential ($\Delta\mu_s$) at the interface, which is then eliminated by spontaneous desorption. Following resuspension and incubation of the particles, the supernatant protein concentration was measured, which represents the desorbed amount. This sequence of resuspension and supernatant collection was repeated for 10 cycles for each protein (Figure 3-4A and B). Data with varying protein/particle ratios were collected to assess the effect of coverage on desorption. The most striking difference in behavior between the two proteins is that the desorbed amount is affected by surface coverage much more significantly for hAR (Figure 3-4B) than the AdhD (Figure 3-4A). For AdhD, there is only a slight decrease in desorbed amount as coverage decreases, while for hAR, desorbed amount varies by over an order of magnitude for the lowest coverage shown, 0.08 mg m^{-2}, than for coverages above 0.52 mg m^{-2}. This indicates the propensity to desorb is decreased when fewer proteins coat the surface. A more subtle difference between the two desorption curves is that while desorbed amount levels off after the third cycle for hAR, this decreases continuously from cycle-to-cycle for AdhD. This indicates that the arrangement of particles for hAR reaches a steady state value earlier in the experiment, while for AdhD a possible redistribution on the surface manifests as a variability of the desorbed amount from cycle-to-cycle. Also, because elutability is expected to increase with molecular weight [104], the higher concentration values of hAR in the supernatant after cycle 5

are consistent with this hypothesis (MW_{hAR}=37.2 kDa, MW_{AdhD}=31.9 kDa).

To assess adsorption/desorption reversibility, surface coverage following each rinse cycle is calculated and desorption isotherms are created, as shown in Figure 3-4C (AdhD) and 4D (hAR). In these figures, the lines represent the Langmuir fits of the adsorbed data (solid line) and desorbed data (dashed line). For AdhD, all six desorbed data sets are used for the Langmuir fit, as each group follows similar trends. This desorption curve in Figure 3-4 varies distinctly from the adsorption isotherm. For reversible adsorption, the ascending and descending branches of the isotherm must overlap at all values of c_{eq}. Therefore, our results indicate irreversible adsorption at time scales assessed here (30 min desorption), and also coverage-dependent desorption (namely a path-dependent hysteresis of desorption). Conversely, for hAR, two desorbed populations are found: at higher coverages (corresponding to transition and plateau values), a single Langmuirian desorption curve can be fit to all the data sets. As before, this desorption curve in Figure 3-4D deviates significantly from the adsorption isotherm, indicating non-reversible adsorption. At low coverages (below 0.53 mg m^{-2}), two data sets reside in a different desorption regime as seen from their position relative to the Langmuir desorption curve. Interestingly, these data sets align closely with the Langmuir adsorption curve.

3.4.5. Desorbed Protein Characterization

To characterize secondary structure of the desorbed protein, far-UV CD spectra were taken from the third resuspension cycle. Native and desorbed protein spectra are shown in Figure 3-5. Three different coverages (corresponding to the plateau, transition and rising portions of the adsorption curve) are shown for the desorbed protein. The results are consistent with the previously

described desorption curves: for AdhD (Figure 3-5A), little variation exists for desorbed protein structure with coverage, while for hAR (Figure 3-5B), the structure at lower coverages is severely perturbed compared to the higher coverages. The results also show that all desorbed samples are slightly less structured than native for AdhD, while there is practically no difference between the high coverage desorbed spectra and native hAR.

Activity assays were also performed on the same desorbed protein populations. The 2,3-butanediol oxidation activity of AdhD using NAD^+ cofactor and the DL-glyceraldehyde reduction activity of hAR using NADPH as cofactor were measured. The results of the kinetic assays are shown as percent of native activity in Figure 3-6 The specific activities are also reported in Table 3-3. These activity results correlate well with the secondary structure characterization. For AdhD, all desorbed protein, independent of surface coverage, lose ~35% native activity. In contrast, for hAR, the four high coverage samples which were grouped together earlier based on lack of secondary structural modification upon desorption, have no apparent activity loss upon desorption. However, the lower coverage samples, which were found to be severely perturbed by CD, show ~ 80% activity loss.

3.5. DISCUSSION

It has long been recognized that a protein's structural stability influences its interfacial behavior, as the presence of a surface can disrupt intermolecular forces and render the protein susceptible to adsorption-induced conformational changes. In previous studies, this role of thermostability has been studied using engineered stability variants. Although using point mutations allows very specific changes to artificially stabilize (or destabilize) the protein without significantly changing

its tertiary structure, we believe applying these systems in adsorption studies have inherent limitations. Only a limited range of thermostabilities can be studied and the approach used to alter stability often changes protein topology. Along these lines, artificially stabilized mutants may have other attributes that would not be favored in naturally evolved systems. To overcome these limitations, we assess the role of thermostability using naturally-evolved homologs. Additionally, we significantly expand the range of surface coverages previously explored.

As shown in Figure 3-1, the use of AdhD and hAR is a fitting model system for the study of the effect of naturally-occurring stability. These two proteins have similar tertiary structures but vastly different thermostabilities: hAR loses approximately half of its helical content at 57ºC, while AdhD is practically unaffected even at 95ºC. Regarding structural similarity of the proteins, it must be noted that Table 3-1 shows some discrepancies between secondary structure fractions determined theoretically from sequence prediction algorithms and direct CD measurement followed by spectral deconvolution. Although the two approaches result in similar trends in distribution of secondary structure, the CD-derived results are lower than the theoretical values. This is likely due to the inherent limitations of deconvolution algorithms used to quantify secondary structure [91]. Although such issues have been documented, CD remains a powerful tool for evaluating comparative structural changes [119, 120] and was used here to examine changes in protein structure upon adsorption/desorption.

The difference in thermal stabilities of the two reductases could be due to many factors. One possible explanation is that since AdhD has a more compact structure, there is more potential for close-range interactions that will stabilize its conformation. Another contributing factor could be

the fraction of amino acids assigned to different secondary structure motifs. For example, AdhD and hAR have 118 and 112 amino acids involved in alpha-helices, respectively. However, because AdhD has an overall lower residue count than hAR this corresponds to 42% amino acids assigned to helices (vs. 34% for hAR). This means that a larger fraction of AdhD is made of a motif that contains a high number of hydrogen-bonds per amino acid, which could translate into increased intrinsic thermal stability of AdhD.

In this study, we chose hydrophilic, unmodified silicon dioxide nanoparticles as the surface for several reasons. On hydrophilic surfaces, in the absence of strong electrostatic forces, protein stability is a key parameters that determines surface activity, as structural rearrangement is the main entropic driving force favoring adsorption [28, 121]. Colloidal silica also has favorable size, refractive index and light scattering properties, which render the particles CD-compatible, allowing *in-situ* structural analysis during adsorption. A final benefit of using colloidal system is our ability to target a wide range of surface coverages. This is a key parameter for our system of interest: proteins in delivery devices, where therapeutic concentration can vary by orders of magnitude. Thus, relevant coverages extend to the plateau region of the adsorption isotherm [122]. To minimize and normalize the effect of electrostatics, experiments were performed at a pH slightly greater than the isoelectric point of each protein, (AdhD IeP = 5.5, hAR IeP = 6.9; system pH = 5.7 for AdhD and 7.2 for hAR) thus imparting a slight negative charge on both proteins. The sodium cacodylate buffer (pK_a 6.3) was selected as its effective buffering range was compatible with the desired conditions. Zeta-potential experiments shown in Figure 3-11 confirm this slight negative charge on each protein, and the data demonstrate that there is no significant charge difference between proteins ($\zeta_{AdhD}^{pH5.7}$ = -4.8±1.7 mV; $\zeta_{hAR}^{pH7.2}$ = -3.2±0.6 mV).

The same silica particles, with a point of zero charge between 2.0 and 3.0, were used in both systems. Therefore, the particles are negatively charged at both pHs and are in both cases more negatively charged than the proteins. However, as Figure 3-11 demonstrates, there is a different in zeta potentials for the two suspensions: ($\zeta_{SiO_2}^{pH\,5.7}$ = -12.0±5.0 mV; $\zeta_{SiO_2}^{pH\,7.2}$ = -26.6±3.4 mV). The difference between the protein solution and the respective silica suspension is greater in the case of hAR (23.4 mV difference) than for AdhD (7.2 mV difference). The potential implications of this charge difference will be discussed in detail further below.

Our results shed new light on the relative role of structural stability in the different kinetic processes depicted in Figure 3-7. During surface attachment (Step I, Figure 3-7), the Langmuir curves in Figure 3-2 compare the surface affinity and adsorbed amounts of hAR and AdhD. Although we anticipated hAR to have a significantly greater affinity for the surface due to its lower thermostability, we find its K value is comparable to that of AdhD. Similarly, the differences in maximum surface coverage can most likely be attributed to the size difference between the proteins. Another reason for the difference in Langmuirian parameters between the two systems may be attributed to the variation in the aforementioned electrostatic potentials. Therefore, these results indicate structural stability does not play a significant role in protein-surface attachment. Figure 3-3 shows hAR and AdhD exhibit similar structural transitions on the surface (Step II, Figure 3-7). While both proteins undergo significant structural perturbation, the extent of α-helical loss and concomitant β-sheet formation is nearly identical. Although such disruption of intermolecular forces upon adsorption was expected for hAR, it is remarkable that the extremely thermostable AdhD undergoes such drastic conformational changes on a hydrophilic surface. Another interesting finding is the lack of correlation between surface

coverage and structural denaturation for either protein (Figure 3-3C). Coverage-dependence of adsorption-induced unfolding has been reported previously [28, 41].

The results of this study reveal differences between hAR and AdhD during detachment and refolding (Steps III and IV, Figure 3-7). The desorption isotherms (Figure 3-4C and D), and structural (Figure 3-5) and kinetic (Figure 3-6) characterization of the desorbed states indicate that while adsorption is irreversible in both cases, desorption follows different pathways for hAR and AdhD. For AdhD, some of the structural loss incurred upon adsorption is regained upon detachment, however native-like refolding is not complete and ~35% enzymatic activity is lost. These findings re-emphasize the surprising effect adsorption-induced instabilities have on a thermally stable protein. AdhD also exhibits hysteresis in its refolding pathways as shown in Figure 3-4C. The pathways appear to be a function of surface coverage (possibly due to microscopic difference in surface arrangement). Although such examples of hysteresis are not commonly reported, Norde found similar behavior for albumin [70]. To schematically capture this incomplete refolding and pathway-dependent hysteresis behavior of AdhD, we believe that the single diagonal arrow in Figure 3-7 (Step V) can be replaced by multiple arrows representing different pathways. In contrast to AdhD, we find two distinct desorbed populations for hAR: at high coverages, the desorption isotherms follow a single pathway to native-like structural refolding and the desorbed protein has no activity loss. These results are unexpected due to the low thermal stability of hAR. At low coverages, desorbed hAR maintains high levels of structural loss and ~80% activity loss, which more closely represents our hypothesis. Unlike AdhD, no hysteresis is found. This coverage-dependent desorption behavior can be represented in Figure 3-7 by a combination of arrows both at Step III (desorption to a perturbed state, the low

coverage case) and at Step V (desorption to a native-like state, the high coverage case).

Two driving forces are likely to govern the adsorption and structural unfolding of the proteins on the silica surface. One driving force is enthalpic-based, due to charge differences between the protein and silica. Although we have set the pH of the system to minimize overall point charge of the proteins, the surface charge profile of the two proteins vary, and localized charged patches can attribute to attractive/repulsive forces with the substrate. 3-D molecular models are shown in Figure 3-12 to illustrate the distribution of surface charge on both hAR and AdhD. Based on these diagrams, qualitative assessment of the differences between the two proteins can be made. While both proteins have a few localized patches (both positive and negative) this charge distribution is generally homogeneous across the surface of the protein for hAR. By contrast, AdhD has more localized patches of both charges, with very few neutral areas. Specifically, positive patches seem to be more prevalent and larger for AdhD. The implication of these differences in surface charge distribution is discussed below. The other, entropic-based, driving force can be due to unfolding of secondary structure which increases conformational entropy of the protein molecule. This has been cited in previous studies [25]. Both proteins demonstrate a helix-to-sheet transition, which indicates that once the protein comes into proximity of an interface, less favorable intermolecular interactions, which constrain the molecular dynamics of the protein, are lost in favor of a more relaxed conformation and more possible surface-interactions.

One possible explanation for the adsorption-induced denaturation of the thermophilic AdhD is the presence of the aforementioned positive patches on the surface of the protein, as seen in Figure 3-12. Because the surface is negatively charged, strong Coulombic attraction would lead

to high levels of surface affinity, with possibly concomitant structural unfolding as favorable attractive forces lead to new protein—surface bond formation.

Unlike previous results that indicate only two states exist: a native-like desorbed and a highly perturbed adsorbed state [122], we see evidence of a non-native like desorbed state. There is also indirect evidence that differentially unfolded states exist on the surface. This hypothesis is supported as follows: first, hAR desorbs in a coverage-dependent manner. This may be a consequence of two (or more) adsorbed protein populations: at low coverages, proteins arriving early have longer residence times, allowing the occupation of more optimal attachment sites, formation of stronger surface bonds, and lateral inter-molecular interactions. The detachment of clusters would require greater free energy consumption, resulting in decreased desorbability [123]. Conversely, at high coverages, a greater packing density may inhibit optimal protein-surface interactions [55]. Second, previous results show differences in elutability, bound fraction and interfacial area in adsorbed proteins, indicating that the existence of a single adsorbed population is unlikely [107, 124]. Finally, evidence for molten globule-like adsorbed states is postulated by studies involving carbonic anhydrase [31], lysozyme [26], and human growth hormone [125].

Our results indicate that overall adsorption behavior of these homologous proteins on silica does not correlate strongly with thermostability. These results are surprising, as the structural stability of mutants has been previously hypothesized to strongly influence their surface affinity, degree of structural perturbation and desorbability. The main difference in our study is that we assess a greater difference in thermostability, by using proteins with naturally evolved structures that have been optimized for their environment. As such, these homologs have similar topology and

tertiary structure, but vastly different primary sequences. In contrast, stability mutants have similar primary and tertiary structure, but often different topologies. Both approaches introduce parameters into the system whose effect on adsorption behavior is unknown: for stability mutants, we hypothesize that altered topology may inhibit optimal protein/surface interaction, thus artificially reducing (or promoting) extent of surface-induced perturbation. However, with naturally-occurring homologs, we cannot be certain that observed adsorption behavior is not due to differences in specific amino acid and surface interactions (due to the differences in primary structure). We argue that although both systems have some limitations, the use of physiologically-relevant systems which allows a wider range of thermostabilities to be studied provides valuable insight which may have been previously overlooked.

We also find interesting differences in the desorption behavior of hAR and AdhD. One explanation is that desorption is sensitive to structural stability because the same intermolecular forces which drive protein folding in solution will determine whether desorption is energetically more favorable. However, we cannot be sure that the observed differences are not protein-dependent. In their natural environments, we know that these proteins are cystolic and may fold with the help of chaperones. Furthermore, thermal stress causes irreversibly unfolding in hAR while having no effect on AdhD. Therefore other intrinsic parameters, such as primary sequence may be the dominant factor in determining desorption behavior.

For more insight into the role of surface adsorption as a catalyst for protein destabilization, we compare the denaturing effects of the surface to other well–known stresses. Figure 3-13 shows the far-UV CD spectra of hAR following thermal, chemical and surface-induced stress. Thermal effects results in almost complete loss in secondary structure, while both surface- and

chemically-induced stress cause only partial structural loss. Such differences are likely due to the probability of breaking the hydrogen bonds which maintain secondary structure in the presence of various disrupting forces [126]. Interestingly, thermal vs. surface-induced stress have a markedly different effect on AdhD: while extreme temperature excursions cause essentially no structural alteration, the surface is capable of irreversibly perturbing its structure.

3.6. CONCLUSIONS

To the best of our knowledge, this study marks the first time that naturally occurring stability variants have been evaluated for interfacial behavior, by studying their differences and interdependencies along each step of the adsorption lifecycle. Our results show that there is little correlation between a protein's thermostability, surface affinity and susceptibility to surface-induced unfolding. Additionally, we show interesting desorption behavior between the proteins and the importance of surface coverage in determining refolding pathway. Our results reveal that role of thermostability in interfacial behavior may be less dominant than previously thought while protein surface properties may be a more important determinant of this behavior. These conclusions shed some doubt on the notion that improving thermostability is the main way to reduce the effects of adsorption-induced changes of proteins.

3.7. TABLES AND FIGURES

	AdhD			hAR		
	Sequence Prediction†	Homology Model‡	CD‖	Sequence Prediction†	Crystal Structure§	CD‖
Helix	0.41 (115)*	0.43 (118)	0.18	0.35 (112)	0.36 (119)	0.21
Sheet	0.14 (39)	0.14 (39)	0.28	0.13 (48)	0.12 (40)	0.27
Disordered	0.45 (125)	0.42 (115)	0.54	0.52 (154)	0.52 (169)	0.52

Table 3-1 Secondary structure domain allocation

* Where applicable, the number of amino acids assigned to each domain is indicated in parentheses

† Predictions based on 6 different algorithms averaged together (JPred, Porter, PsiPred, Prof, SCRATCH, 3DJigsaw)

‡ Homology model obtained as previously described [114]

§ Crystal structure obtained from PDB file 2ACQ

‖ Deconvolutions of CD Spectra performed using CDPro Software

A

```
AdhD    MAKRVNAFNDLKRIGDDKVTAIGMGTWGIGGRETPDYSRD 40
hAR     MRGSHHHHHHAMASRLLLNNGAKMPILGLGTWKSPPG--- 37
        *    : .:.          ..  *   *:*  ::*

AdhD     KESIEAIRYGLELGMNLIDTAEFYGAGHAEEIVGEAIKEF 80
hAR      -QVTEAVKVAIDVGYRHIDCAHVYQN---ENEVGVAIQEK 73
          :  **:: .:::* . ** *..*     *: ** **:*

AdhD    E------REDIFIVSKVWPTHFGYEEAKKAARASAKRLG- 113
hAR     LREQVVKREELFIVSKLWCTYHEKGLVKGACQKTLSDLKL 113
              **::*****:* *:.    .* *.: : . *

AdhD    TYIDLYLLHWP------------------VDDFKKIEETL 135
hAR     DYLDLYLIHWPTGFKPGKEFFPLDESGNVVPSDTNILDTW 153
         *:****:***                  * .  .:* :*

AdhD     HALEDLVDEGVIRYIGVSNFN-LELLQRSQEVMRKYEIVA 174
hAR      AAMEELVDEGLVKAIGISNFNHLQVEMILNKPGLKYKPAV 193
          *:*:*****::: **:**** *::    ::   **: ..

AdhD    NQVKYSVKDRWPETTGLLDYMKREGIALMAYTPLEKG--- 211
hAR     NQIECHP---YLTQEKLIQYCQSKGIVVTAYSPLGSPDRP 230
        **::      :     *::* : :**.: **:** .

AdhD    -------TLARNECLAKIGEKYGKTAAQVALNYLIWEENV 244
hAR     WAKPEDPSLLEDPRIKAIAAKHNKTTAQVLIRFPMQRN-L 269
              :* .:  :  *. *:.**:*** :.: : .: :

AdhD    VAIPKASNKEHLKENFGAMGWRLSEEDREMARRCV----- 279
hAR     VVIPKSVTPERIAENFKVFDFELSSQDMTTLLSYNRNWRV 309
        *.***: . *:: *** .:.:.**.:*

AdhD     ------------------ 279
hAR      CALLSCTSHKDYPFHEEF 327
```

B

C

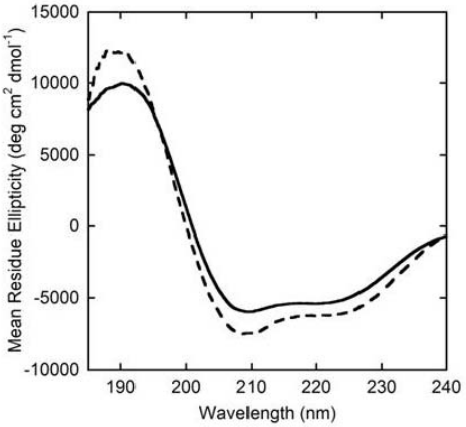

Figure 3-1 Comparison of primary and secondary structures of AdhD and hAR

(A) Amino acid sequence alignment of AdhD and hAR showing < 30% sequence homology between the selected proteins; (B) 3-D homology model of AdhD (left) and crystal structure of hAR (PDB:2ACQ) (right) showing similarities in secondary and tertiary structure; (C) Far-UV CD spectra of native AdhD (——) and native hAR (– – –) quantitatively demonstrating the

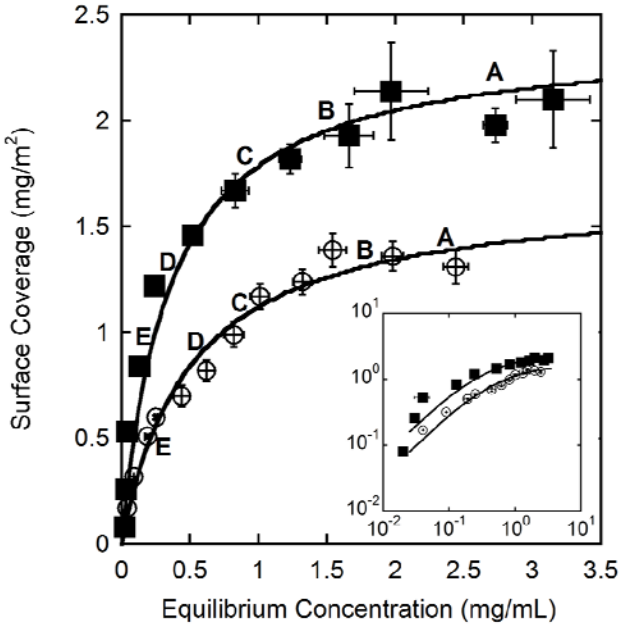

similarities in secondary structure between the two.

Figure 3-2 Adsorption isotherms of AdhD and hAR

Isotherms for AdhD, ○ (K=0.50 mg mL^{-1}, Γ_{max} = 1.68 mg m^{-2}) and hAR, ■ (K=0.35 mg mL^{-1}, Γ_{max} = 2.40 mg m^{-2}) with least-squared fits to a Langmuir isotherm. Inset contains adsorption isotherms on logarithmic axes. Labels A-E indicate points selected for subsequent data sets. Error bars represent the standard deviation of three independent replicates.

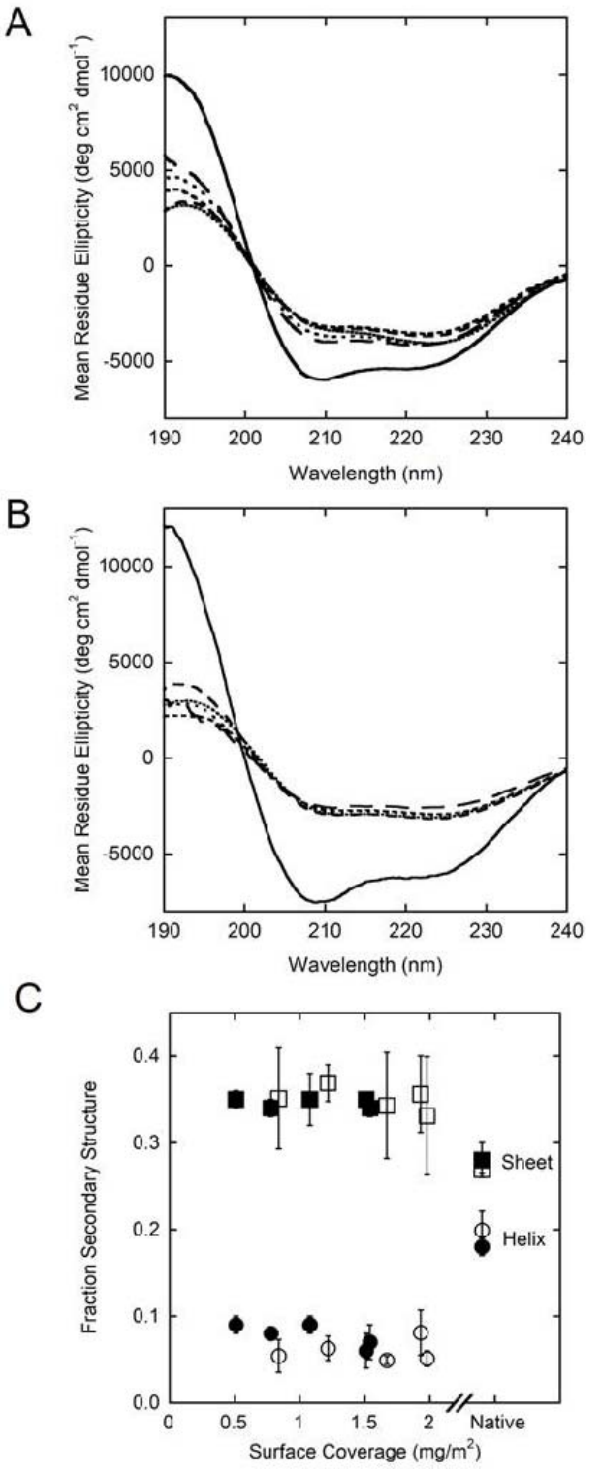

Figure 3-3 Adsorbed CD spectra of AdhD and hAR as compared to native

AdhD (A) and haR (B) spectra as compared to the native spectra (——), of each protein.

Starting with the highest surface coverage, the line types indicate (Surface coverage and C_{eq} follow each line type): ..... (AdhD: 1.54 mg m^{-2}, 2.44 mg mL^{-1}; hAR: 1.98 mg m^{-2}, 2.73 mg mL^{-1}), ••••••••• (AdhD: 1.51 mg m^{-2}, 1.62 mg mL^{-1}; hAR: 1.93 mg m^{-2}, 1.66 mg mL^{-1}), ▬ ▬ ▬ ▬ (AdhD: 1.08 mg m^{-2}, 0.85 mg mL^{-1}; hAR: 1.67 mg m^{-2}, 0.83 mg mL^{-1}), ▬▬ ▬▬ ▬▬ (AdhD: 0.78 mg m^{-2}, 0.50 mg mL^{-1}; hAR: 1.22 mg m^{-2}, 0.24 mg mL^{-1}), and ▬▬▬ ▬▬▬ (AdhD: 0.51 mg m^{-2}, 0.24 mg mL^{-1}; hAR: 0.84 mg m^{-2}, 0.13 mg mL^{-1}); (C) Fraction of secondary structure that exists as α-helical (circle) and β-sheet (square) domains for AdhD (● and ■) and hAR (○ and □) for native protein and adsorbed protein.

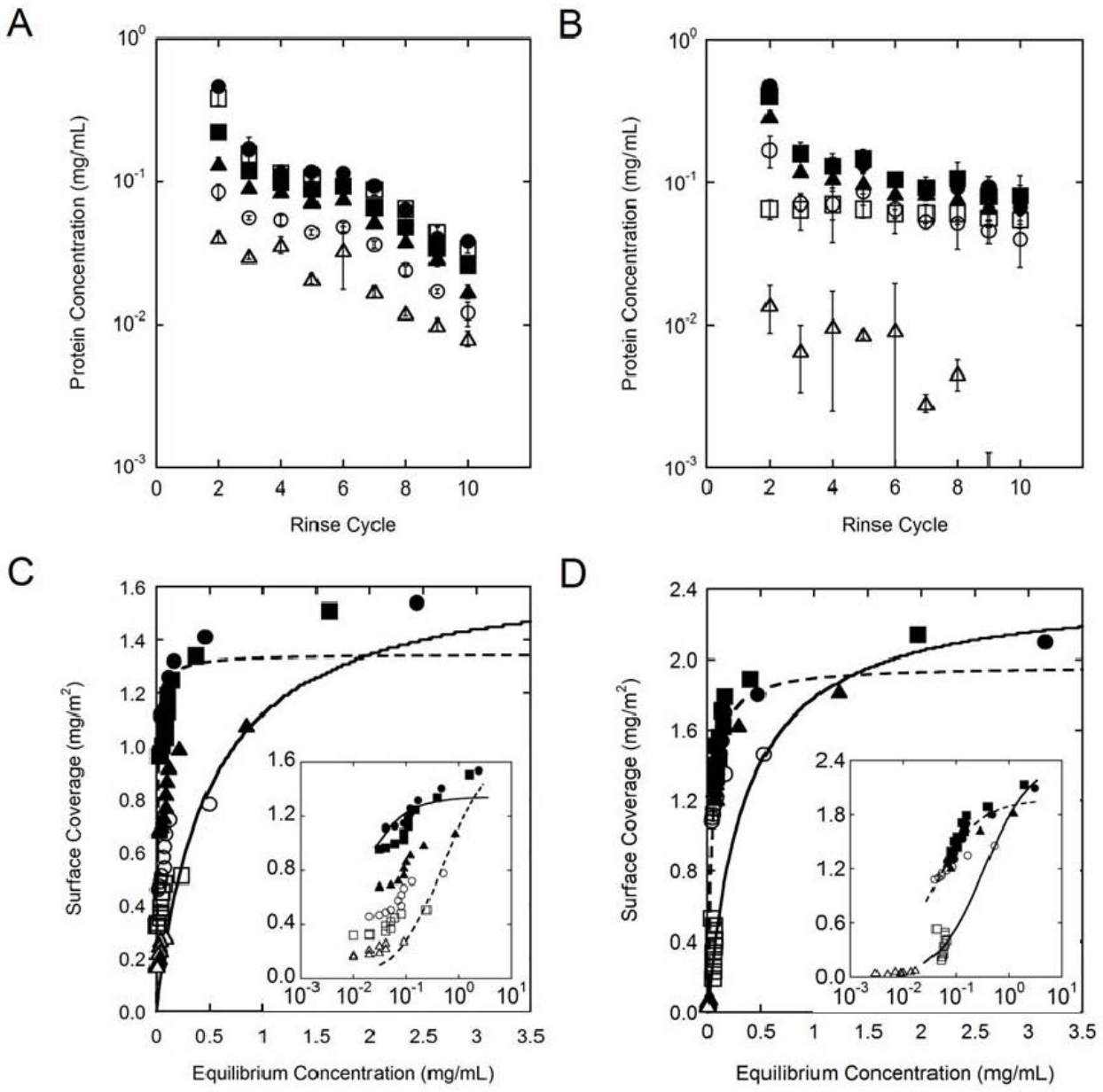

Figure 3-4 Desorbed protein concentration as a function of rinse cycle for AdhD and hAR

Data shown for AdhD (A) and hAR (B) for rinse cycles 2-10. Protein/particle ratios corresponding to five different regions along the adsorption isotherm (as labeled A-E in Figure 3-2) were used (surface coverage and C_{eq} follow each sample). AdhD: ● Sample A: 1.4 mg m^{-2}, 1.9 mg mL^{-1}; ■ Sample B: 1.2 mg m^{-2}, 1.3 mg mL^{-1}; ▲ Sample C: 0.82 mg m^{-2}, 0.62 mg mL^{-1}; □ Sample D: 0.60 mg m^{-2}, 0.25 mg mL^{-1}; ○ Sample E: 0.32 mg m^{-2}, 0.09 mg mL^{-1}; hAR: ● Sample A: 2.1 mg m^{-2}, 3.2 mg mL^{-1}; ■ Sample B: 2.1 mg m^{-2}, 2.0 mg mL^{-1}; ▲ Sample C: 1.8 mg m^{-2},

1.23 mg mL^{-1}; □ Sample D: 1.46 mg m^{-2}, 0.52 mg mL^{-1}; ○ Sample E: 0.53 mg m^{-2}, 0.04 mg mL^{-1}. Each point is the average of three distinct replicates and error bars represent their standard deviation. Not shown on the graphs is the limit of detection of each assay, as all concentration values shown are above this limit. Desorption isotherms are shown in (C) AdhD and (D) hAR. Data for all 10 cycles are depicted, and symbols are consistent with those used in A and B. The solid line represents the Langmuir fit for the adsorption isotherm data and the dashed line represents a Langmuir fit for the desorption data. Insets show the same data sets on a logarithmic x-axis.

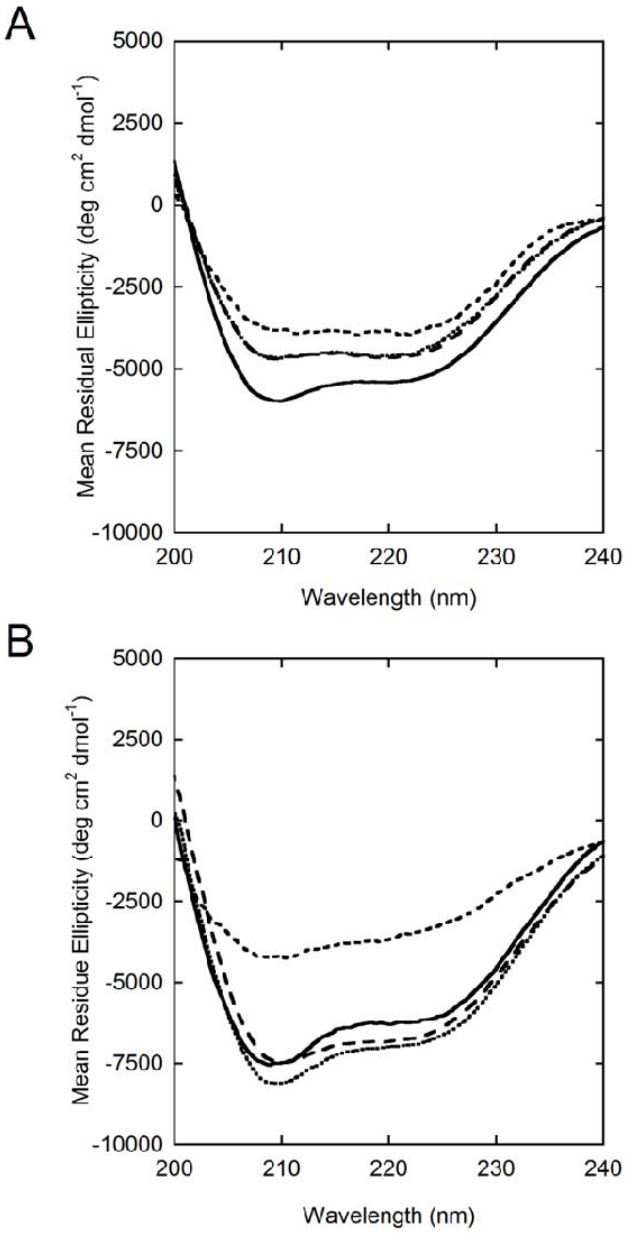

Figure 3-5 Desorbed protein structure

CD spectra of native protein (solid line) vs. desorbed protein (obtained from cycle 3 of the desorption experiments captured at a surface coverages along the plateau value ..... , transition region — — and rising portion of the adsorption isotherm – – –) for (A) AdhD and (B)) hAR

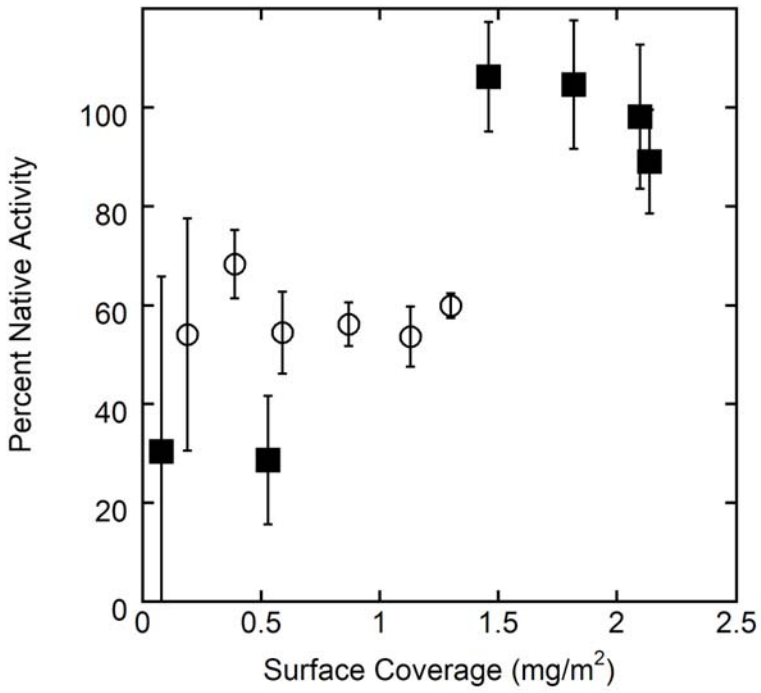

Figure 3-6 Kinetic activity of desorbed protein

Kinetic data showing percent native activity for desorbed AdhD (○) and hAR (■) at various levels of surface coverage. Desorbed protein has been taken from the third rinse cycle of the desorption experiments. Error bars represent standard deviations of three independent samples. Coverages targeted are the same 5 data sets as have been used in Figure 3-5, for direct comparison.

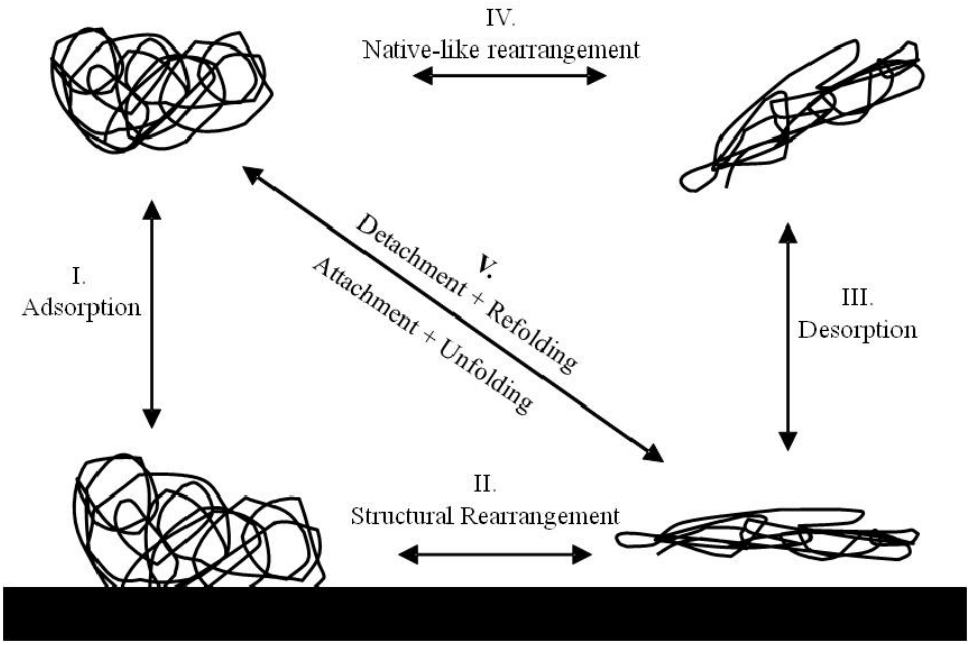

Figure 3-7 Classical 4-state kinetic model

Classical 4-state kinetic model, representing the native state in bulk before adsorption, the adsorbed state before unfolding, followed by structural rearrangement while on the surface, desorption into bulk, and refolding into native-like state.

3.8. SUPPLEMENTARY INFORMATION

3.8.1. Further Experimental Detail

Cloning. The following primers were used for the hAR: The forward primer OE1F 5'-AGCAGCCATGGCAAGCCGTCTCC-3' was used with the reverse primer OE1R 5'-GGACACGTGGGCGGCAATGGAAGAGCTGGTGG-3' to generate the first part of the gene, while the forward primer OE2F 5'-CCACCAGCTCTTCCATTGCCGCCCACGTGTCC-3' was used with the reverse primer OE2R 5'-ATCGAAGCTTTCAAAACTCTTCATGGAAGG-3' to generate the second part of the gene. The pieces were denatured, annealed and extended to yield the full-length hAR gene. This strategy introduced an *Nco*I restriction site (underlined in OE1F) and a *Hind*III restriction site (underlined in OE2R).

Protein Concentration. Standards for the BCA assays and protein samples for extinction coefficient measurements were made from purified lyophilized protein. 12 - 30 mL of purified protein were dialyzed against 2 L of 25 mM ammonium bicarbonate at 4^{o}C with buffer replacement every 8-12 hours. The dialyzed protein samples were then lyophilized for 36 hours. Pure lyophilized protein was weighed and resuspended to a known concentration.

3.8.2. Supplementary Tables and Figures

Figure 3-8 Swiss model program output for AdhD and hAR

Swiss model program output for AdhD (top) and hAR (bottom). [127-129]

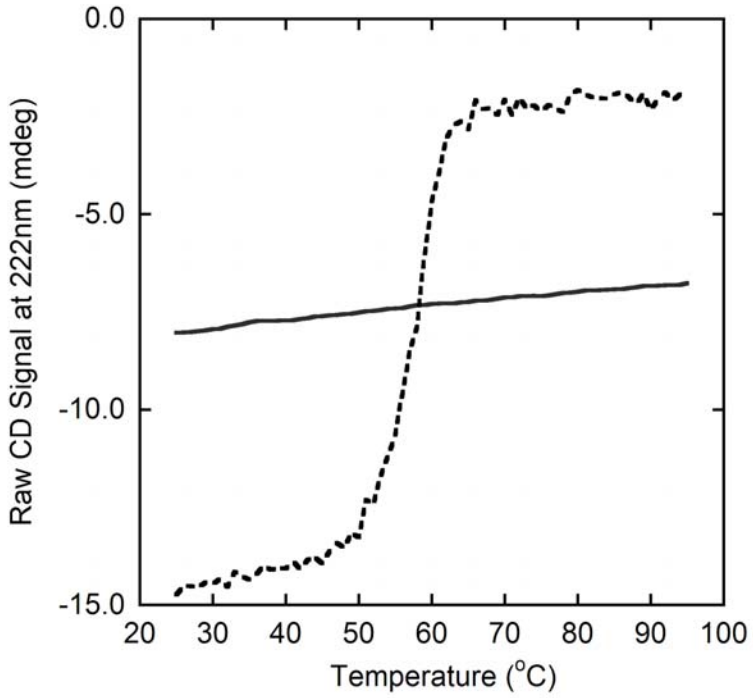

Figure 3-9 Melting curves for hAR and AdhD

Curves for AdhD (solid line) and hAR (dashed line) obtained by following the CD spectra of both proteins at 222nm between 25 and 95°C. Samples were run in 1mm cuvettes. Buffer used is 10mM sodium cacodylate buffer at pH=5 (AdhD) and pH=6.9 (hAR). Only hAR exhibits unfolding behavior under these conditions, and the midpoint temperature of a sigmoidal fit (T_m = 57°C) is assigned as the melting temperature of this protein.

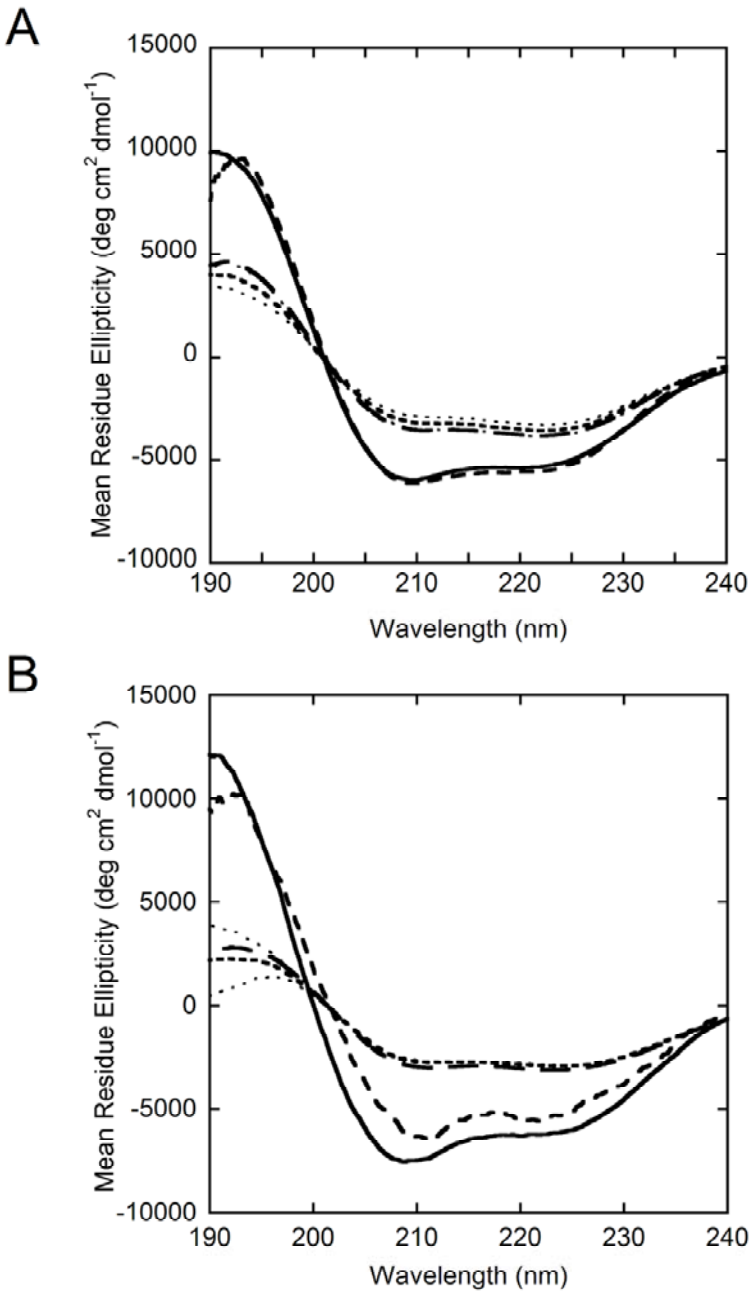

Figure 3-10 CD spectra of various adsorbed states of AdhD and hAR

Spectra used for determining adsorbed protein structure for AdhD (A) and hAR (B). Spectra shown: native (——), resuspended adsorbed protein-particle pellet (— —), supernatant from resuspended pellet (— — —), adsorbed protein (- - - -), error in adsorbed spectrum (·····). Error bands are obtained by adding the standard deviations of three replicates to the average spectrum.

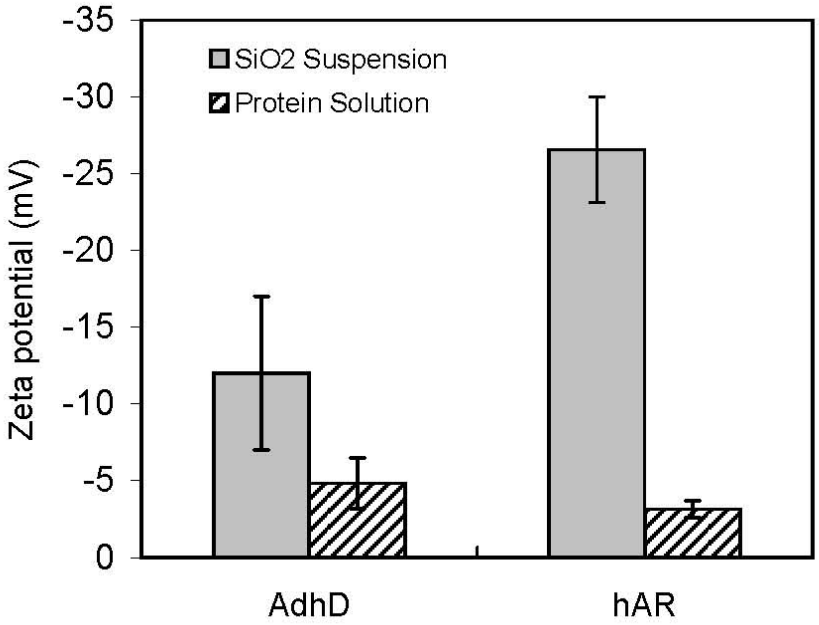

		pH 5.7 Condition for AdhD	pH 7.2 Condition for hAR
6mg/mL SiO_2	Average	-12.0	-26.6
	St Dev	5.0	3.4
Protein Solutions	Average	-4.8	-3.2
	St Dev	1.7	0.6

Figure 3-11 Zeta-potential measurements on proteins and particle suspensions

Conducted on the 6 mg/mL silica suspensions and proteins solutions for AdhD and hAR in pH=5.7 and pH=7.2 buffers, respectively.

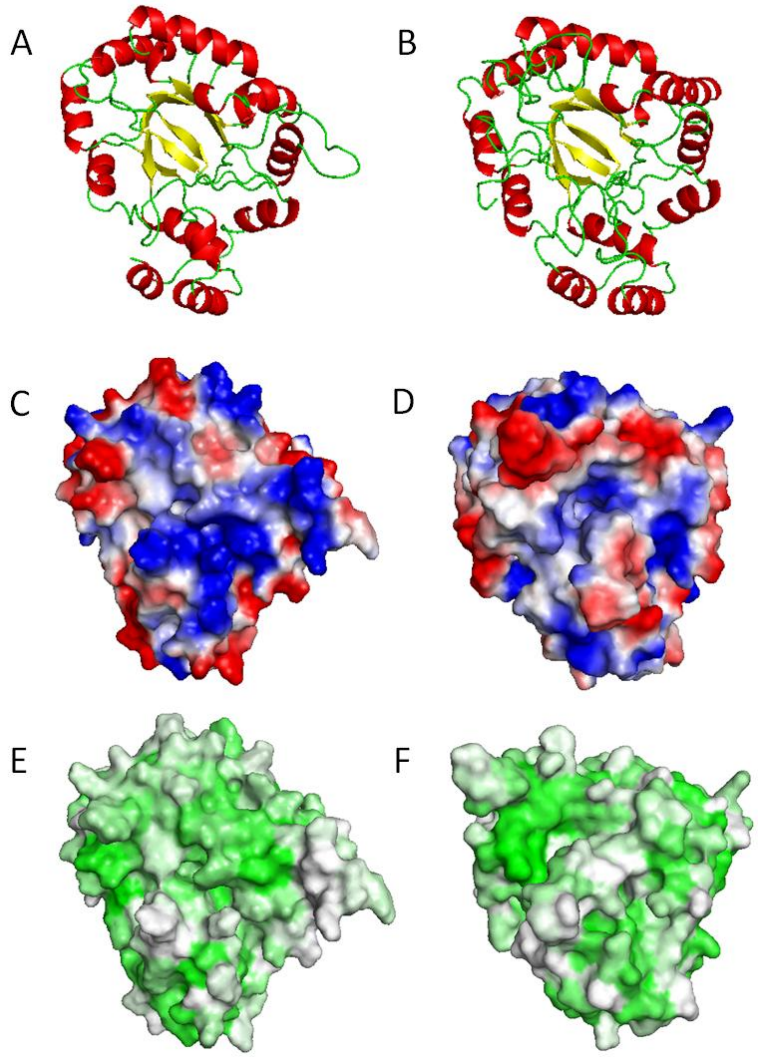

Figure 3-12 3-D molecular cartoons for AdhD and hAR showing surface charge and hydrophobicity distributions

Cartoon diagrams for (A) AdhD and (B) hAR showing the similarities in secondary structure and surface representations of surface charge for (C) AdhD and (D) hAR and surface hydrophobicity for (E) AdhD and (F) hAR.

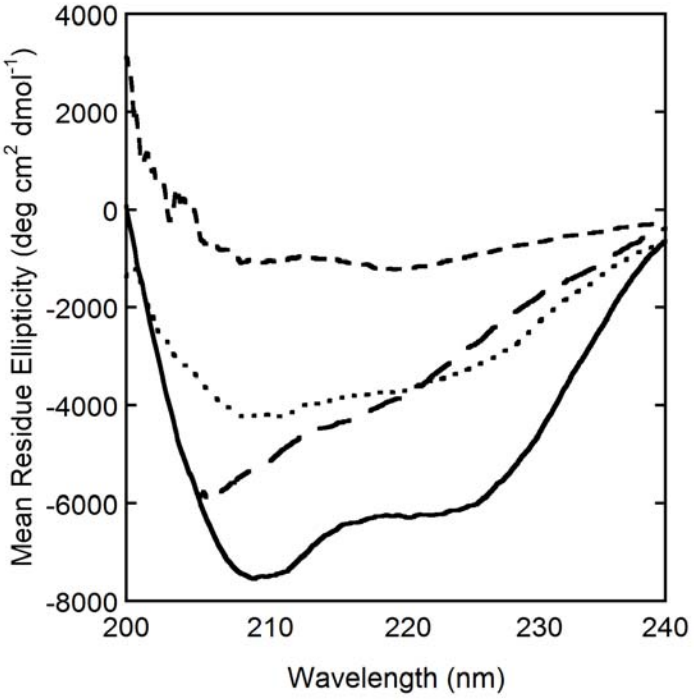

Figure 3-13 Far-UV CD spectra of hAR showing effect of thermal, chemical and surface-induced denaturation

Far-UV CD spectra of hAR in the native state (solid), following chemical denaturation by 6M GdHCl (— —), surface-induced denaturation, i.e. desorbed protein (••••••••) and following thermal denaturation upon heating to 95°C (- - - -).

(A)

Surface Coverage (mg m^{-2})	Helix fraction	Sheet fraction	Random fraction
Native	0.20	0.27	0.51
1.98	0.05	0.33	0.49
1.93	0.08	0.36	0.47
1.67	0.05	0.34	0.50
1.22	0.06	0.37	0.52
0.84	0.05	0.35	0.48

(B)

Surface Coverage (mg m^{-2})	Helix	Sheet	Random
Native	0.18	0.28	0.50
1.54	0.07	0.34	0.53
1.51	0.06	0.35	0.51
1.08	0.09	0.35	0.49
0.78	0.08	0.34	0.52
0.51	0.09	0.35	0.52

Table 3-2 Adsorbed proteins secondary structure following deconvolution of CD spectra
Data for AdhD (A) and hAR (B). This is a numerical representation of the data graphed in Figure 3-4.

	Specific Activity (min^{-1})	
	AdhD	hAR
Published	60	96
Native	63	85
Point A	37 (1.30)	83 (2.10)
Point B	34 (1.13)	75 (2.14)
Point C	35 (0.87)	89 (1.82)
Point D	34 (0.59)	90 (1.46)
Point E	43 (0.39)	24 (0.53)
Point F	34 (0.19)	26 (0.08)

Table 3-3 Specific activity values for AdhD and hAR

Specific activity values of native protein and desorbed protein at various coverages. Surface coverage in mg m^{-2} is given in parentheses for each point. Values from literature for both AdhD [114] and hAR [130]

CHAPTER 4. EFFECT OF ELECTROSTATIC INTERACTIONS ON PROTEIN ADSORPTION TO SILICA USING SUPERCHARGED GFP VARIANTS‡

4.1. INTRODUCTION

Electrostatic interactions play important roles in many colloidal phenomena and have been studied extensively. Specifically, the dominant role of electrostatics in protein adsorption is well established, and it is widely accepted that on hydrophilic surfaces, entropic driving forces govern the interfacial behavior of proteins [51, 98]. However, few studies have been conducted to assess the role of protein surface charge in isolation, without altering other key system parameters.

Past studies have been conducted on mixtures of proteins with varying isoelectric points [98, 131] and substrates with varying surface charge densities [102]. These studies report an increase in adsorbed protein mass as surface/protein charge contrast increased. In mixtures, proteins with more favorable charge interactions readily out-compete adsorbed proteins for surface attachment, displacing the bound molecules. McGuire *et al* created charged variants of T4 lysozyme (charges ranged from +3 to +9) [51]. Surprisingly, no significant difference between the adsorption of the charged mutants was found on hydrophilic surfaces. Only on the hydrophobic surface did the

---

‡ A version of this chapter is being prepared for a future manuscript. Sara Chuang provided help in performing experiments and analyzing data.

variant with the more favorable surface charge interaction show higher levels of adsorption. Furthermore, no real correlation between net charge and elutability was observed on either hydrophilic or hydrophobic surfaces.

Previously, as described in Chapter 2, we determined that the adsorption of lysozyme onto silica occurred in a reversible manner, on a relatively short timescale. We found that although surface-induced structural perturbation of the protein occurs, the desorbed protein is able to refold into its native-like conformation. We hypothesized that our results were system-specific: lysozyme has a complex, globular structure and a highly favorable electrostatic attraction to silica. Therefore, we aimed to evaluate structural stability and electrostatics separately to better understand the roles of each. In another study, described in Chapter 3, we assessed the impact of intrinsic structural stability (keeping most other system parameters constant) on interfacial behavior and found little correlation between a protein's thermostability, surface affinity and susceptibility to surface-induced unfolding. In this study, we now assess the impact of electrostatics (also keeping other system parameters constant) on adsorption/desorption behavior.

A more global motivation for this study is to gain further insight into the impact of electrostatics on adsorption-related events on hydrophilic surfaces. We aim to re-evaluate the conclusions reached by McGuire, by using a system to achieve a wider range of charge differences. While McGuire's mutants ranged in charge by 6 units, and all mutants were positively charged, here we employ "supercharged" green fluorescent protein (GFP) variants. These proteins have been mutated at their surface-exposed residues, resulting in extremely high theoretical net charges ranging from -30 to +48 [132]. These proteins were originally developed as a platform for the

delivery of proteins into mammalian cells [133]. The widely varying protein surface charge, yet very similar size, secondary structure and structural stability render this group of proteins an ideal candidate for our proposed adsorption studies.

4.2. EXPERIMENTAL SECTION

4.2.1. Materials

Plasmids for the supercharged GFP variants (st, +15 and -30) were generously provided by Dr. David Liu (Harvard University). Isopropyl β-D-1-thiogalactopyranoside (IPTG) was obtained from Promega (Madison, WI). Untreated, fumed, colloidal silicon dioxide (Cab-O-Sil, M5, purity >99.8) was obtained from Cabot Corp (Boston, MA). All water was purified using a Millipore water filtering system. Bicinchoninic acid (BCA) and QuantiPro BCA Assay kits were purchased from Thermo Fisher Scientific (Rockford, IL). All other chemicals were obtained from Sigma-Aldrich (St. Louis, MO).

4.2.2. Protein Expression and Purification

The supercharged GFP plasmids were a kind gift from Dr. David Liu (Harvard University). The plasmid sequences are described in a previous publication [133]. The plasmids were transformed into the BLR Escherichia coli cell line (Qiagen). Cells were grown in 1 L batches of Terrific Broth media supplemented with 1000 μg mL-1 ampicillin. Expression was induced with 0.7 mM of Isopropyl b-D-1-thiogalactopyranoside upon reaching an OD600 of 0.6-0.7. Expression was allowed for 18 hr at 25 °C prior to harvesting. Cells were harvested by centrifugation at 10,000g for 10 minutes and resuspended in 100 mL of 20 mM PBS buffer, 2M NaCl, and 40 mM

imidazole (pH 7.5) and supplemented with 1x HALT protease inhibitor cocktail (Thermo-Fisher). The cells were lysed by sonication with a 6 minute run time with pulses of 5 seconds with a 5 second rest between each pulse. The cell debris was pelleted by centrifugation at 15,000xg for 30 minutes. The GFP was purified from the clarified lysate using a HisTrap column (GE Healthcare) on a GE ÄKTA FPLC. The fractions containing GFP, (verified by SDS-PAGE) were pooled and concentrated using Amicon (EMD Millipore) centrifugal filters with a 30 kDa MWCO. Samples were further purified by size exclusion chromatography (SEC; HiLoad 16/20, Superdex 200, GE HealthCare) with 100 mM NaCl, 50 mM potassium phosphate pH 7.5, Protein stocks were stored at 4^{o}C.

4.2.3. Concentration Measurements

Concentration of the GFP variants was measured by absorbance at 488nm assuming an extinction coefficient of 8.33 x 104 $M^{-1}cm^{-1}$. The solution of each protein was adjusted to 10 mg mL^{-1} to start the adsorption experiments. A SpectraMax M2 spectrophotometer (Molecular Devices, Sunnyvale, CA) was used. The stGFP variant was used to make a standard curve and the BCA total protein assay was used for all subsequent concentration measurements. Standards ranged from 1-0.010 mg mL^{-1} (BCA Macro) and 0.05-0.0005 mg mL^{-1} (BCA Micro).

4.2.4. Adsorption Procedure

Colloidal silica was resuspended in 50 mM potassium phosphate, 100mM NaCl, pH 7.5, at 12 mg mL^{-1} and vortexed immediately before use. Equal volumes of silica and protein solutions were mixed to achieve protein concentrations between 0.1 - 5.0 mg mL^{-1}, and a constant silica surface area, 1.2 m^2 mL^{-1}. For equilibrium adsorption measurements, samples were maintained at

25°C and rotated end-on-end for 16 hr using a standard laboratory rotator. Supernatants were collected and surface coverage calculated as described previously [122].

4.2.5. Desorption Procedure

Pellets obtained from the adsorption experiments were resuspended in a volume of fresh buffer corresponding to half the volume of the original protein-particle mixture volume. The pellet was resuspended by pipetting. Pellets and resuspension weights were recorded, and values were converted to volume using ρ=1.02 g/mL to calculate exact adsorbed amounts. Samples were incubated for various times (between 16hr and 14 days). Separate samples were used for each time point. Following the appropriate incubation time, the sample was centrifuged, and the supernatant removed. These supernatant concentrations were measured and reported. Based on these values, as well as amounts adsorbed on the pellets at t=0, surface coverages were calculated.

4.2.6. Far-UV CD and Melting Curve Measurements

A J-815 CD spectrometer (Jasco, Inc, Easton, MD) equipped with a Peltier junction temperature control was used to perform CD measurements. Quartz cuvettes with 0.01, 0.02, 0.05, or 0.1 cm pathlengths were used. Pure protein solutions and protein-particle mixtures were measured, using buffer or silica blanks, respectively, for baselining. Far-UV spectra were collected between 185-240 nm in 0.1nm intervals (190-240 nm for desorption samples) using a 1nm bandwidth, 8 sec response time and 50nm/min scanning speed. Temperature was held at 25°C. Three accumulations were averaged during each run. Raw CD signal was converted to mean residue ellipticity according to: $[\theta]_{MRE} = \frac{\theta}{10\, C_r\, \ell}$, where C_r represents concentration (M*residue number)

and ℓ the cuvette pathlength. Calculation of the adsorbed protein spectra is described elsewhere [122]. Desorbed protein structure was measured from rinsing the pellet following adsorption with two resuspensions of 30 min each and collecting the final supernatant. Melting curves were conducted by tracking the 222nm CD signal between 25 -95°

4.2.7. Charge comparison

To compare the charge difference between the silica and each GFP variant, the point of zero charge of the silica (3.0) was compared to the isoelectric point of GFP-st (6.13), GFP-30 (4.64), and GFP+15 (9.75) and charge difference reported as $IeP_{protein}$-$IeP_{silica.}$ This method yields an absolute value of charge difference.

4.2.8. Modeling of Desorption Data

Kinetic desorption data were fit with the stretched exponential function:

$$c = c_o e^{-(t/\tau)^{-\beta}} \qquad \text{Eq. 4-1}$$

Using a first order Taylor approximation to simplify the exponential term, the equation was transformed into a linear relation between $\ln\left(1 - c/c_\infty\right)$ and $\ln(time)$ whose slope represents β, the parameter used to describe desorption.

4.3. RESULTS AND DISCUSSION

4.3.1. Characterization of the Supercharged GFP Variants

In Table 4-1, we list various properties related to size, charge and conformation of the three

proteins we evaluated in this study. While the size and secondary structure of the GFP variants remain constant, their charges vary drastically, as was the intent in designing these constructs. The size of the proteins following gel filtration was verified by gel electrophoresis, as shown in Figure 5-1. For this study, we have selected wild-type GFP (stGFP) and two other variants which have approximately the same amount of charge difference to wild type in both the positive and negative directions. Thus, the proteins are ordered in Table 4-1 from having the least, GFP(-30), to most, GFP(+15), favorable electrostatic interaction with the silica nanoparticles. Based on isoelectric points, GFP(-30) and stGFP have a repulsive interaction with the surface, while GFP(+15) has a strong attractive interaction. The IeP of these proteins has been verified elsewhere [133].

4.3.2. Adsorption

Due to its unique fluorescence qualities, the distribution of GFP populations between the surface and solution can be easily visualized. Figure 4-2 compares the protein/surface mixtures along the adsorption isotherm for stGFP and GFP(+15). The samples shown are centrifuged following 16 hours of incubation. stGFP, which has lower affinity for the surface, has a substantial amount of protein remaining in the supernatant at all coverages except the lowest one. In contrast, GFP(+15) has a much stronger surface affinity and almost all protein leaves the solution for the surface at the three lowest coverages. The adsorption isotherms of these two GFP variants as well as GFP(-30) are shown in Figure 4-3. As expected, the stronger the electrostatic interaction between protein and silica, the steeper the initial portion of the adsorption becomes. GFP(+15) behaves much like lysozyme, as the initial portion of the isotherm overlays with the y-axis. The only protein which exhibits a plateau level of coverage is GFP(+15). The stGFP data seem to indicate

that a plateau level may be similar to that of GFP(+15), but GFP(-30) shows no sign at all of reaching surface saturation. Without extending the range of protein concentrations studied for these latter two proteins, the Langmuir isotherm fits the stGFP and GFP(-30) data sets poorly. However, to get some sense of comparison between the adsorption behaviors of the three variants, the Langmuirian parameters of the least-squares fit shown in Figure 4-3 are reported in Table 4-2. While these values do not make much sense for GFP(-30), the difference in K value and the similarity if Γ_{max} between stGFP and GFP(+15) reflects that attractive electrostatics has a dramatic effect on the binding affinity of the proteins, but the same amount of protein can eventually adsorb to both surfaces due to similar molecular dimensions. In order to obtain acceptable Langmuir fits, adsorption data points at higher supernatant coverage must be tested for stGFP and GFP(-30).

4.3.3. Desorption

Raw kinetic data of desorption are shown in the left-hand column of Figure 4-4. The first observation is the protein with the least favorable charge interactions with silica shows the least amount of time-dependence, while stGFP and GFP(+15) exhibit increasingly greater levels of time-dependence. This behavior is quantified in Table 4-2: The β value is lowest for GFP(-30) at all coverages, while it is the same order of magnitude between stGFP and GFP(+15). The surface coverage values for desorption are shown in Figure 4-5. The black curve, which represents the Langmuir fit of the adsorption data, has known error associated with it for the GFP(-30) and stGFP data sets, therefore, we only report with its position with confidence in Figure 4-5 for GFP(+15). While the average values for the high coverage data fall on the isotherm, approach the isotherm for medium coverage and overshoot the isotherm at low coverages, the error bars on

each data set are quite high. The main conclusion we can make from these data sets is that none them show significant deviation from equilibrium. However, this conclusion must be reassessed for stGFP and GFP(-30) once the adsorption isotherm has been extended.

4.3.4. Secondary Structure Characterization

Figure 4-6 depicts the CD spectra of the native GFP protein compared to the adsorbed populations at various coverages. As expected, the native spectra of the three GFP variants are very similar, as the charge-altering mutations did not affect secondary structure. Similarly, the adsorbed populations for all three variants are similar: some level of perturbation is present (indicated by the decreased signal amplitude at 208, 218 and 222 nm). However, no discernible difference can be identified between the variants. Further spectral comparison algorithms or deconvolutions need to be run to identify any potential difference. It must also be noted that the adsorbed signal for the GFP(-30) was especially high and only one of the coverage levels could be reported.

Figure 4-7 shows the CD spectra of the desorbed protein populations as compared to native. The data indicate that full native-like refolding is achieved for all three variants. We find this results very interesting, as our original hypothesis was that favorable charge interactions between the protein and surface [58] play an important role in lysozyme's reversible adsorption behavior and in its tendency to regain native-like structure upon desorption.

4.4. OUTLOOKS AND CONCLUSIONS

To the best of our knowledge, this is the first study in which the interfacial behavior of green

fluorescent protein has been evaluated in a comprehensive manner. Due to the widespread use of this protein, such information is useful when designing system where interaction with surfaces and other interfaces is expected. Unlike previously reported results by McGuire, we find that surface binding affinity on hydrophilic surfaces correlates strongly to charge difference between the protein and surface. Furthermore, we observe that the time-dependence of desorption is also impacted by these electrostatic effects: Our results indicate that the more favorable the charge interaction, the stronger the time-dependence of surface detachment.

We do not perform detailed assessments of the correlation between the electrostatic properties of the proteins and their observed adsorption/desorption behavior. Before performing such an analysis, experimental measures of protein/surface charge should be taken, and these values used for subsequent analysis. We present a principal component analysis in Chapter 5, and a similar type of analysis could be done on these data sets.

While we feel that further experiments are needed with our system to obtain a more complete understanding of the role of electrostatics in the different kinetic pathways involved in adsorption, our preliminary data indicate that surface attachment and detachment are strongly influenced by surface charge while level of surface-induced protein unfolding does not correlate strongly to this parameter.

4.5. TABLES AND FIGURES

Variant	MW (kDa)	Length (aa)	n_{pos}	n_{neg}	Q_{net}	IeP	Charge difference with silica	Fraction Helix	Fraction Sheet
GFP(-30)	27.8	248	19	49	-30	4.6	0.1	0.24	0.34
stGFP	27.8	248	27	34	-7	6.1	1.6	0.21	0.37
GFP(+15)	28.2	248	41	26	15	9.8	5.3	0.21	0.36

Table 4-1 Calculated and experimentally determined properties of supercharged GFP

n_{pos}, number of positively charged amino acids

n_{neg}, number of negatively charged amino acids

Q_{net}, theoretical net charge at neutral pH

IeP, isoelectric point (theoretical)

Charge difference with silica defined as $Q_{protein}$-Q_{silica}, where $Q_{protein}$ = $IeP_{protein}$ -7.5 and Q_{silica} = 3.0 – 7.5 = -4.5 (where 7.5 is the pH of the system and 3.0 is the point of zero charge of the silica)

Fraction helix and sheet are calculated from deconvolution of experimental Far-UV CD measurements

Variant	Charge difference (silica)	K	Γ_{max}	β_{high}	β_{med}	β_{low}
GFP(-30)	1.6	9992	1866	5.1E-03	1.2E-02	3.2E-03
stGFP	3.1	1.0	1.5	8.7E-02	1.7E-01	6.5E-01
GFP(+15)	6.8	0.0018	1.5	5.3E-02	2.0E-01	3.3E-01

Table 4-2 Adsorption and desorption parameters of the GFP variants

Langmuirian parameters, K and Γ_{max}, provided, and desorption β values at high, medium and low surface coverages.

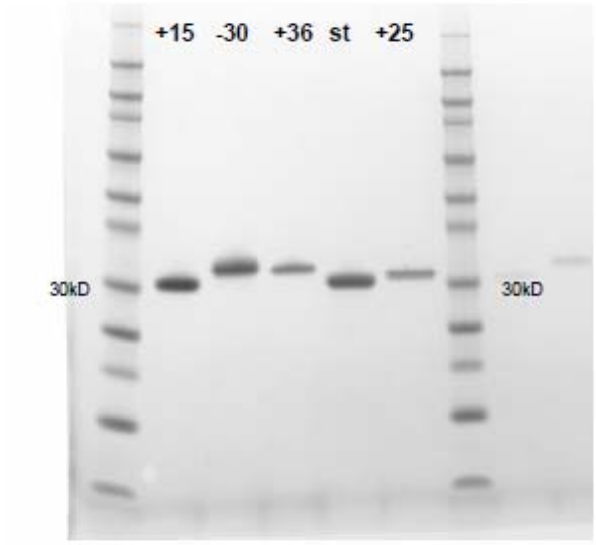

Figure 4-1 Protein gel of supercharged GFP variants
Samples obtained following gel filtration

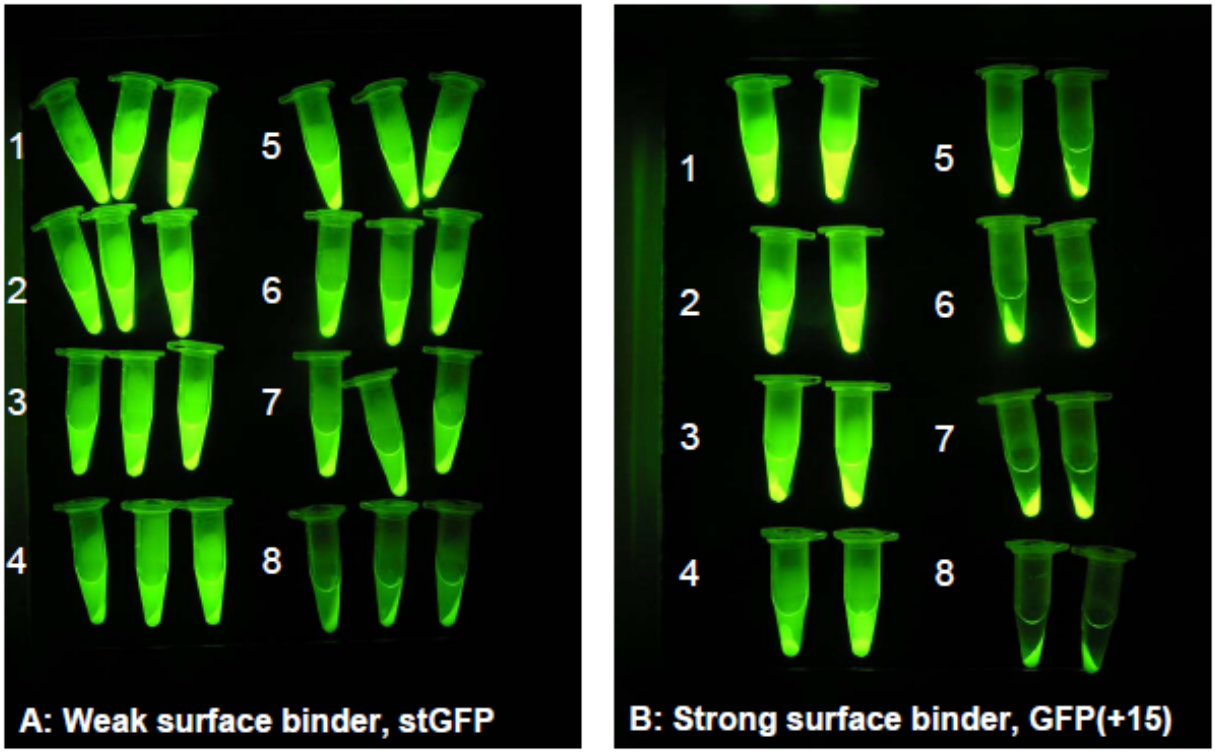

Figure 4-2 Photographs of GFP adsorption samples

Samples pictured after 16 hour incubation and centrifugation. The triplicate (or duplicate) samples represent points from the highest (1) to lowest (8) surface coverages for stGFP (A) and GFP(+15) (B)

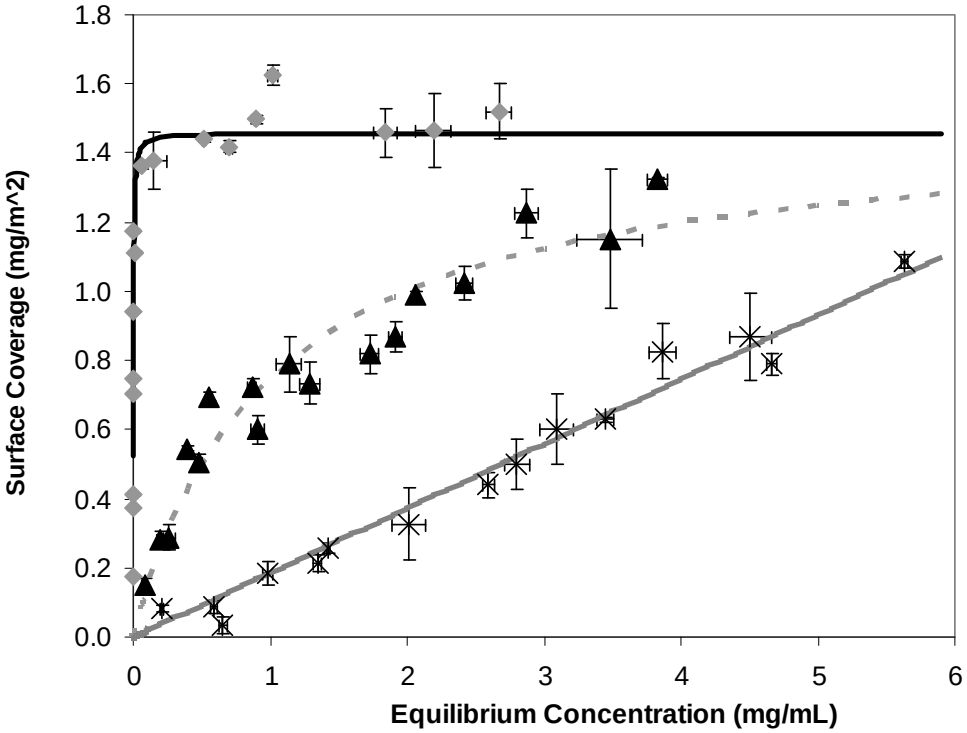

Figure 4-3 Adsorption isotherms and Langmuir fits for supercharged GFPs

Adsorption data for GFP(+15) (♦), stGFP (▲) and GPF(-30) (*). Data presented is the accumulation of two different experiments, error bars represent averages of three replicates. Lines represent Langmuir fits for GFP(+15) (solid black), stGFP (gray, dashed) and GPF(-30) (solid gray).

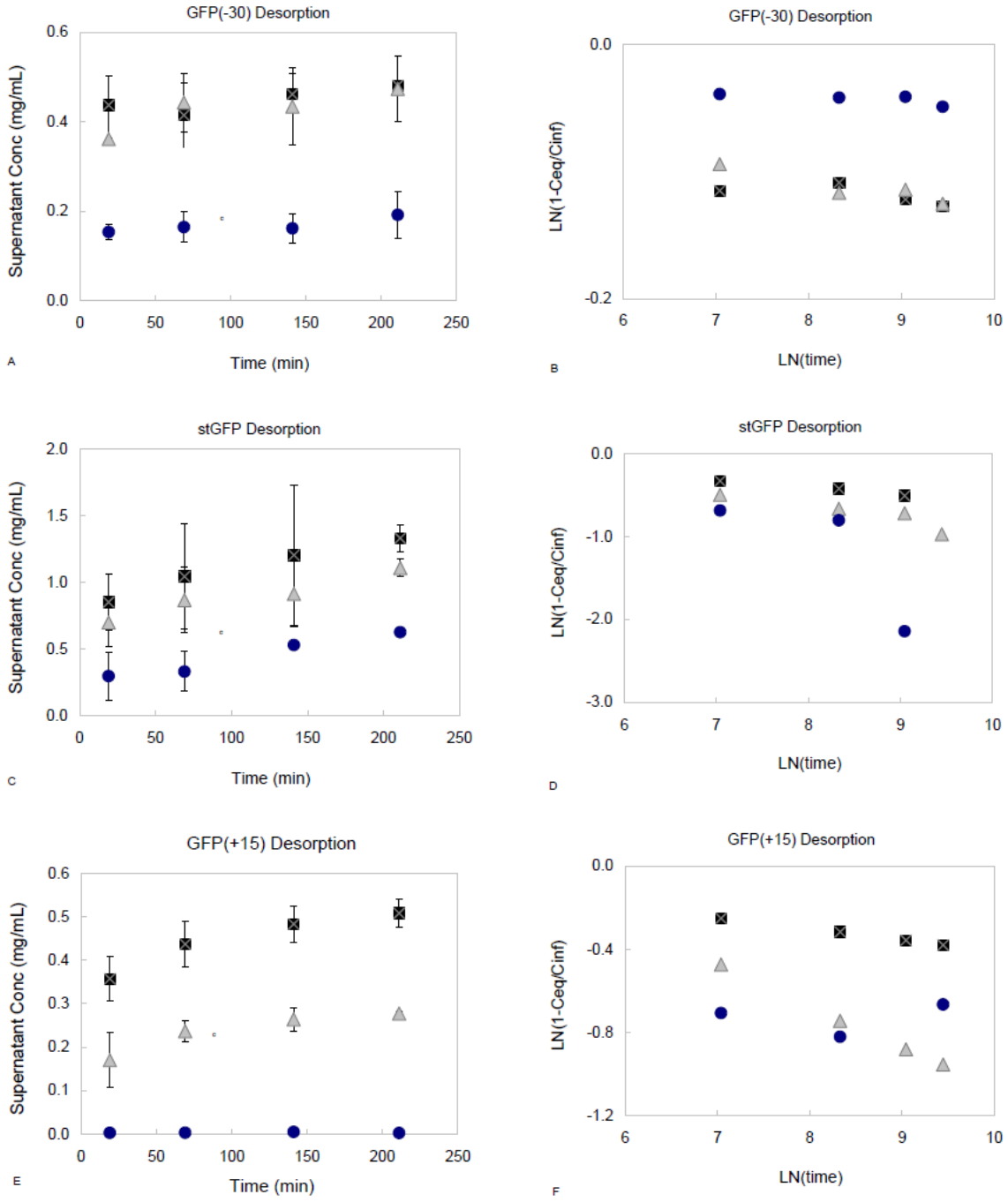

Figure 4-4 Raw desorption kinetics and stretched exponential fits for GFP variants

Desorption kinetics shown for (A) GFP(-30), (C) stGFP and (E) GFP(+15). Stretched exponential fits shown for (B) GFP(-30), (D) stGFP and (F) GFP(+15). The slope of these lines was used to calculate the desorption parameter β. For each data set, 3 coverages are presented: high ■ (isotherm plateau), medium ▲ (transition region) and low ● (rising protein of isotherm).

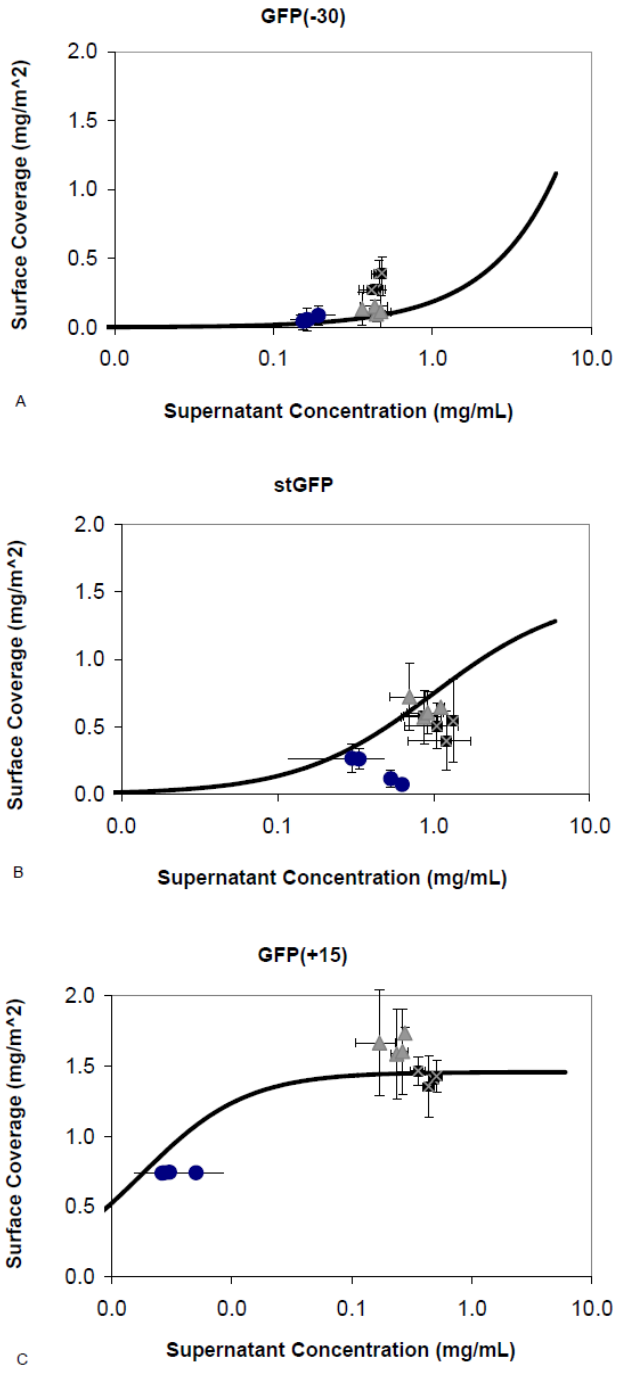

Figure 4-5 Desorption curves for GFP variants

Desorption isotherms for each individual time point overlaid with Langmuir fit of adsorption data. For each coverage, data from 4 time points measured (individual time points are shown in Figure 4-4). 3 coverages are presented: high ■ (isotherm plateau), medium ▲ (transition region) and low ● (rising protein of isotherm).

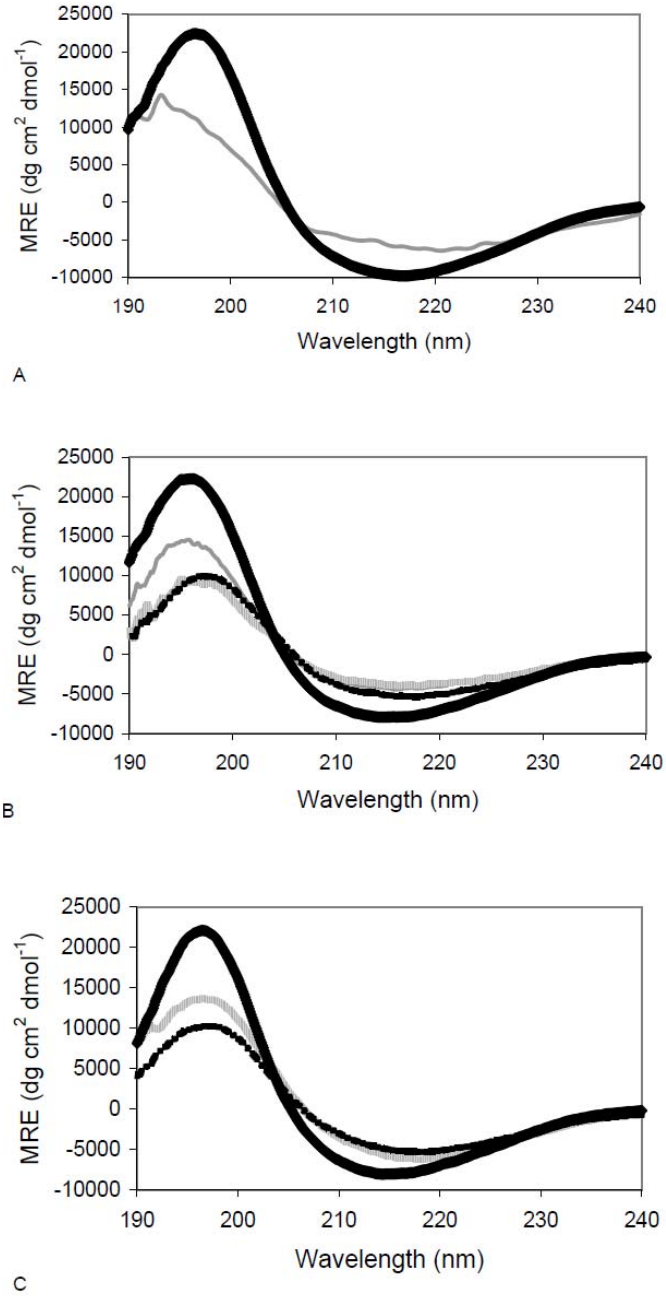

Figure 4-6 Far-UV CD spectra of adsorbed and native GFP variants

CD spectra of (A) GFP(-30), (B) stGFP, and (C) GFP(+15). The solid lack line represents the native spectra for all three variants, while the dashed and grey lines represent various adsorbed populations.

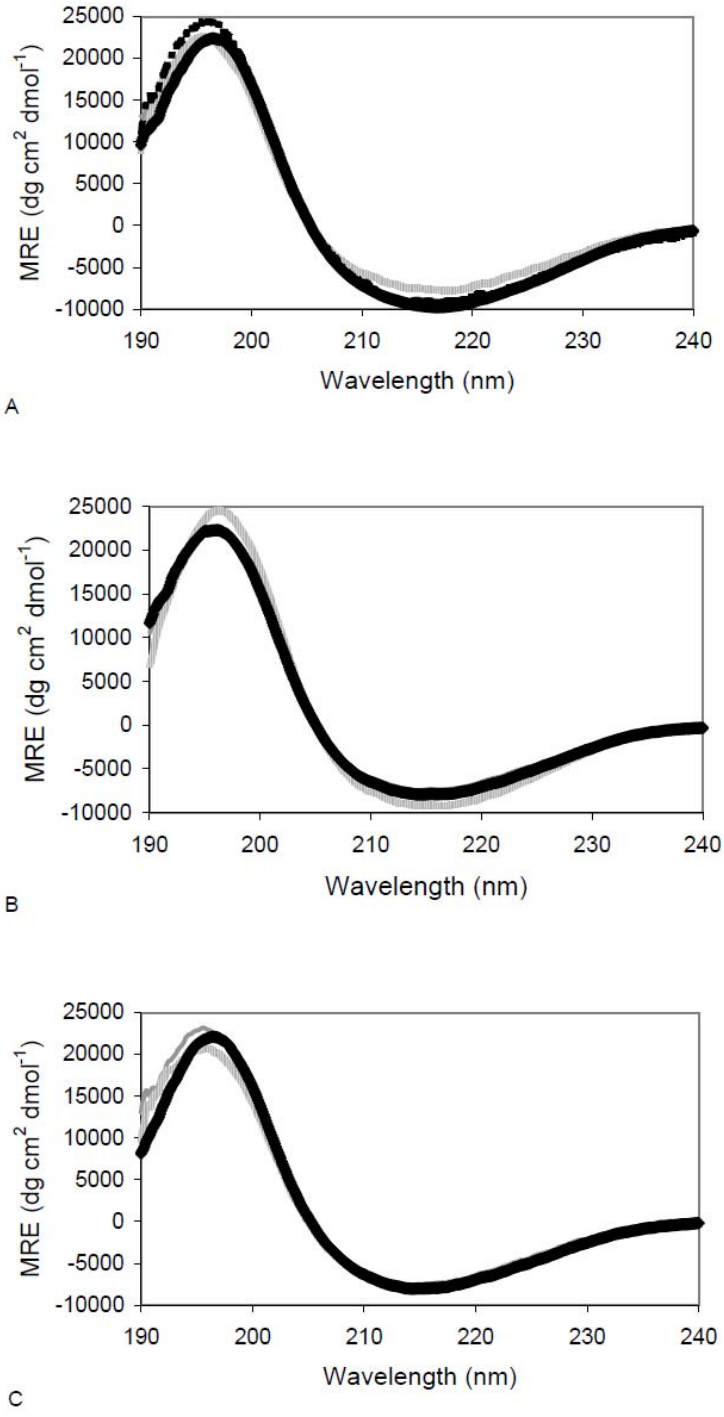

Figure 4-7 Far-UV CD spectra of desorbed and native GFP variants

CD spectra of (A) GFP(-30), (B) stGFP, and (C) GFP(+15). The solid lack line represents the native spectra for all three variants, while the dashed and grey lines represent various adsorbed populations.

CHAPTER 5. TOWARDS THE PREDICTABILITY OF PROTEIN DESORPTION FROM HYDROPHILIC SURFACES ‡

5.1. ABSTRACT

The complexity of protein structure, multi-segment surface binding and surface-induced structural perturbations contribute to the widely accepted notion that in most cases, protein desorption irreversible. However, relatively little is known about the mechanisms governing protein desorption from solid/liquid interfaces. In some isolated cases, reversible protein adsorption processes have been reported. We seek to strengthen our general understanding of the history-dependence of protein/surface attachment and synergistic effects of adsorption-related subprocesses. Our interdisciplinary approach is motivated by findings in the polymer field related to the complex chain dynamics of surface-adsorbed, low molecular weight polymers and the time-dependence of achieving equilibrium in these systems. Here, we evaluate desorption of various proteins with diverse charges, stabilities and conformations. We aim to highlight the role surface coverage and intrinsic protein parameters play in determining the consequences of

---

‡ A version of this chapter is being prepared for a future manuscript with co-authors Paolo Mangiagalli, Sanat K. Kumar, and Scott Banta. FF designed the experiments, performed the experiments, analyzed data, and wrote the manuscript.

protein adsorption. Our results reveal new similarities between protein and polymer adsorption mechanisms and find interesting insight into the heterogeneity of the adsorbed protein layer. Because we find that all proteins exhibit reversible (or quasi-reversible) binding and structural refolding, we confidently report and analyze the roles of the Langmuirian parameters, K and Γ_{max}. We uncover strong multivariate correlations between protein parameters and surface-induced structural perturbations, and reveal a promising approach towards predicting desorption time scales from K and Γ_{max}. The ability to predict adsorption-induced outcomes from such parameters which can be easily obtained can be invaluable when designing systems where interfacial behavior must be strictly regulated.

5.2. INTRODUCTION

The complexity of protein structure and the interdependencies among the adsorption subprocesses contribute to the intricacies associated with the behavior of proteins at interfaces. Understanding the reversibility of protein adsorption to a solid/liquid interface is pertinent in the wide range of applications and industries [67, 68, 134] in which this ubiquitous phenomenon plays a role. A system of interest in which the consequences of adsorption-induced effects must be especially well-characterized is the interaction of high-value biologics with prefilled drug container systems [59, 60]. Here, proteins are exposed to delivery device surfaces for extended time periods and surface-induced changes in concentration and conformation of the protein therapeutic are strictly regulated [7, 135].

Adsorption isotherms are most often used to present adsorption data. Here, the concentration of free protein in solution (C_{eq}) is related to the amount adsorbed to a given substrate surface (Γ). Adsorption is defined as a reversible process when the ascending and descending branches of the isotherm overlap. Only in the case of reversibility can the adsorption isotherm be used to derive the equilibrium binding constant, K. In such situations, the Langmuir equation is often used to model the data and derive values for K and Γ_{max}, maximum surface coverage.

Protein adsorption is most often reported as irreversible [10, 11, 15, 28, 33, 50-54] or as quasi-reversible [55]. This phenomenon has often been studied on hydrophobic surfaces [10, 50] or at low surface coverages [28]. Irreversible adsorption is often linked to conformational unfolding of the protein and the level of relaxation to the energetics of overcoming multi-segment protein/substrate detachment. Few studies report the presence of reversibly-bound molecules,

and these studies often report that desorption follows first order kinetics [56-58]. We aim here to gain a more general understanding of the mechanisms governing protein desorption.

To design our system and interpret the data, we turn to studies on the adsorption lifecycle of simple polymer chains at solid surfaces [48, 136]. An overall conclusions from these studies is that the kinetics of desorption can be very slow and depends on polymer chain length and the number of polymer-surfaces linkages [137, 138]. The complex surface dynamics of the entangled polymer chains results in high activation energies needed for displacement of the many linked segment. Resulting time-dependence of desorption can be both exponential and nonexponential. Due to this complex system dynamics, the stretched exponential (Kohlrausch function) has been successfully applied to model the wide variety of microscopic mechanisms at play in these systems.

We compare the long-term desorption (time scale of weeks) behavior of six proteins listed in Table 5-1. Proteins with a diverse level of surface charge, size and native conformation were targeted. We study desorption as a function of coverage and induce desorption using pure solvent, in order to not confound subsequent structural characterizations. We assess protein structural changes, *in situ*, associated with surface-unfolding and refolding upon release. Furthermore, a principal component analysis (PCA) is applied to assess the predictability of Langmuirian parameters and other adsorption-related events from intrinsic protein parameters.

Our data indicate that all proteins bind reversibly with widely varying timescales of desorption. As the assumption of reversibility is satisfied, we can confidently report and compare K and Γ_{max} values and correlate them to intrinsic protein parameters. Although we cannot deduce these

Langmuirian parameters using our principal components, we show strong correlations between our protein parameters and changes in secondary structure following adsorption and desorption. We can also use K and Γ_{max} to develop a predictive framework for desorption time scales. We strengthen the hypothesis that electrostatics is more influential than intrinsic protein stability in determining protein interfacial behavior. However, our results indicate that the relationship between protein parameters and adsorption-induced outcomes is an intricate, multivariate relationship where no single parameter dominates. We propose that with the ability to predict various aspects of adsorption, we can attain favorable adsorption-related outcomes by controlling the protein's environment to regulate electrostatics. Finally, the coverage- and affinity-dependence of desorption timescales provide valuable insight into the heterogeneous arrangement of the adsorbed protein layer.

5.3. EXPERIMENTAL SECTION

5.3.1. Materials

Lysozyme (from chicken egg white, purity ≥98%, Ref: L4919), Human Serum Albumin (Cohn IV purification, purity ≥97%, Ref: A9511) and Cytochrome c (from bovine heart, purity ≥95%, Ref: C2037) were purchased from Sigma (St. Louis, MO) and Ribonuclease A (Molecular biology Grade, Ref LS003431) from Worthington Biochemical Corp. (Lakewood, NJ). For AdhD and hAR expression, Integrated DNA Technology (IDT; Coralville, IA synthesized the DNA oligonucleotides. Isopropyl β-D-1-thiogalactopyranoside (IPTG) was obtained from Promega (Madison, WI). Untreated, fumed, colloidal silicon dioxide (Cab-O-Sil, M5, purity >99.8) was obtained from Cabot Corp (Boston, MA). All water was purified using a

Millipore water filtering system. Bicinchoninic acid (BCA) and QuantiPro BCA Assay kits were purchased from Thermo Fisher Scientific (Rockford, IL) and restriction enzymes NcoI and HindIII, T4 DNA Ligase, and Phusion DNA Polymerase from New England Biolabs (Ipswich, MA). All other chemicals were obtained from Sigma-Aldrich (St. Louis, MO).

5.3.2. Protein Preparation

AdhD (from hyperthermophilic archaea Pyrococcus furiosus) and hAR (from human placental DNA) were recombinantly produced and purified according to previous methods [114, 122]. The proteins were buffer exchanged into 10mM sodium phosphate buffer (pH7.0) using 30 kDa MWCO Amicon (EMD Millipore) filters. The other lyophilized proteins were reconstituted in the same buffer and filtered through a 0.22μm membrane (EMD Millipore).

5.3.3. Protein Concentration

The concentration of bulk protein solutions was determined by UV absorbance at 280 nm for all proteins except Cytochrome c. Concentration was derived using Beer-Lambert's law with the following experimentally-measured extinction coefficients: $\varepsilon_{280}^{AdhD} = 1.97\ mL\ mg^{-1}\ cm^{-1}$, $\varepsilon_{280}^{hAR} = 1.10\ mL\ mg^{-1}\ cm^{-1}$, $\varepsilon_{280}^{LYZ} = 24.39\ mL\ mg^{-1}\ cm^{-1}$, $\varepsilon_{280}^{RNaseA} = 6.90\ mL\ mg^{-1}\ cm^{-1}$, $\varepsilon_{280}^{HSA} = 5.30\ mL\ mg^{-1}\ cm^{-1}$. For Cytochrome c, the oxidized form of the heme iron was used to determine the concentration, using $\varepsilon_{550}^{CytC} = 8.40\ mM^{-1}\ cm^{-1}$ [139]. SpectraMax M2 spectrophotometer (Molecular Devices, Sunnyvale, CA) was used. Bulk protein solutions were used to make standard curves and the BCA total protein assay was used for all subsequent concentration measurements. Standards ranged from 1-0.010 mg mL^{-1} (BCA Macro) and 0.05-0.0005 mg mL^{-1} (BCA Micro).

5.3.4. Adsorption Procedure

Colloidal silica was resuspended in 10 mM sodium phosphate buffer (pH 7.0) at 12 mg mL^{-1} and vortexed immediately before use. Equal volumes of silica and protein solutions were mixed to achieve protein concentrations between 0.1 - 5.0 mg mL^{-1}, and a constant silica surface area, 1.2 m^2 mL^{-1}. For equilibrium adsorption measurements, samples were maintained at 25°C and rotated end-on-end for 16 hr using a standard laboratory rotator. Supernatants were collected and surface coverage calculated as described previously [122].

5.3.5. Desorption Procedure

Pellets obtained from the adsorption experiments were resuspended in a volume of fresh buffer corresponding to half the volume of the original protein-particle mixture volume. The pellet was resuspended by pipetting. Pellets and resuspension weights were recorded, and values were converted to volume using ρ=1.02 g/mL to calculate exact adsorbed amounts. Samples were incubated for various times (between 16hr and 14 days). Separate samples were used for each time point. Following the appropriate incubation time, the sample was centrifuged, and the supernatant removed. These supernatant concentrations were measured and reported. Based on these values, as well as amounts adsorbed on the pellets at t=0, surface coverages were calculated.

5.3.6. Far-UV CD and Melting Curve Measurements

A J-815 CD spectrometer (Jasco, Inc, Easton, MD) equipped with a Peltier junction temperature control was used to perform CD measurements. Quartz cuvettes with 0.01, 0.02, 0.05, or 0.1 cm pathlengths were used. Pure protein solutions and protein-particle mixtures were measured, using

buffer or silica blanks, respectively, for baselining. Far-UV spectra were collected between 185-240 nm in 0.1nm intervals (190-240 nm for desorption samples) using a 1nm bandwidth, 8 sec response time and 50nm/min scanning speed. Temperature was held at 25°C. Three accumulations were averaged during each run. Raw CD signal was converted to mean residue ellipticity according to: $[\theta]_{MRE} = \frac{\theta}{10\, C_r\, \ell}$, where C_r represents concentration (M*residue number) and ℓ the cuvette pathlength. Calculation of the adsorbed protein spectra is described elsewhere [122]. Desorbed protein structure was measured from rinsing the pellet following adsorption with two resuspensions of 30 min each and collecting the final supernatant. Melting curves were conducted by tracking the 222nm CD signal between 25 -95◦C.

5.3.7. Theoretical Maximum Surface Coverage Calculation

The Random Sequential Adsorption (RSA) [117] packing density (Θ = 0.547) was multiplied by the total surface area of the particles to obtain the available surface area per molecule [140]. For all proteins with known crystal structures, molecular dimensions were used to estimate projected surface area. For AdhD, molecular volume from modeling was used for this estimation.

5.3.8. Deconvolution

The CDPro software package [141] was used to analyze CD spectra using three different algorithms (Continll, Selcon3 and Cdstr) and two bases: (SP37, SDP42). α-helix and β-sheet content is reported as the sum of the distorted and regular classes. For selected adsorbed spectra a Savitzky-Golay smoothing algorithm (filter width=25), was applied prior to deconvolution, using the Spectra Manager software (Jasco, Inc,).

5.3.9. Spectral Similarity

The spectral characteristics of far-UV CD data were quantified and compared by using a spectral similarity algorithm found in the Omnic Software Suite (Thermo Electron) originally designed for FTIR second-derivative spectra comparison but applied to CD spectra in a previous study [128]. The QC Compare function [142] was used to compare both the adsorbed and desorbed data sets to the native reference in the 185-240nm or 190-240 nm range. The output is a correlation value between 0 and 1, 1 indicating identical spectra.

5.3.10. Electrophoretic Mobility

The zeta potential of 6 mg mL^{-1} silicon dioxide suspension and 0.1 mg mL^{-1} protein suspensions (in 10mM sodium phosphate buffer, pH 7.0) was measured with a Zetasizer Nano-ZS (Malvern) at 25°C. A 50mW laser operating at 532nm was used. Scattering intensities were recorded at a 90° angle. Folded capillary cells were used for the zeta potential measurements. Absolute charge differences, defined as $\zeta_{protein}^{pH\,7.0} - \zeta_{SiO_2}^{pH\,7.0}$ are reported and used for the PCA.

5.3.11. Statistical Analysis

Minitab 15 software was used for statistical analyses. A PCA was run on the protein parameter data set (inputs: size, measured charge difference, melting temperature, fraction helix, fraction sheet, number of disulfides) and the first two components were used for further modeling, as they account for > 80% of data variability. A general linear model was built on these principal component scores and output values analyzed. We identified data sets with high levels of correlation based on following criteria: R^2 > 60% and p-value of principal components < 0.3. For prediction of outputs based on K and Γmax, a general linear model was built around these

parameters using similar criteria as above to identify highly correlated data sets.

5.3.12. Modeling of Desorption Data

Kinetic desorption data were fit with the stretched exponential function:

$$c = c_o e^{-(t/\tau)^{-\beta}} \qquad \text{Eq. 4-1}$$

Using a first order Taylor approximation to simplify the exponential term, the equation was transformed into a linear relation between $\ln\left(1 - c/c_\circ\right)$ and $\ln(time)$ whose slope represents β, the parameter used to describe desorption.

5.4. RESULTS

5.4.1. Protein Characterization

Six different proteins were investigated in this study. Their intrinsic parameters are shown in Table 5-1. Abbreviations of the proteins listed in the second column of the table will be used. Size and isoelectric point (IeP) are theoretical values obtained from primary protein structure. The zeta potential of the proteins and the silica suspensions were measured to evaluate the protein/surface charge difference in each system. We compared these measured values of the proteins to their theoretical IePs. While the values had similar trends, the measured values showed positive charge only for Lyz; all other measurements were negative. Based on the IeP, we expected that Cyt and RNase would also be negative. We report here absolute charge differences between lysozyme and silica based on the experimental values. We rely on this natural scale to measure level of electrostatic attraction (rather than positive and native integers)

due to its better applicability to the subsequent PCA. CD-derived deconvolutions show three different groups with respect to secondary structure: HSA contains solely alpha-helices, Lyz and Cyt contain predominantly helices with some sheet content, while RNase, hAR and AdhD have approximately equal distribution of these two secondary components. Due to some known shortcomings of deconvolution algorithms [143], only helix and sheet content are reported. Because secondary structure has been the focus of this study, melting temperature is obtained in terms of unfolding of α-helices. AdhD, which was chosen for this study specifically for its high thermostability [114, 115] has the highest melting temperature. Cyt, Lyz, and HSA have intermediate levels, while RNase and hAR have the lowest values. Finally, we consider the number of disulfide bridges, as this impacts molecular flexibility and can therefore affect interfacial behavior [144].

5.4.2. Adsorption

Adsorption isotherms of various proteins, following 16 hr incubation with the silica nanoparticles are shown in Figure 5-5. As can be seen from the raw data, the six proteins have widely varying behavior with respect to the initial slope and maximum coverage values. Langmuir fits, according to Eq. 1-1 are also graphed. K and Γ_{max} values are presented in Table 5-2. Proteins are listed in terms of increasing K value (decreasing surface affinity). Lyz, Cyt and hAR have the highest affinities for the surface ($K < 0.05$) while RNase, HSA and AdhD have increasingly lower affinities. Measured Γ_{max} values compare well with theoretical maximum surface coverage calculations listed in Table 5-2 (all values within in a factor of ~2). Both the graphs in Figure 5-5 and the root mean square deviation (RMSD) values in Table 5-2 indicate that this equation accurately models the data.

5.4.3. Desorption

We evaluated the desorption kinetics of the six proteins from silica nanoparticles following a constant adsorption time (16hr). We chose this time length for adsorption because our previous experiments, and results reported in literature, indicate this time is sufficient to achieve steady state adsorption. We assume that this amount of desorption time results in system equilibrium; however, we will reassess this assumption in Section 1375.5 in light of our current results. The raw data for desorption kinetics can be found in Figure 5-6. These data have been converted to surface coverage at each time point. We compare these values to adsorption isotherms (shown as the Langmuir fit for simplicity) in Figure 5-1. In this way, we evaluate reversibility based on the overlap of the two pathways. We also studied the coverage-dependence of desorption and report data at three coverages ("high" indicates starting point on the plateau, "medium" on the transition region, and "low" on the rising portion of the isotherm).

Figure 5-1 shows that over the time course of these experiments (2 weeks), desorbed protein concentration in all cases, achieved equilibrium (or quasi-equilibrium in the case of HSA), which we define based on the state of the system following adsorption. More specifically, three different behaviors with respect to desorption kinetics can be identified from Figure 5-1. The first is slow desorption whereby equilibrium values are achieved on the order of weeks. In fact, for HSA, which appears to have the slowest desorption kinetics, desorbed concentration only approaches the adsorption isotherm. We assume that the trending of the data suggests that these values will overlap with the isotherm provided that desorption time is extended. However, other explanation for this behavior, which call into question the definition of system equilibrium, will be discussed below. AdhD and RNase, Figure 5-1B-C, also show slow desorption kinetics,

however, the final time point has reached adsorption equilibrium. The second classification involves Cyt and hAR (Figure 5-1D-E), which appear to have fast desorption kinetics: even at the first 16 hr time point equilibrium has been achieved. Finally, Lyz (Figure 5-1F) shows equilibrium-state desorption values at 16hr, but desorption concentrations continue to increase as surface coverage remains constant.

Finding a model to fit all data in Figure 5-6 was complicated by varying behavior between proteins and surface coverages. We considered the application of the stretched exponential function to our data. Upon being satisfied by the linearity of $\ln(1-c/c_o)$ and ln(time), shown in Figure 5-7, we solved for the β and τ parameter (Eq. 4-1). For subsequent analysis, we report the β parameter which represents the measure of departure from normal relaxation dynamics. $\beta = 0$ represents zeroeth order kinetics (i.e. no time-dependence) while $\beta=1$ represents the standard exponential relaxation kinetics. β values are shown in Table 5-2. We note that some β values were calculated as negative. These values are attributed to error associated with our concentration measurement assay. We assign a value of zero to these numbers for subsequent PCA analysis. The first important observation is that β seems to correlate strongly with coverage and binding affinity (K). All high-coverage β values, representing the plateau region of the adsorption isotherm, approach zero indicating no time sensitivity. For Lyz, Cyt and hAR, the trend continues: β increases with coverage. The correlation between β and K is apparent in the low coverage β values (where the maximum amount of surface binding can occur per protein molecule). Two groups emerge: For high affinity binders ($K < 0.1$), β_{low} is greater than 0.1, indicating that desorption has a greater level of time dependence. The low affinity binders ($K > 0.1$) have virtually no time-dependence.

5.4.4. Secondary Structure Characterization

Following 16-hour adsorption, we assessed the structure of the protein in its adsorbed state which is calculated from the CD spectra of the protein/particle mixture and protein in the supernatant. The far-UV spectra which revealed information about secondary structure can be found in Figure 5-8. We deconvolute these spectra to obtain fraction of α-helix and β-sheet based on a comparison with a reference set of known proteins. We also applied a correlation coefficient to these spectra, and compared their deviation from the native spectra from a purely mathematical standpoint. These values can be found under the "Adsorption" heading in Table 5-3. The deconvolution results show that all adsorbed proteins have altered structure as compared to native. More specifically, all proteins undergo an α helix → β sheet transition upon adsorption. The trends represented by the correlation coefficient correspond much more closely to the change in sheet than with change in helical content.

The comparison of CD spectra of the desorbed and native protein populations are shown in Figure 5-9. Based on the spectra, we concluded that Cyt, Rnase, and Lyz (which have favorable electrostatic interactions) have the highest level of similarity to the native spectra, whereas hAR, AdhD, and HSA exhibited some levels of deviation from native. To quantify these changes, we show again deconvolution and correlation coefficient results in Table 5-3 under the heading "Desorption". The correlation coefficient shows that all protein spectra deviate minimally from the native. The deconvolutions mirror our spectra-based observations: Lyz, Cyt and RNase show almost no change in helical or sheet-like content, while hAR, AdhD and HSA have nearly identical secondary structure between the desorbed and adsorbed states, indicating that these proteins cannot recover from surface-induced perturbations.

5.4.5. Principal Component Analysis and Statistical Predictions

PCA can be a valuable tool in analyzing the complex relationship between protein properties and observed adsorption/desorption behavior by reducing the dimensionality of a multivariate data set. A PCA has been performed on protein parameters listed in Table 5-1. The first output of interest of a PCA are the principal component weights assigned to the different input parameters, which are shown graphically in Figure 5-2 and numerically in Table 5-4. Because the Scree plot in Figure 5-10B shows that the Eigenvalues of the first two principal components account for over 80% of system variability, all analyses have been conducted on the first two principal components. Because the third component does have minimal contribution to the Eigenvalues, its loading plots can be found in Figure 5-10C and D. From Figure 5-2, we can make some interesting observations. The first component is dominated by effects related directly to the protein primary and secondary structure: helix and sheet content, number of disulfide bonds and size. The second component, however, is dominated by charge effects. The first two principal component scores as they apply to the various proteins in this study are shown in Figure 5-10A. HSA (presumably due to its size and large number of disulfide bridges) is most strongly influenced by the first component.

Before implementing a general linear model based on the principal component scores, we analyze the data sets one-by-one to identify any strong correlations which exist between input parameters and measured behavior. A matrix plot is presented in Figure 5-11 to represent the data grouped by desorption parameters, adsorbed protein structure and desorbed protein structure. Visually, the relationships which exhibit strong correlation are identified and highlighted. We see that in all three data sets the majority of these hits involve protein charge and size.

We generate a linear model of the first two principal component scores and assess their predictability of the measured outputs. Three data sets are identified which meet the R^2 and p-value criteria stated previously. Each data set is related to structural parameters: change in helical and sheet content in the adsorbed state and change in helical content of the desorbed state. The accuracy of the predictions is shown in Figure 5-3. For a practical application of these models, a regression based on the PCA scores is generated for the identified data sets. Weighted scores are then are linked back to the original protein input parameters to obtain an equation that predicts the behavior. A linear combination of the input parameters, weighted by the coefficients defined in Table 5-5 yields the prediction model. By multiplying these coefficients by the range of each parameter we identified the dominant input parameter in each data set which are highlighted in Table 5-5, and are β-sheet content, charge and size for the three data sets. Table 5-5 also contains the R^2 value of each prediction to assess goodness-of-fit. We originally hypothesized that K and Γ_{max} could also be predicted in this way. However, the selection criteria were not met and the poor correlation between predicted and measured values are shown in Figure 5-12.

Finally, we tested the predictability of the measured adsorption behavior based on K and Γ_{max}. Three data sets, all related to desorption behavior pass the selection criteria. High coverage, medium coverage and average β values were all predicted fairly accurately by K and Γ_{max}, as can be seen in Figure 5-4. R^2 values as well as coefficients needed to conduct predictions can be found in Table 5-6. Low coverage predictions were also evaluated, but the poor correlations can be seen in Figure 5-13.

5.5. DISCUSSION

Often conflicting findings regarding the desorbability of proteins from interfaces have motivated us to reassess the notion that interfacial protein adsorption is a thermodynamically irreversible process. Our approach of expanding the design space, in terms of coverage levels and time scales, demonstrates that on a hydrophilic surface protein detachment is a relatively slow process, but does return to equilibrium, which we define as the state the system has achieved following 16hr of adsorption. In light of this result, we confidently extract equilibrium parameters related to binding affinity and maximum coverage to characterize surface attachment. Similarly, we strive to identify a meaningful parameter which best characterizes our observed desorption behavior. Variations between proteins, non-exponential behavior, and diverse time scales prevent the applicability of traditional models to the data. We turned to polymer theory for a solution. The stretched exponential function has been used to model the large-scale dynamics of polymer systems [145]. Because the β-parameter was shown to characterize the entanglement of polymer chains, we postulate that proteins may behave similarly to simple polymers in this respect. Our data confirm that this model can be successfully applied to characterize protein desorption. Combining these newly acquired desorption parameters with the equilibrium adsorption constants and intrinsic protein parameters, we identify strong, multivariable correlations which we integrate into a model to predict specific surface-induced outcomes.

Previously, we determined that the adsorption of lysozyme onto silica occurred in a reversible manner, on a relatively short timescale (hours). We found the Langmuirian adsorption parameters could predict desorbed amounts [122]. We hypothesized that our results were system-specific: lysozyme has a complex, globular structure and a highly favorable electrostatic attraction to silica. Here, we aim to generalize our understanding of the mechanisms governing

desorption from hydrophilic surfaces. Table 5-1 lists the proteins we evaluate in this study. Due to our focus on electrostatics, our main protein selection criterion targeted a wide range of protein surface charges. We have proteins with both strong (Lyz, RNase, Cyt) and weak (HSA, AdhD, hAR) electrostatic interactions with the silica. As we keep the system pH constant between proteins, the same negative charge is imparted on the silica for each system. By using different proteins to achieve variability in surface change, we inherently also changed other parameters (size, melting temperature, secondary structure) which we also evaluate here. Although the limitation of this approach is that no single parameter can be assessed in isolation, we believe it is beneficial to use natural proteins rather than engineered mutants [146].

We measured desorbed protein concentration at various time points between 16hr and 2 weeks, and from the kinetic data we constructed desorption isotherms at three levels of coverage for each protein. From Figure 5-1, we can see three groups of behavior. The proteins either trend toward equilibrium throughout the 2 week study (HSA, AdhD, RNase), reach equilibrium adsorption values after 16 hr and not change much after that (Cyt, hAR), or reach equilibrium after 16hr and then overshoot adsorption values at later times (Lyz). From our definition of reversibility, based on overlapping of the adsorption/desorption isotherms, our data indicate that given enough time, protein desorption is a reversible process in all cases. The second aspect of reversibility relates to the ability of the protein to regain its native-like conformation. Our results indicated that all proteins undergo helix to sheet transition on the surface. Three of the proteins, with the highest isoelectric points, achieve native-like refolding. For hAR, AdhD and HSA, however, surface perturbations are retained, and the data indicated that while the protein are able to detach from the surface, intermolecular bonds cannot all be rebuilt. Therefore, we found it

remarkable that using only pure solvent to induce desorption, Lyz, RNase and Cyt all exhibit reversible behavior, while HSA, hAR, and AdhD exhibit quasi-reversible adsorption.

Some of our findings call into question whether or not the allotted adsorption time is sufficient for the system to reach equilibrium. In the case of HSA, we assume that the desorption rate will eventually reach equilibrium, which we define by the adsorption isotherm. However, another possibility is that our assumption that the adsorption isotherm is at equilibrium is incorrect, and given more time, higher level of adsorption will occur and the adsorption curve in Figure 5-1A will shift upward. We explain our observation for lysozyme in Figure 5-1F similarly. Lyz has the highest binding constant and the most favorable charge attraction with the silica. We postulate that due to a strong electrostatic driving force, a large amount of protein initially adsorbs to the surface. Over time, slow rearrangement, structural relaxation (as our CD data supports) and lateral protein-protein interaction may favor lower levels of surface coverage, shifting the adsorption curve down. It is possible that this change takes more than 16 hr to occur. This could explain why desorption values overshoot the adsorption isotherm. In light of these alternative explanations, more effort must be taken to ensure that adsorption equilibriums has been achieved. However, the emphasis of this paper is to compare the desorption behavior of the proteins. We chose the same starting point for all our adsorption studies, which in most cases does present steady state.

After successfully applying the stretched exponential function to our desorption data, we found interesting coverage- and affinity-dependence of β. Because all proteins, independent of binding affinity, desorbed with little time-dependence at high coverage, this indicates that a specific

characteristic of the adsorbed protein layer causes the proteins to desorb more readily than at lower coverages. Furthermore, the lower affinity binding proteins (AdhD, RNase and HSA) retained this type of desorption behavior along the entire adsorption isotherm. In contrast, Lyz, Cyt and hAR exhibited increasingly different desorption kinetics at medium and low coverage. β increases (reaching 1 for Lyz) meaning that longer time scales dominate and the kinetics approached an exponential relationship with time. We have previously represented a model hypothesizing that coverage-related differences in desorption may be correlated with local descriptors such as the number of surface contacts [122]. Combining all our current results, we expand upon this model. We postulate that high affinity binding proteins exhibit a heterogeneous surface arrangement relative to coverage. At high coverage, the number of surface attachments is more uniform across all adsorbed proteins, therefore any protein has equal probability of desorbing and time-dependence is not relevant. At low coverage, number of attachment sites vary. Proteins with fewest number of attachments desorb first, followed by those which are more strongly bound with more attachments, thus imparting a time dependence in the system. In contrast, low affinity binders have a homogenous arrangement across the entire adsorption isotherm, and number of surface attachment sites are uniform across all bound proteins.

The applicability of the stretched exponential to both polymer and protein desorption emphasizes similarities between the two molecular systems. We have also found the applicability of the Langmuir model for protein adsorption, which is also often used to describe simple polymer adsorption. Based on these we find from a mechanistic standpoint, the attachment and detachment of proteins to and from the surface are more similar to simple, low molecular polymers than previously thought. While most dramatic differences between protein and

polymer interfacial behavior seem to come from unfolding of the molecule on the surface and lateral interactions actions between adsorbed molecules, our results surprisingly show that on hydrophilic surfaces, surface-induced conformational changes do not result in dramatically different desorption behaviors.

Our initial hypothesis that electrostatics plays an influential role in adsorption is strengthened by our results. Table 5-1 and 4-2 emphasize the strong correlation between charge differences and binding affinity. Figure 5-11 shows that desorption behavior, adsorbed structure and refolding upon desorption all have strong correlations to electrostatics. However, in our predictive models, where multi-dimensional relationships rather than single correlative relationships are examined, we see that observed behavior is intricately related to several other parameters tested. Electrostatics alone does not dominate these models.

The two predictive models we presented in this study provide information about the timescales of desorption (model based on K and Γ_{max}) and about adsorption-induced structural changes (proteins input parameter model). The R^2 values for both models in Table 5-5 and 4-6 show relatively high levels of correlation. These correlations can be valuable tools because measuring desorption kinetics and surface-induced structural changes is experimentally demanding. On the other hand, acquiring the protein parameters listed in Table 5-1 as well as the Langmuirian parameters is relatively simple. Therefore, complex adsorption behavior can be estimated from these simple measurements.

Figure 5-2 depicts the distribution of first and second principal component. The first component includes parameters which are strictly related to primary protein structure: helical and sheet

content, size and number of disulfide bonds. Changing these parameters to impact adsorption behavior would involve fundamentally changing the properties of the proteins (i.e. use of protein engineering). On the other hand, the second principal component is dominated by electrostatics. Because protein and substrate surface charge is strongly influenced by the aqueous environment, altering solution conditions provides a more simplistic strategy to influence the protein's interfacial behavior. This approach, combined with predictive capabilities presented earlier, provide powerful tools in designing systems with specific adsorption-related outcomes.

5.6. CONCLUSIONS

In this study, we set out to strengthen our understanding of the history-dependence of protein/surface attachment and the interdependencies of adsorption-related subprocesses. We show that on hydrophilic surfaces, all proteins we evaluate bind reversibly with widely varying timescales of desorption. These results show that equilibrium binding constant as well as surface coverage play a critical role in defining these desorption timescales. We hypothesize that high affinity binding proteins exhibit a heterogeneous surface arrangement relative to coverage. We also present a framework for predicting the level of structural transitions a protein will undergo during adsorption and upon desorption from the surface.

5.7. TABLES AND FIGURES

Protein	Abbreviation	Size [1] (kDa)	Theoretical Isoelectric Point [2]	Charge Difference [3] (mV)	Fraction Helix [4]	Fraction Sheet [5]	Melting Temperature [6] (°C)	Number of Disulfides [7]
Lysozyme	Lyz	14.3	11.1	36.2	0.36	0.14	76	4
Cytochrome C	Cyt	11.6	9.5	26.1	0.30	0.18	87	0
Ribonuclease A	RNase	13.7	8.6	20.7	0.19	0.25	58	4
Human Aldose Reductase	hAR	37.2	6.9	14.2	0.22	0.27	55	0
Human Serum Albumin	HSA	69.4	5.9	18.9	0.74	0.02	72	17
Alcohol Dehydrogenase	AdhD	31.9	5.5	17.1	0.24	0.25	100	0

Table 5-1 Intrinsic protein parameters

[1] From following pdb files: Lysozyme (2vb1), Cytochrome c (2b4z), hAR (2acq), Ribonuclease A (5rsa), Human Serum Albumin (1e78); [2] Lysozyme [147], all other proteins from theoretical calculations; [3] Data from zeta potential measurement: absolute differences reported between silica nanoparticle suspensions and protein solutions; [4, 5] As measured by far-UV CD, and deconvoluted using CDPRO; [6] Measured by monitoring 222nm wavelength signal on CD during temperature excursion between 25◦C and 95◦C, [7] Source: [148]

	Langmuirian Parameters				Desorption Rate Constants							
	K (mg/mL)	Γ_{max} (mg/m^2)	RMSD	Theoretical Γ_{max} (mg/m^2)	β_{high}		β_{med}		β_{low}		β_{AVE}	$\beta_{vs\ \Gamma}$
					Avg.	*error*	Avg.	*error*	Avg.	*error*		
Lyz	0.0060	1.1	0.023	1.8	2.6E-02	*0.008*	3.8E-01	*0.100*	1.0E+00	*0.4*	4.8E-01	3.0E+00
Cyt	0.020	1.1	0.0094	0.58	1.2E-02	*0.004*	1.2E-01	*0.02*	3.6E-01	*0.57*	1.6E-01	4.3E-01
hAR	0.032	2.3	0.041	2.3	-3.9E-02	*0.007*	6.1E-01	*0.33*	4.7E-01	*0.37*	3.5E-01	2.9E-01
Rnase	0.16	0.86	0.017	1.0	2.1E-03	*0.005*	1.8E-02	*0.011*	5.7E-02	*0.020*	2.6E-02	2.1E-01
HSA	0.45	0.68	0.0025	1.6	1.6E-02	*0.005*	2.9E-02	*0.007*	2.8E-02	*0.008*	2.5E-02	3.1E-02
AdhD	1.5	1.5	0.038	2.2	-7.1E-03	*0.002*	-1.3E-02	*0.005*	-1.0E-02	*0.013*	-9.9E-03	6.9E-03

Table 5-2 Measured adsorption- and desorption-related parameters

Langmuirian Parameters, associated RMSD values for the Langmuir fits, theoretical surface coverage, and desorption parameter β (at high, medium, and low coverage as well as average and coverage-dependence) for the various proteins. For β, the average value of 3 replicates and error is presented. Error represents the average standard error (with a 95% confidence interval) around the slope of the linear regressions used to fit the data as shown in Figure 5-7. Values of "0" represent β values where the slope yielded negative numbers. These were rounded to 0, but the error has been included to a precision on three decimal places.

	Adsorption			Desorption		
	Deconvolution		Correlation Coefficient	Deconvolution		Correlation Coefficient
	Change in % helix	Change in % sheet	Overall Change	Change in % helix	Change in % sheet	Overall Change
LYZ	-19	15	0.17	-3	3	0.02
Cyt	-11	10	0.09	-4	5	0.01
hAR	-8	7	0.14	-8	5	0.03
Rnase	-14	13	0.21	-2	1	0.06
HSA	-22	6	0.02	-22	9	0.03
AdhD	-12	9	0.11	-10	9	0.05

Table 5-3 Measured adsorption-induced structural transitions

Secondary structural transitions in the adsorbed state and upon desorption. All values refer to change compared to the native conformation. Two measures of structural change are provided: deconvolution values give percentages of helical loss and beta-sheet gain, whereas the correlation coefficient represents deviation of the spectra from the native spectra.

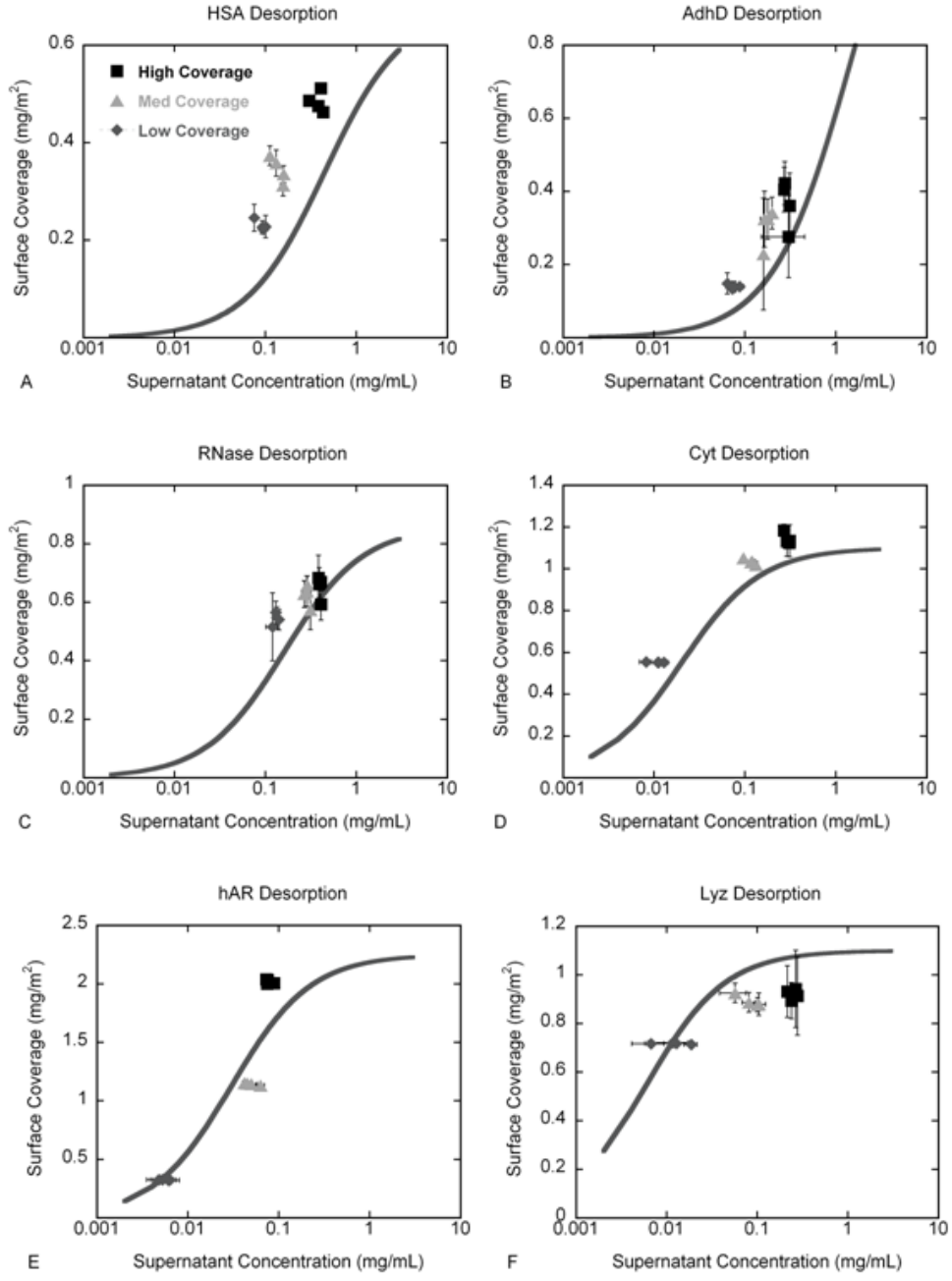

Figure 5-1 Desorption isotherms for various proteins

Desorption isotherms for each protein (individual data points) overlaid with Langmuir fit of adsorption data (solid line). For each protein, 3 coverages are presented: high ■ (plateau region of isotherm), medium ▲ (transition region) and low ● (rising protein of the isotherm). For each coverage, data from 4 time points measured (individual time points are shown in Figure 5-6) are presented.

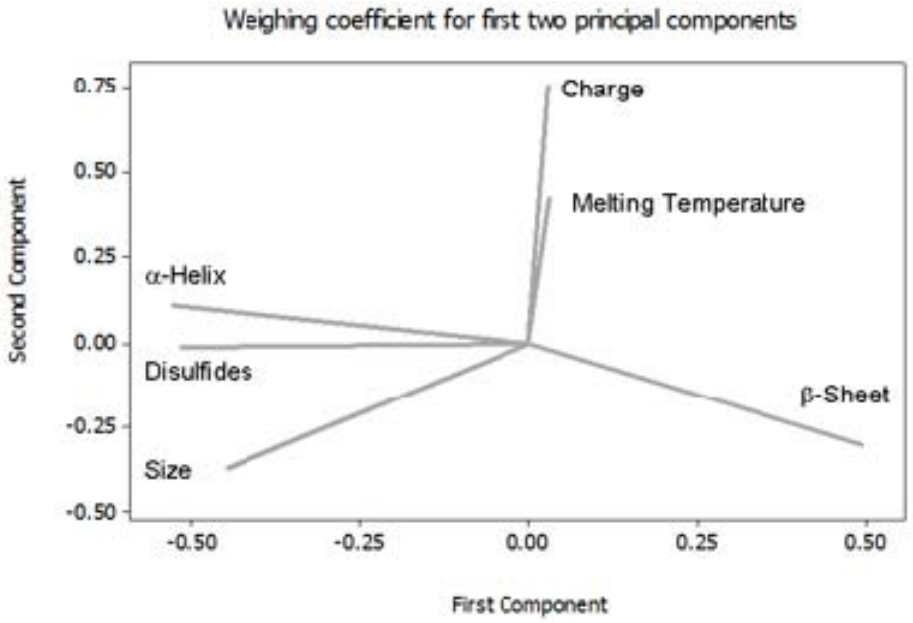

Figure 5-2 Loading plots of first and second principal components

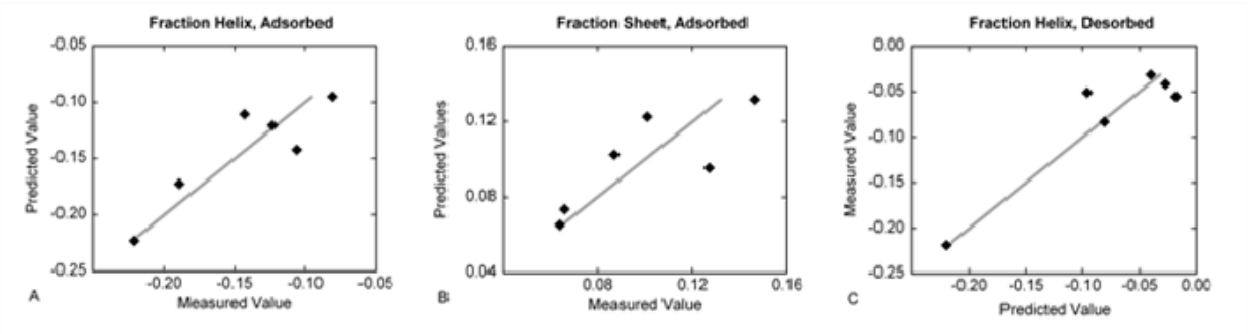

Figure 5-3 Accuracy of predicted values for adsorption-induced structural transitions

Predicted vs. actual values for change in helix (A) and sheet (B) content for proteins in the adsorbed state, and change in helix (C) content for desorbed proteins. Predictions based on PCA of intrinsic protein parameters..

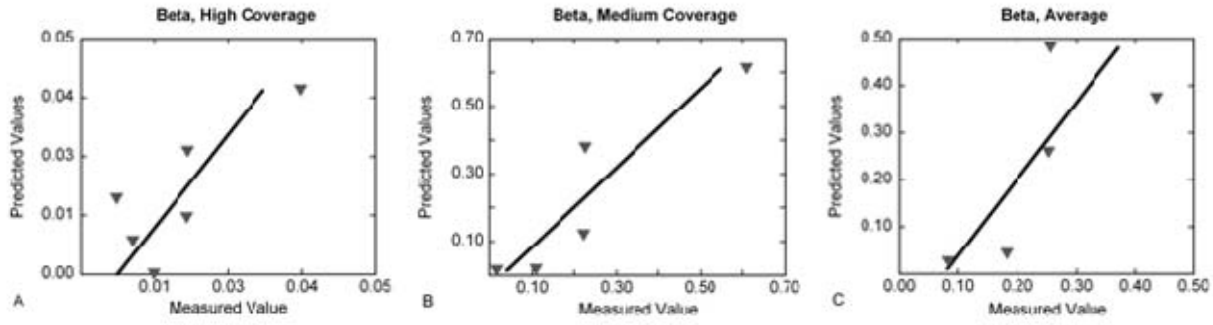

Figure 5-4 Accuracy of predicted values for desorption parameters

Predicted vs. actual values for (high coverage (A), medium coverage (B) and average (C) β values as predicted from the Langmuirian parameters K and Γ_{max}.

5.8. SUPPLEMENTARY INFORMATION

5.8.1. Supplementary Tables and Figures

	Principal Components Weights		
Protein Parameters	Weight1	Weight2	Weight3
Size	-0.45	-0.37	-0.25
Charge Difference	0.03	0.76	0.36
Melting Temperature	0.03	0.43	-0.88
Fraction Helix	-0.53	0.11	-0.03
Fractin Sheet	0.50	-0.30	-0.05
Number of Disulfides	-0.52	-0.01	0.16

Table 5-4 Weights of first three principal components

Prediction Coefficients for PCA Prediction of Selct Adsorption Behavior

	Constant	Size	Charge Difference	Melting Temp.	Fraction Helix	Fraction Sheet	Number of Disulfides	R-sq
Δ_{HELIX}, Adsorbed	-0.0740	-0.0003	-0.0016	-0.0004	-0.0779	**0.1938**	-0.0021	79.6
Δ_{SHEET}, Adsorbed	0.0472	-0.0005	**0.0018**	0.0005	-0.0090	-0.0202	-0.0006	63.2
Δ_{HELIX}, Desorbed	-0.1182	**-0.0010**	0.0020	0.0006	-0.0804	0.1211	-0.0028	86.6

Table 5-5 Structural transition prediction coefficients

Coefficients used to predict change in helix (Row 1) an d sheet (Row 2) structure in the adsorbed state and change in helix (Row 3) following desorption based on intrinsic protein parameters. R-squared values of the fit are also included in the last column.

Prediction of Desorption Rates for K and Γ_{max}

	Constant	K	Γ_{max}	R-sq
β_{high}	-0.0003	-0.0111	0.0168	63.7
β_{med}	-0.1440	-0.2380	0.3380	85.4
β_{Ave}	0.0810	-0.2360	0.1610	61.6

Table 5-6 Desorption rate prediction coefficients

Coefficient used to predict high coverage (Row 1), medium coverage (row 2) and average (Row 3) β values based on K and Γ_{max} parameters. R-squared values of the fit are also included in the last column.

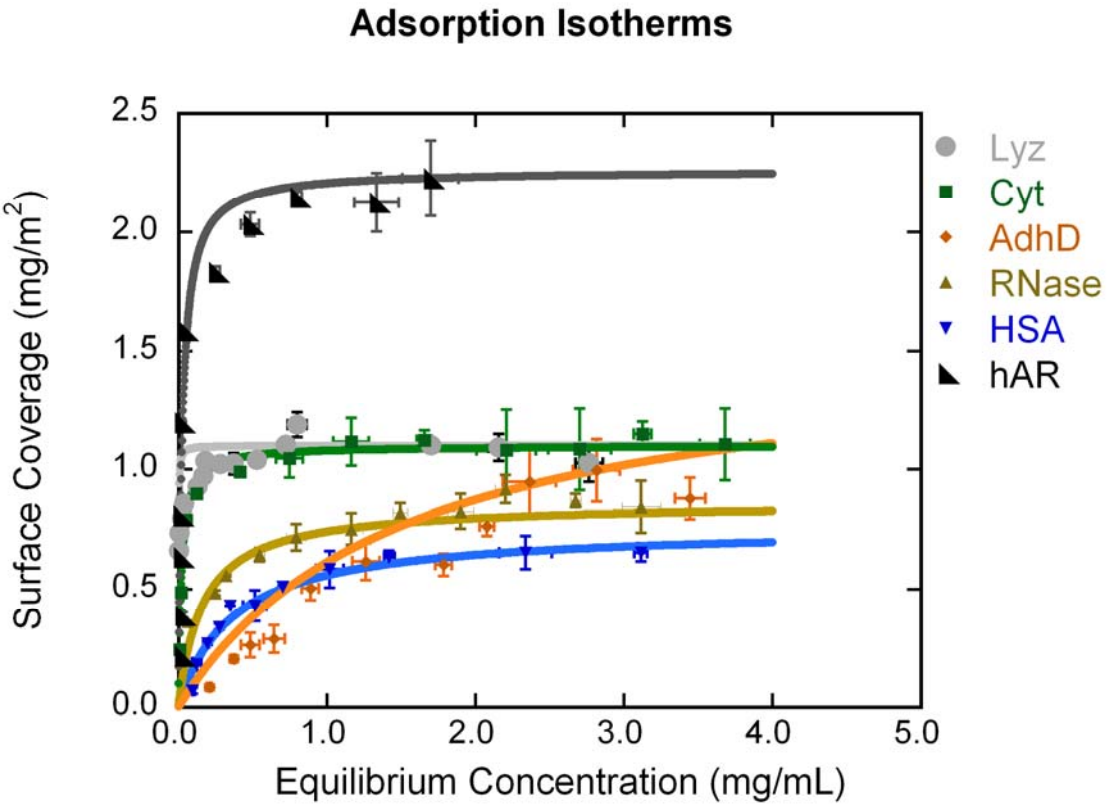

Figure 5-5 Adsorption isotherms for various proteins and Langmuir fits

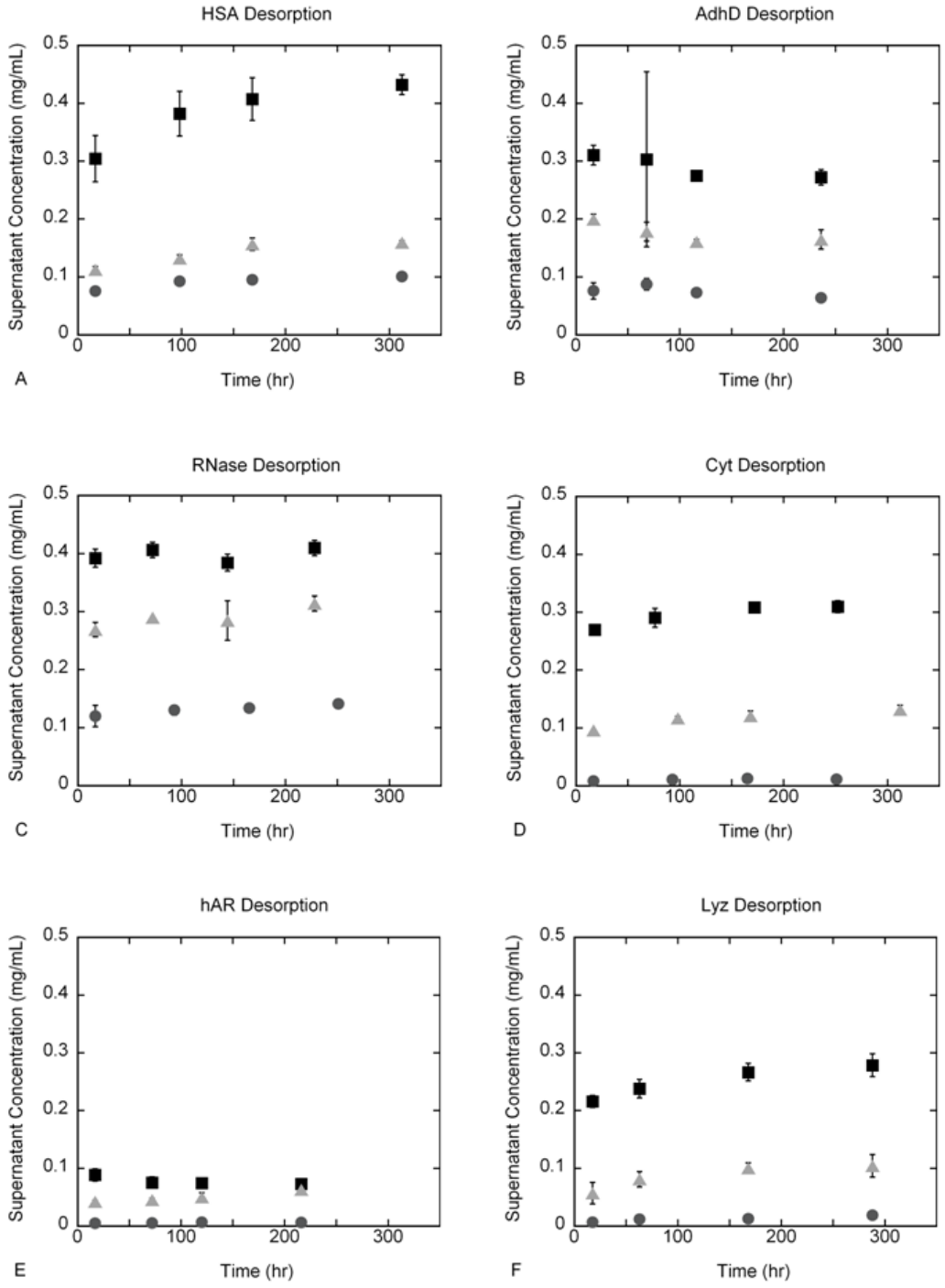

Figure 5-6 Raw desorption data for various proteins

Raw desorption data for all six proteins. For each data set, 3 coverages are presented: high ■ (plateau region of isotherm), medium ▲ (transition region) and low ● (rising protein of the isotherm).

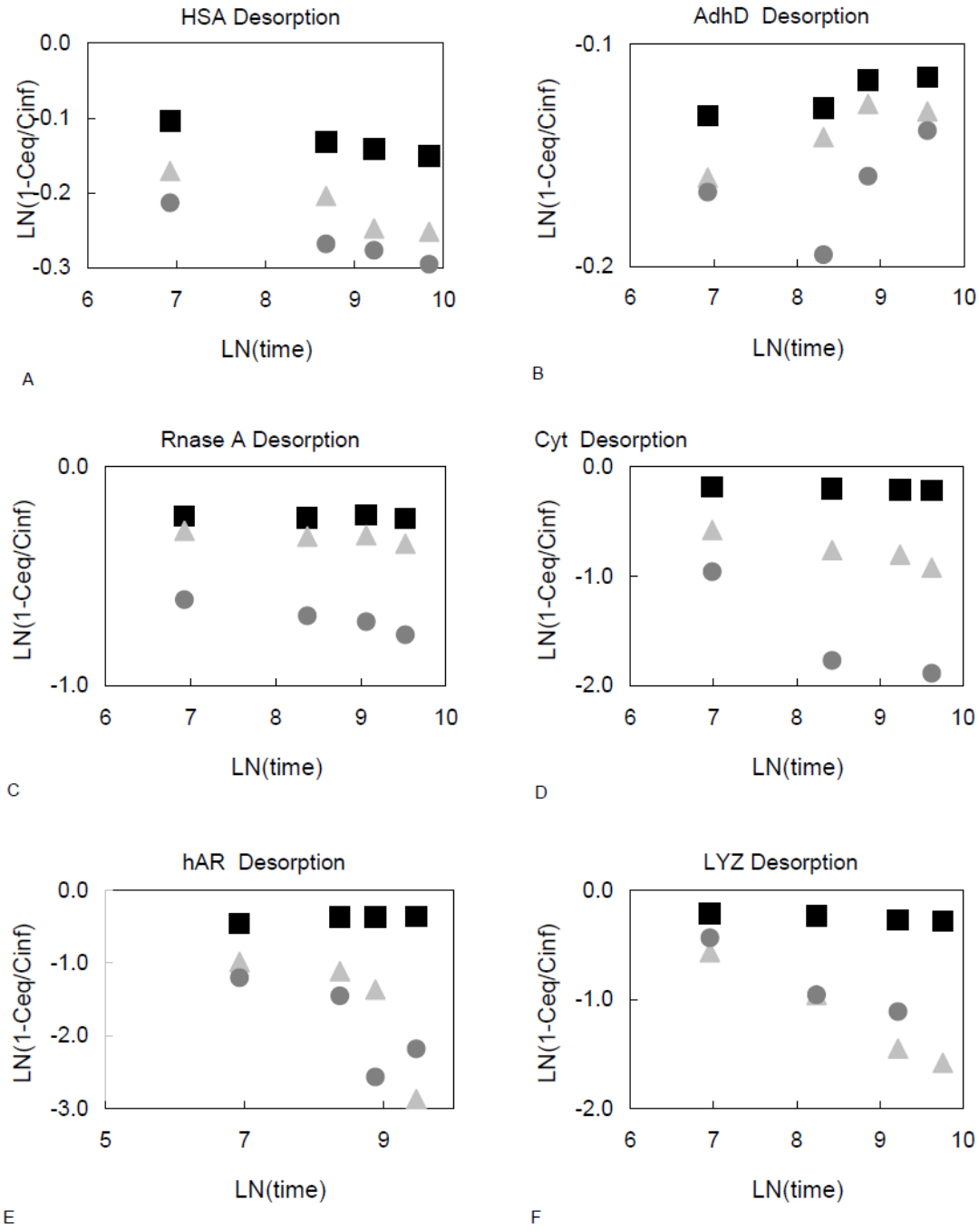

Figure 5-7 Stretched exponential fit of desorption data

Stretched exponential fit of desorption data. The slope of these lines was used to calculate the desorption parameter β. For each data set, 3 coverages are presented: high ■ (plateau region of isotherm), medium ▲ (transition region) and low ● (rising protein of the isotherm).

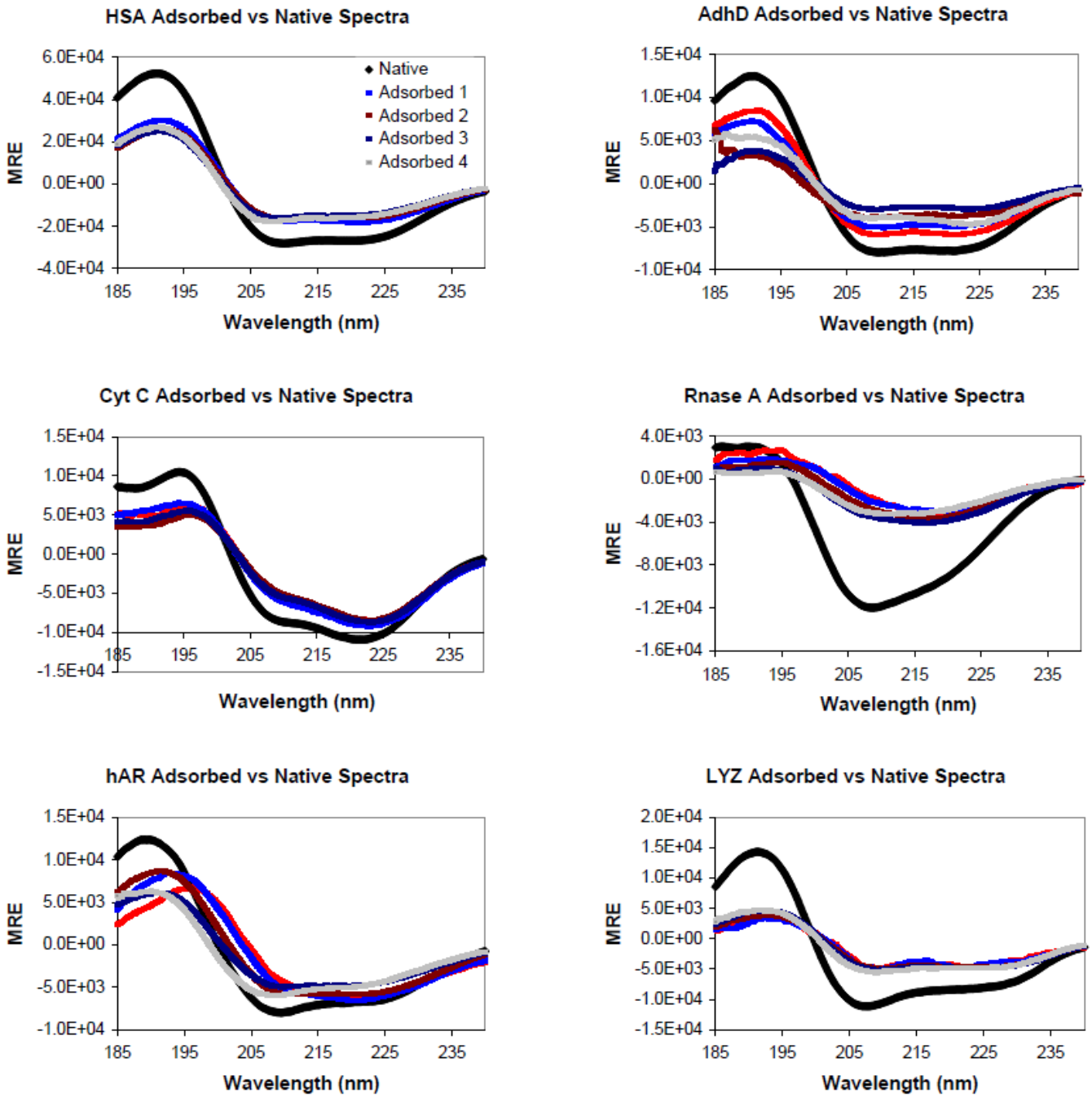

Figure 5-8 Far –UV CD Spectra of adsorbed and native protein

Black lines represent the native spectra, while the colored lines show adsorbed spectra at various levels of coverage

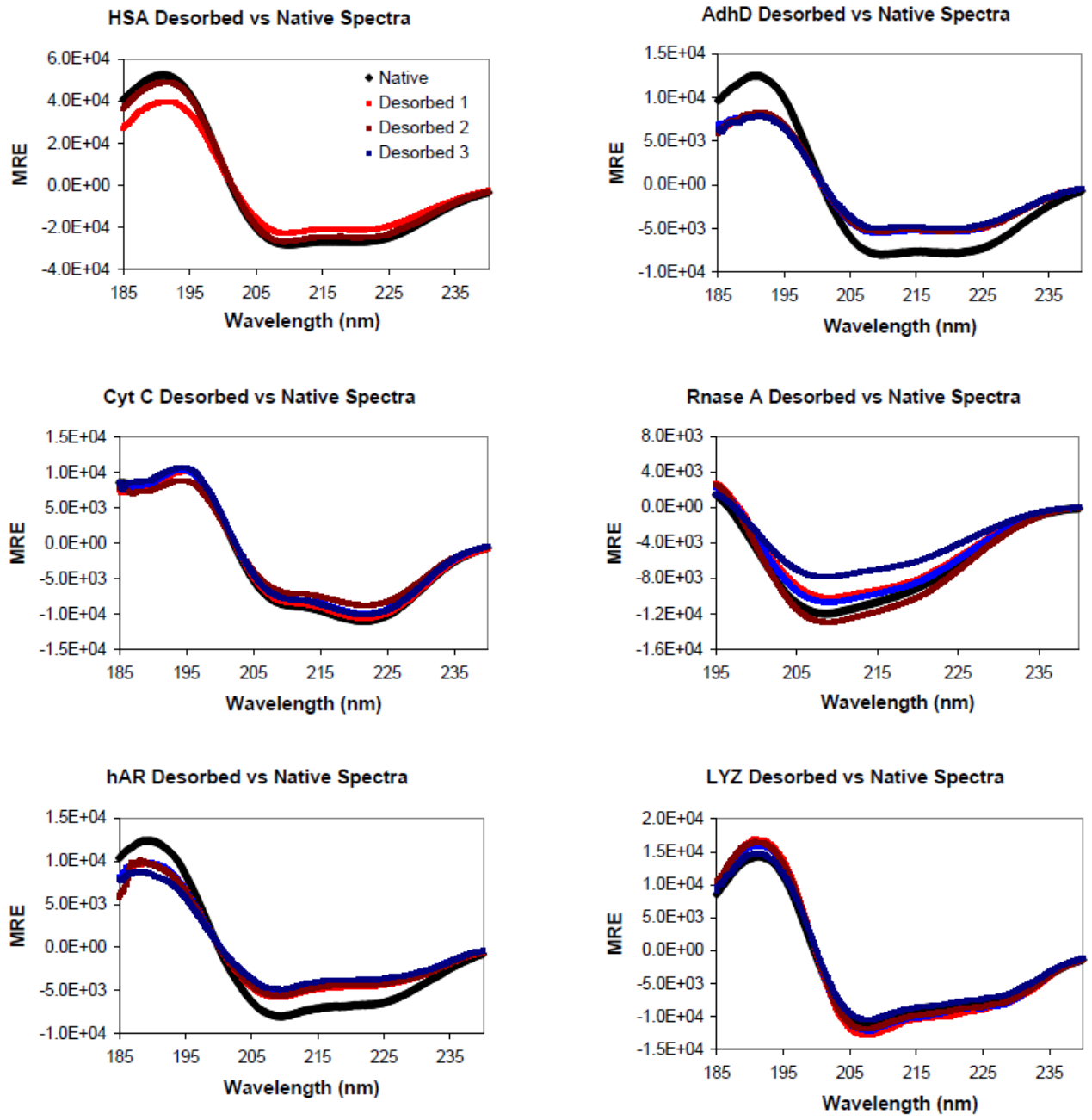

Figure 5-9 Far –UV CD spectra of desorbed and native protein

Black lines represent the native spectra, while the colored lines show adsorbed spectra at various levels of coverage

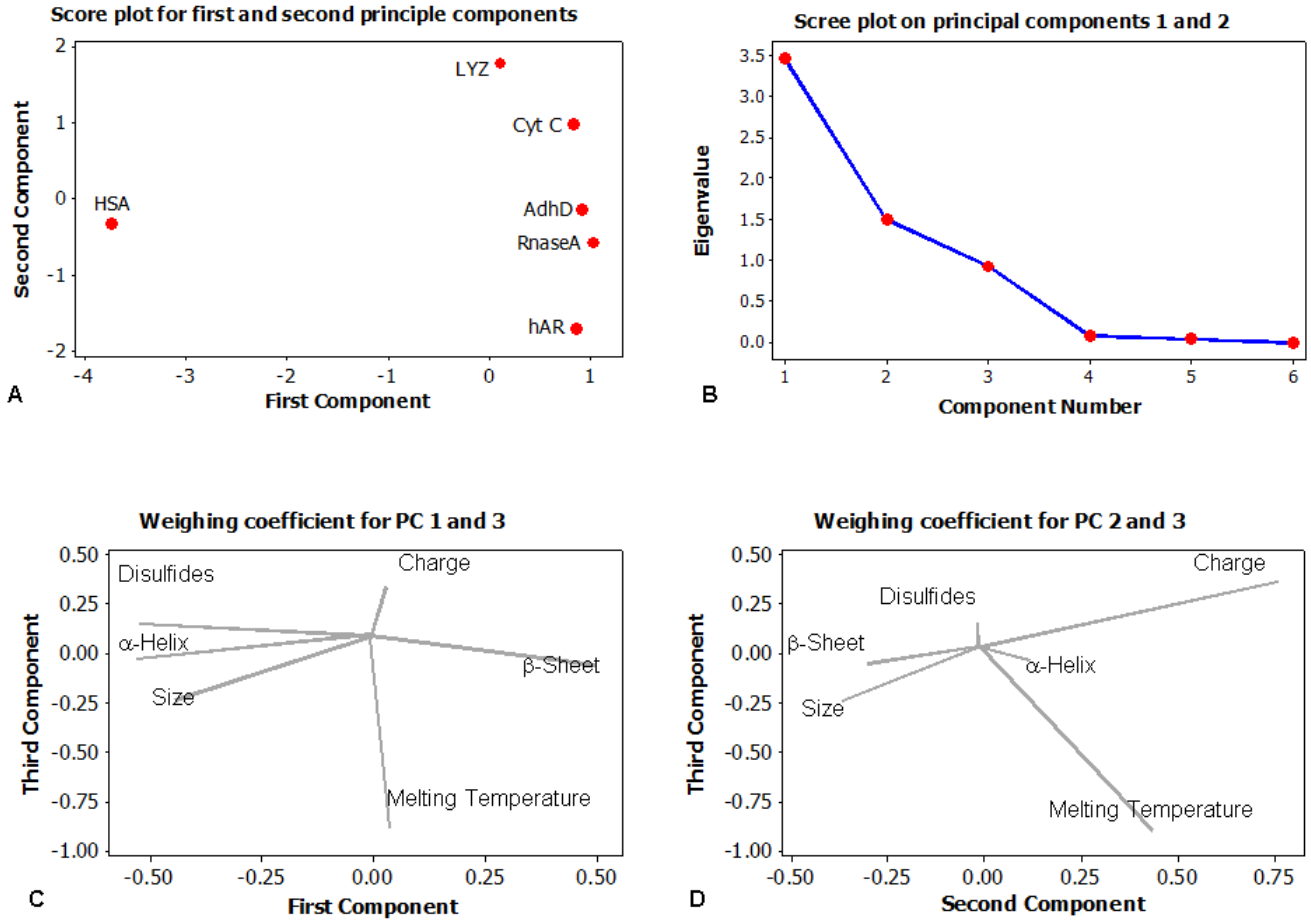

Figure 5-10 PCA scores and Scree plots for 1st, 2nd and 3rd principal components

(A) PCA scores of first two principal components, (B) Scree plot showing Eigenvalues of all six principal components, and relative weights of third principal components against (C) first and (D) second principle component

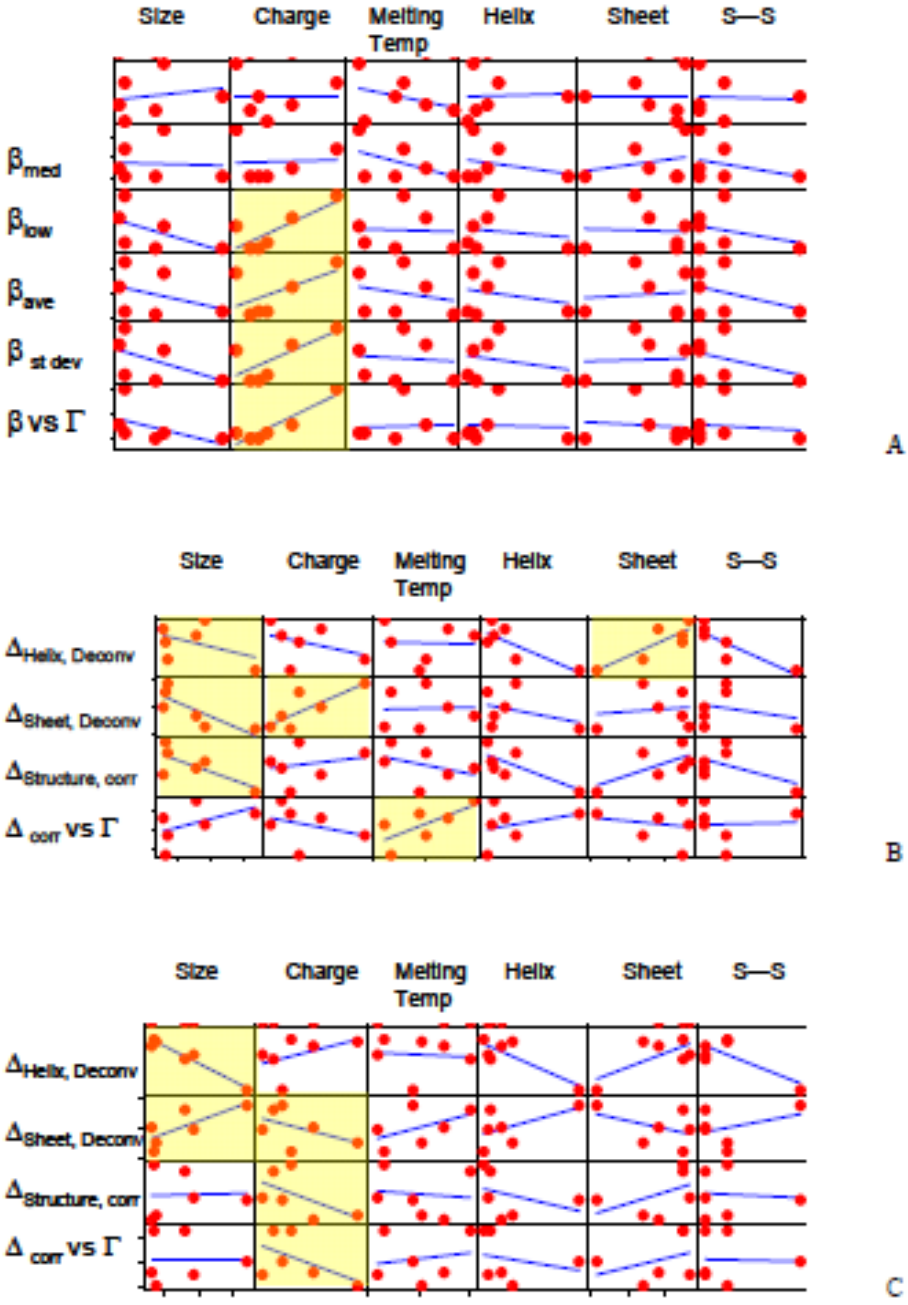

Figure 5-11 Correlation matrix of protein parameters

Correlation of input protein parameters to (A) Desorption behavior, (B) Adsorbed protein structure, and (C) Desorbed protein structure. Data sets with relatively high levels of correlation (evaluated visually) are highlighted in yellow. Each graph represents the comparison of the parameters defined by the column header (x-axis) and row header (y-axis).

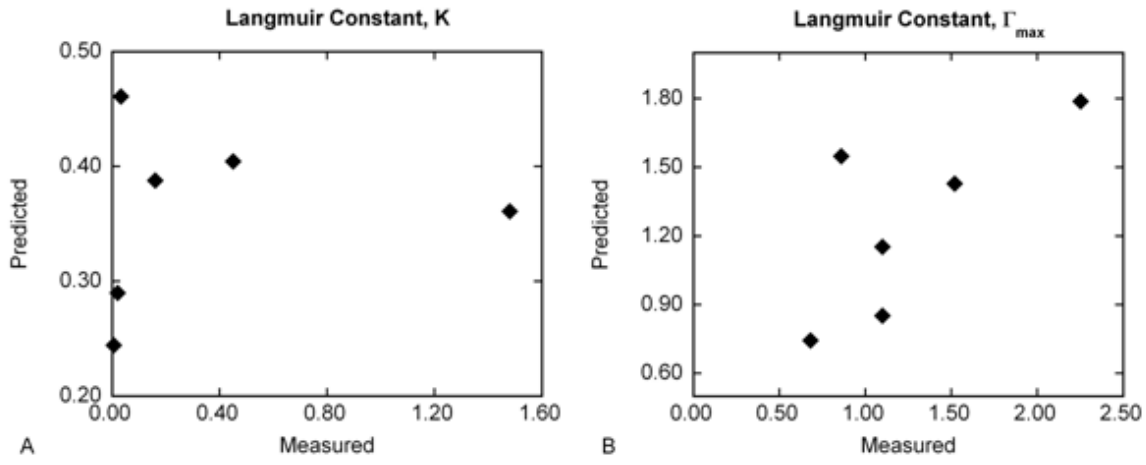

Figure 5-12 Predicted vs. actual values K and Γ_{max} using PCA model

Predicted vs. actual values for Principal Component Analysis model for (A) K and (B) Γ_{max}

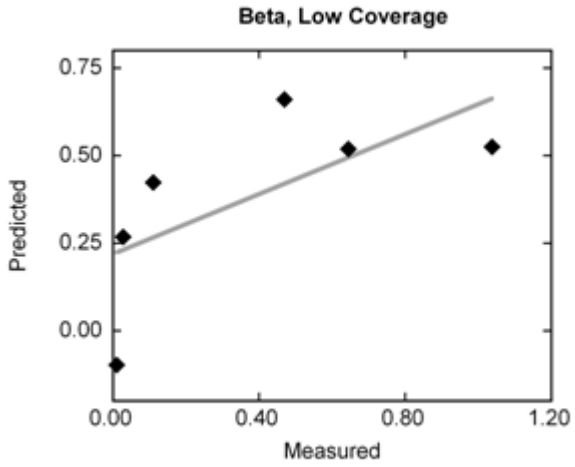

Figure 5-13 Predicted vs. actual values of low β from K and Γ_{max} model

CHAPTER 6. PERSPECTIVES, OUTLOOKS AND CONCLUSIONS

6.1. EXTENSION OF SYSTEM TO OTHER SURFACES

6.1.1. Introduction

The various surfaces which protein therapeutics encounter during drug manufacturing, storage, and delivery are highly diverse. The surfaces vary in their hydrophobicity, charge, morphology, roughness, and exposed functional groups. It has long been known that surface hydrophobicity plays an important role in the interfacial behavior of proteins. However, the impact of substrate hydrophobicity is difficult to study experimentally because varying this parameter is often coupled with changes in other parameters, such as surface charge [149]. Effects of surface hydrophobicities have been studied using latex nanoparticles [150] and gradient polymer surfaces [63]. While these methods have shown that increase in hydrophobicity causes higher levels of surface binding, adsorbed layer thickness and binding strength, less research has been done on understanding surface-induced structural perturbations and desorption kinetics. Here, we present feasibility studies aimed at extending the previously presented silica-based system to surfaces which have lower surface energies. We anticipate that reversible binding as well as refolding upon desorption will be less prevalent in these systems.

6.1.2. Approach and Methods

To evaluate surfaces which are more hydrophobic than the untreated silica nanoparticles, we screened various other surfaces, including functionalized gold, silica, poly(methyl methacrylate)

and polystyrene. Our ability to obtain a sharp (and experimentally uncomplicated) separation between the particles and the supernatant following adsorption, as well as CD-compatibility, led us to use polystyrene. We chose plain polystyrene spheres (Ref 2498, Bangs Laboratories, Fishers, IN) with a diameter of 290 nm to match the approximate size of the fumed silica particles from our previous studies. These polystyrene microspheres generally have highly hydrophobic surfaces. While surfactants are routinely added to stabilize the beads, we use surfactant-free suspensions for this study, and we demonstrate in Figure 6-1 that the mean particle diameter of this solution remained at 290 nm.

As received, the concentration of the suspensions was 10% polystyrene. The solution was too concentrated and yielded an unacceptable CD signal below a wavelength of 210 nm. We found that a 12x dilution with 10mM sodium phosphate buffer (pH=7) rendered the solution dilute enough to be compatible with the CD signal to 185 nm. We verified that the size distribution remained unaltered after this dilution. Therefore, 6x bulk solutions of the polystyrene were added to the protein solutions in a 1:1 ratio. To separate the particles out of solution required a 10-minute spin cycle at 13,000G. Otherwise, the same adsorption and desorption procedures were used as are outlined in the previous chapters. The stretched exponential function, as discussed in Section 5.3.12, is used to quantify the kinetics of desorption.

6.1.3. Results

In our initial set of experiments, we set out to compare the adsorption isotherm of lysozyme and human serum albumin (HSA) on silica vs. polystyrene. However, we found it challenging to create adsorption isotherms in a reproducible manner. Variation between replicates, within

various points along the isotherm, and between separate experiments were large, and prevented us from drawing conclusions about the adsorption behavior of these proteins on polystyrene.

We attempted to solve this issue by performing a two-part sonication on the polystyrene particles: once on the original 10% bulk solution, before performing the 6x dilution, and again on this diluted solution, immediately before aliquoting the particles into the adsorption samples. Each sonication step had a 6-minute run time with pulses of 5 seconds with a 5 second rest between each pulse. With this method, we improved our results. Before running full isotherms, we tested the supernatant concentration following centrifugation on select points along the isotherm (low, medium and high coverage). The decrease in sample-to-sample variability following this sonication step is evident from the data in Table 1-1, especially when using different polystyrene suspensions for setting up the isotherm samples. Improvements are further apparent in Figure 6-2 and 6-3, where we show the full adsorption isotherm of albumin and ribonuclease on polystyrene. We decided to conduct these studies with ribonuclease instead of lysozyme because this protein also represents a high-affinity binder (to silica), but it has a K value which is slightly less than that of lysozyme. If the polystyrene increases binding affinity, we will be able to detect this change, whereas we do not think we can discern such differences for lysozyme.

In Figure 6-2 and 6-3, we compare the adsorption isotherms of HSA and ribonuclease of each protein on polystyrene and silica, and in Table 6-1, we present the Langmuirian parameters of these systems. For both proteins, the adsorption isotherm has a significantly different shape with polystyrene than with silica. The maximum surface coverage increases several-fold in both cases, indicating that more protein binds to the polystyrene surface, perhaps due to the formation of

multiple layers. Because the isotherms do not reach a plateau, this also supports the multiple layer hypothesis. From Table 6-2, we see that the K value for HSA increases slightly for polystyrene and by an order of magnitude for ribonuclease. This result is somewhat unexpected: we originally hypothesized that the binding affinity of the protein to the surface would increase with hydrophobicity. One explanation for this behavior is an incomplete separation of the adsorbed from non-adsorbed protein. If some protein/particle complexes remain in the supernatant, the measured concentration would be artificially increased, thus leading to lower adsorbed amount calculations.

Next, we evaluate the desorption of HSA from polystyrene. Figure 6-4 shows this data in terms of surface coverage, while Figure 6-6 depicts the raw kinetic data. In the first graph, we see a significant difference in the desorption behavior of HSA between silica and polystyrene. First, we observe that overall desorbed amounts are an order of magnitude less for polystyrene than silica. While desorption kinetics progress slowly with silica and do not reach equilibrium even after 2 weeks, the polystyrene data achieve adsorption-level values even after the first time point of 16 hours at all three surface coverages. This behavior is captured in terms of the stretched exponential parameter, β, in Table 6-3. At high and medium coverages, the difference between the parameters is several orders of magnitude. This indicates that desorption of HSA from polystyrene has less time-dependence than desorption from silica. While previous studies have found decreased levels of elutability on hydrophobic surfaces [107], our results indicate that the adsorbed layer that is created is significantly different between the two surfaces. It is possible that in the case of polystyrene, protein which has no surface attachment is contributing to the relatively fast desorption kinetics. The large error bars associated with the desorption data also

indicate that more method development is needed to improve the accuracy of detecting desorbed concentration in this system.

For ribonuclease, Figure 6-5 and 6-7 show the surface coverage and raw kinetic data, respectively, for polystyrene. While desorbed amounts are also about an order of magnitude lower for the polystyrene system, from Figure 6-5 we find that the desorption kinetics have similar levels of time-dependence for the two surfaces. The β parameters in Table 6-3 show that there is about one order of magniture difference between their time-depence. As with HSA, the polystyrene system exbihits lower levels of time dependece.

6.1.4. Conclusions

Future experiments include structural characterization of the surface-bound and desorbed protein. Comparing this data to previous results on silica may reveal interesting effects of hydrophobic surface adsorption. We hypothesize that two populations may emerge: one which belongs to the less strongly attached protein (perhaps protein which is bound to an already adsorbed layer and not directly to surface sites). This population may be subject to lower levels of structural perturbation as there is little contact with the surface. The second, tightly bound layer is likely to be more dramatically altered, and we suspect that native-like refolding may not occur for this population upon desorption.

Because many of the base substrates, as well as coatings, added to the surfaces of medical devices have lower surface energies than glass, it is crucial to understand what impact these surfaces have on proteins during desorption. While our current data suggest the structure of the adsorbed protein layer is significantly different between the two systems, we still need more

detailed information about how the integrity of the protein is impacted.

6.2. SYSTEM LIMITATIONS AND AREAS OF IMRPOVEMENT

6.2.1. Understanding the Effects of Surface Curvature

The silica particles we use in our studies consist of 250-300 nm aggregates which are made up of primary particles 14 nm in diameter [151]. The aggregates are at least an order of magnitude larger than the average dimensions of the proteins studied, while the individual monomers are several-fold larger. HSA is the largest protein we evaluate, with a maximum dimension of 8nm [152]. We make the assumption that from the perspective of the protein, the surface is "flat". However, we do not account for localized curvature effects stemming from the individual monomers.

Various studies have shown that surface curvature effects can significantly impact the secondary structure of adsorbing peptides [153]. One study found that for 5, 10 and 20 nm gold particles, secondary structure becomes more perturbed as curvature increases. On flat surfaces, the effect of adsorption is less prevalent [154]. The authors note that peptide rigidity may have a dominant impact on this effect. This implies that the effect of curvature is highly dependent upon intrinsic protein parameters such as molecular geometry and secondary structure. However, results are contradictory, as other studies find that adsorption-induced unfolding of lysozyme (a highly globular protein) is most dominant on the surface with least amount of curvature [90, 155].

The primary goal of our studies is to obtain direct comparison of the adsorption behavior of various proteins from the same surface. Our secondary goal is to use a surface that is

representative of what a protein would contact in a delivery/storage device. Use of the fumed silica nanoparticles satisfies these two goals. However, for more detailed insight into the effects of curvature, and a comparison of the surface morphology of the nanoparticles used in this system, and of typical surfaces in delivery devices, more surface characterization is needed.

6.2.2. Limitations of Structural Characterization

In Chapter 2-4, we present a method for evaluating the secondary structure of the protein in an adsorbed state and upon desorption, using the same technique. Once desorption is induced, measuring the CD spectra of a protein in a dissolved state was not challenging, as this is how CD is most often used for structural characterizations. However, to use this instrument to evaluate proteins in the adsorbed state was more challenging. Our ability to conduct such experiments limited the types of surfaces we could use, and *in situ* CD-compatibility dictated our particle selection criteria. We chose fumed silica nanoparticles which have been used successfully by the seminal studies of Norde and colleagues [22, 28, 90-93]. To expand upon and improve previous systems, we introduce an algorithm which allows us to evaluate the contribution of only the adsorbed populations to the CD signal. We have validated this approach, as discussed in Section 2.8.1. This novel approach allows us to extend the range of coverages evaluated to all regimes of the adsorption isotherm. However, using CD to evaluate secondary structure on the surface has limitations. First, we assume that the difference in CD spectra with and without particles is due to the restructuring of proteins when they adsorb to the surface. However, it is also possible that the changes we see in the CD spectra are due to difference in the environment sensed by the adsorbed protein compared to the protein in solution. Second, we are only able to capture global changes in secondary structure. When we observe variations in the spectra, we cannot discern

whether a specific population of bound protein is highly perturbed, or all bound protein is somewhat perturbed. These localized effects, which are valuable to understand the true nature of protein/surface interactions are lost. We do, however, feel that the helix-to-sheet transitions we observe on the surface are substantial enough that we can report these changes with confidence. Furthermore, the fact that we see no coverage-dependence of the adsorbed proteins gives a strong indication that the previous hypotheses about heterogeneity with respect to secondary structure as a function of coverage need to be reassessed. We also compare our assessment of the adsorbed structure of lysozyme on particles to similar studies conducted on flat surfaces with FTIR. As mention in Section 2.5, the values of loss in helix and gain in sheet structure are similar. Therefore, we have confidence in the large-scale structural transitions we measure, however, we emphasize that there may be specific surface-induced artifacts, as well as buried structural rearrangements we cannot measure.

6.2.3. Limitations of Desorption Studies

In Chapter 4, we present data on desorption kinetics. Two assumptions that we make are that the starting point of the desorption studies (following 16 hours of adsorption) is at thermodynamic equilibrium, and that the desorption process eventually returns to this same state. While we performed preliminary kinetic studies of lysozyme and HSA on silica to show that adsorption achieves an apparent steady state over the time course of 16 hours (and this conclusion is supported by research on other hydrophilic systems), we did not perform extensive kinetic studies beyond this timeframe. We also did not perform similar evaluations for the other proteins. Some of the results in Section 5.4.3, namely for HSA and lysozyme, indicate that even after allowing desorption to progress for two weeks, the system does not return to the post-adsorption

state. Specifically, for HSA, the adsorption curve is not yet reached (meaning less protein has desorbed than was anticipated for the steady state), and for lysozyme the desorption values overshoot the adsorption isotherm (meaning that higher amounts of proteins desorb). One explanation for these observations is that our assumption that our system has achieved thermodynamic equilibrium following 16 hours of adsorption is inaccurate. If this is the case, the data indicate two opposing effects. For HSA, the actual adsorption isotherm may be shifted to the left, meaning that even after 16 hours, protein continues to adsorb onto the surface. This may be caused by slow rearrangement of protein on the surface allowing more adsorption to occur. Because the adsorption isotherm achieves a plateau value, we believe this additional attachment does not present itself as multi-layer adsorption, but rather as higher levels of crowding and surface packing in a single monolayer. For lysozyme, it is possible that the adsorption curve shifts to the right at longer times. This would occur if protein which was originally adsorbed to the surface in the 16-hour timeframe eventually desorbs at longer times. This can also be explained by a slow rearrangement process, but in this case, the reorganization allows certain proteins to occupy greater surface area, causing other proteins to detach. Given that lysozyme has the most favorable electrostatic interaction with the surface, it is possible that initially more proteins are drawn to the surface by charge interactions and other effects dominate, such as formation of higher number of surface attachments at longer time scales.

We must also acknowledge that while our current technique allows us to confidently compare general desorption trends between proteins, and it allows us conclude that all proteins have a tendency to return back to a steady state or quasi-steady state, our method of measuring desorption on particles using the depletion method are not as sensitive as some other methods on

flat surfaces. Ellipsometry [17, 156, 157], isothermal titration calorimetry [158], quartz crystal microbalance [159, 160], and total internal reflection fluorescence microscopy [161, 162] may allow more sensitive desorption data to be collected on flat surfaces. We limit our assessment of desorption to reporting only the β value from the stretched exponential, but with these other techniques, the time and rate constant may also be reported. Furthermore, some of the errors associated with these β values, as well as error bars on the raw desorption data seen in Sections 4.35.4 and 6.1.3 may be decreased.

6.2.4. Applicability of Langmuir Isotherm

The validity of the Langmuir isotherm to model protein adsorption remains an open question. Various other isotherm models, including the linear, Fowler, Freundlich, Freundlich–Langmuir and bi-Langmuir, have been applied to model adsorption at the solid/liquid interface [163]. Most of these other models are empirical and not all have theoretical derivations. The Langmuir model is the one that is most often used due to its simplicity and good agreement with the data [163]. Often, however, the Langmuir equation is erroneously applied to systems which are not at equilibrium, and the K value is used to represent the equilibrium binding constant. We demonstrate reversibility in our systems, and therefore confidently use the Langmuir equation as a tool to compare binding affinity of proteins as well as their maximum surface coverage. In our data, we see specific cases where the Langmuir model fits some data better than others. As a general rule, in the case of extremes (particularly high or low affinity binders) the Langmuir fit deviates slightly from specific subsets of data, such as the transition region between the plateau and rising protein of the isotherm. Proteins such as HSA and RNase which are neither very high- nor very low-affinity binders, seem to have the best fits, as is supported by small root mean

square error term in Table 5-2.

6.3. FUTURE STUDIES

6.3.1. Expansion of Predictive Models

In Chapter 4, we present a framework for using various intrinsic protein parameters, along with the Langmuirian parameters, to predict time scales associated with desorption and surface-induced structural transitions. This approach would allow the ability to model and predict the behavior of complex adsorption phenomena from easily measured parameters. However, these models must be tested on various systems and the accuracy of the prediction must be validated. A controlled system, where specific parameters are tested in isolation, such as the supercharged GFP system presented in Chapter 5, would be a logical way to begin testing the predictive power of our models. Also, adding other intrinsic protein parameters into the system, such as measure of surface energy, or a more accurate measure of surface potential, may improve the predictability of the model.

6.3.2. Evaluation of More Pharmaceutically Relevant Systems

We present in this research a model system which simulates certain aspects of our actual system of interest: biologically active proteins interacting with storage and delivery devices. The surface we use represents bare, uncoated glass, which is a widely used base substrate in vials and syringes. Our experimental parameters target various surface coverages, of which the high-plateau levels best capture the protein/surface area ratios present in such a system. We also induce desorption in a manner similar to what protein stored in containers for extended time

periods would experience. However, there are various ways in which we could further develop our model so that it is an even more realistic representation of our system of interest. One area of improvement would be to study the adsorption and desorption behavior of more complex proteins, such as antibodies or immunoglobulins. These proteins are larger, have more complex structural characteristics, and have been engineered at length to withstand the destabilizing effects of the drug manufacturing processes. Similarly, studying other therapeutically relevant peptides, such as insulin and human-growth hormone would also be of interest as their prevalence in prefilled systems is growing. Only a handful of studies have assessed the interfacial behavior of biologics [156, 162-166].

6.4. ASPECTS OF ADSORPTION RELATED TO PROTEIN THERAPEUTICS

6.4.1. Protein and Surface Engineering Opportunities

As technological capabilities to engineer materials with very specific properties are advancing, the ability to incorporate surfaces into protein delivery systems which have minimal effects on protein is possible. It has been shown that surfaces can be engineered to control specific adsorption-related attributes, such as the rigidity of the adsorbed protein layer [167], biological activity of attached proteins [168] and adsorption patterns [155].

Adsorption resistance can also be engineered into the protein itself. While improving the structural stability of proteins to reduce their surface activity is one way to achieve this, we show in Chapter 3 that even highly thermostable proteins are susceptible to adsorption-induced structural perturbation. More promising approaches include attaching oligosaccharides [169],

polyethylene glycol [170] or fatty acid chains [171] to proteins to avoid adsorption through steric hinderance mechanisms. Another approach which can either prevent or achieve specific levels of adsorption, depending on the constructs used, involves the insertion of very specific amino acid sequences into parts of the protein which are likely to be highly attracted or repelled by the surface, such as highly localized charge or hydrophobicity patches. [99] Tethering proteins to achieve specific orientations on the surface is also a promising way to control interfacial behavior. [172]

In Chapters 4 and 5, we evaluate the role of electrostatic effects in influencing adsorption and desorption behaviors. From our assessment of the various protein parameters through the principal component analysis, we see the second principal component is dominated by electrostatics. Because protein and substrate surface charge is strongly influenced by the aqueous environment, altering solution conditions provides a more simplistic strategy to influence the protein's interfacial behavior, than by modifying either the protein or surface. Our results support the idea that significant levels of control can be exerted upon adsorption behavior by modifying the aqueous environment of an interfacial system. Making subtle changes in the dielectric properties of the protein formulation with the specific intent to control adsorption behavior is an area for research.

6.4.2. Newly Emerging Applications of Protein Adsorption

Various new, innovative applications of protein adsorption are emerging. In vaccine delivery, proteins are adsorbed to adjuvant by design, as a way to achieve controlled release and to modify the antigen's immunogenicity [153]. For example, in products such as Adju-Phos® and

Alhydrogel®, certain regulatory agencies require 80% of the vaccine to be adsorbed to adjuvants [153, 173]. In other fields, such as in designing diagnostic systems and biosensors, new innovations are emerging for greater control over protein adsorption [174].

6.5. SUMMARY

Proteins encounter solid/liquid interfaces in a wide range of applications. In many cases, such as with therapeutic agents, the adsorption process and adsorption-induced consequences must be well understood and controlled. Unfavorable outcomes must be regulated. While protein adsorption has been studied comprehensively over the past 40 years, and much is understood about various aspects of the interfacial behavior of proteins, it remains difficult to link the existing knowledge to pharmaceutically relevant system [153].

Our strategy is to expand the traditional design space of protein adsorption studies to target a wider range of surface coverages, longer desorption time scales and proteins with unique characteristics, so as to gain more insight into this system of interest. Furthermore, a more global goal of this research is to further our understanding about the factors affecting protein adsorption and desorption and the interplay between various adsorption-related subprocesses.

We begin by evaluating a simple system: lysozyme adsorption to silica. Although such a system has been studied extensively in the past, we gain new insight into the impact of surface coverage and surface-induced structural transitions on adsorption reversibility. Despite significant levels of structural unfolding on the surface, the adsorption of lysozyme is reversible. Furthermore, we find that the Langmuirian adsorption parameters can also be used to describe desorption behavior.

Building upon our results for lysozyme, we postulate that observed adsorption/desorption behavior was strongly influenced by either the high level of intrinsic stability of the protein or the favorable protein/surface charge interaction. We design two unique systems to test both hypothesis. To explore the relationship between stability and adsorption, we use two naturally occurring stability variants from the aldo-keto reductase superfamily. Surprisingly, we find little correlation between the protein's thermostability, surface-affinity and susceptibility to surface-induced unfolding. Our results question the idea that thermal stability is an accurate predictor of adsorption behavior. To evaluate the role of electrostatics in protein adsorption we use supercharged GFP variant. In this system, we do find that protein/surface affinity and desorption kinetics are strongly impacted by electrostatic interactions. These results highlight the more dominant role of electrostatics, compared to intrinsic structural stability, in determining protein interfacial behavior.

Finally we seek to reach some general conclusions about the reversibility of proteins on silica. Our results refute the widely accepted notion that due to the complex, multi-segment binding of proteins and surface-induced unfolding, protein adsorption is a thermodynamically irreversible process. We find that all proteins we evaluate exhibit reversible binding and structural refolding. Our results indicate that the relationship between protein parameters and adsorption-induced outcomes is an intricate, multivariate relationship where no single parameter dominates. We also reveal new similarities between protein and polymer adsorption mechanisms and find interesting insight into the heterogeneity of the adsorbed protein layer. Finally, we develop a framework for predicting protein desorption behavior. Such new insight can be invaluable when designing systems where interfacial behavior must be strictly regulated.

6.6. FIGURES AND TABLES

	CV within study		CV between suspensions	
C_{SN} (mg/mL)	with sonication	without sonication	with sonication	without sonication
3.30	2%	5%	2%	11%
1.50	4%	5%	6%	16%
0.70	3%	4%	3%	12%

Table 6-1 Repeatability of polystyrene adsorption studies

Coefficient of variance is reported for replicates within a single study (left side of table) and between samples in separate studies (in which different suspensions of polystyrene were used to aliquotting).

	Silica		Polystyrene	
	K (mg/mL)	Γ_{max} (mg/m^2)	K (mg/mL)	Γ_{max} (mg/m^2)
HSA	0.45 (0.10)	0.68 (0.07)	0.77 (0.28)	2.8 (0.3)
Rnase	0.16 (0.04)	0.86 (0.03)	2.0 (0.86)	4.3 (1.2)

Table 6-2 Comparison of Langmuirian adsorption parameters between silica and polystyrene

K and Γ_{max} parameters for human serum albumin and ribonuclease A adsorption on silica (left) and polystyrene (right). Averages of from separate experiments for silica, and for separate replicates within the same experiments for polystyrene provided, as well as standard deviations in parentheses

		β_{high}	β_{med}	β_{low}
HSA	Polystyrene	8.1E-04	2.6E-07	7.0E-03
	Silica	1.6E-02	2.9E-02	2.8E-02
RNase	Polystyrene	1.0E-04	-4.3E-03	2.7E-03
	Silica	2.1E-03	1.8E-02	5.7E-02

Table 6-3 β values for desorption for albumin and ribonuclease on polystyrene and silica

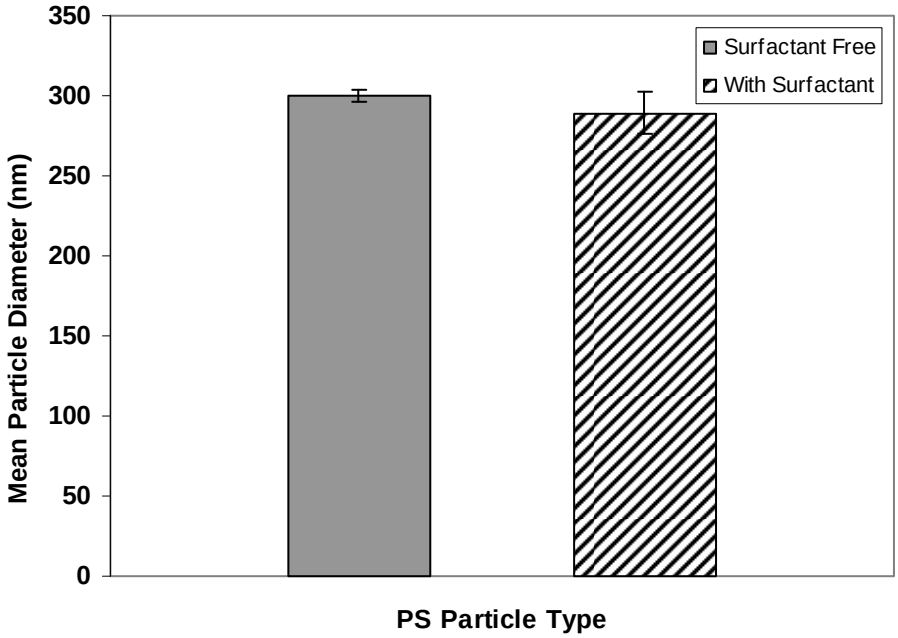

Figure 6-1 Mean particle diameter of polystyrene suspensions with and without surfactant

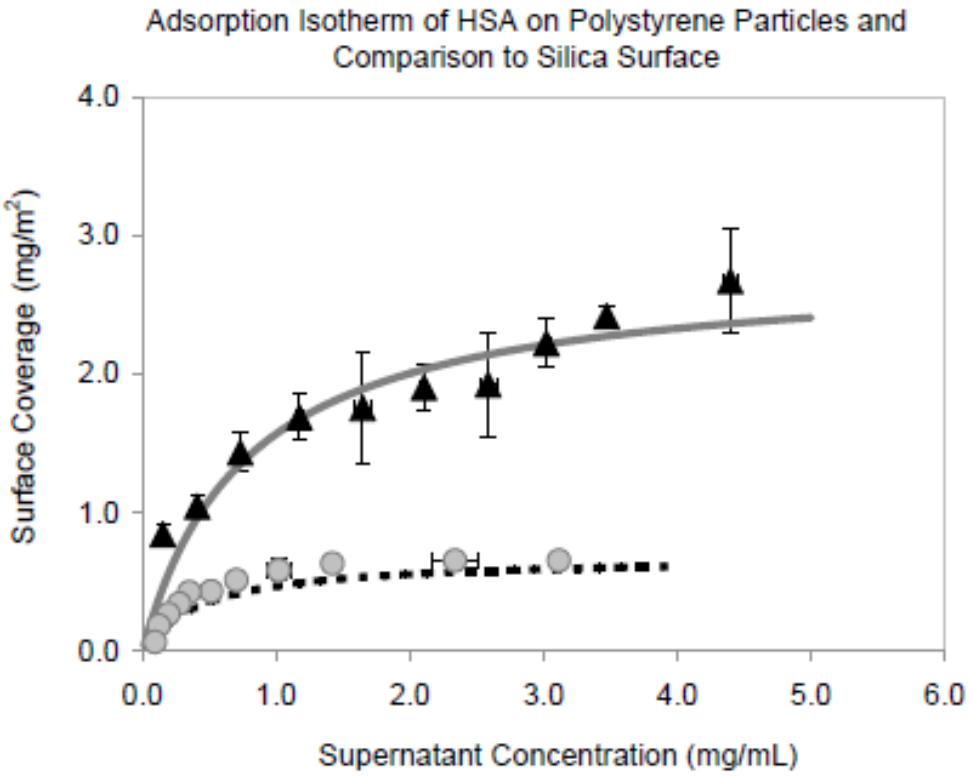

Figure 6-2 Adsorption isotherms of albumin on polystyrene and silica

Adsorption values for RNase on 290 nm polystyrene particles (▲) and 290 nm silica particles (●). Error bars represent the average of three separate replicate, and lines represent the Langmuir fit for polystyrene (solid) and silica (dashed).

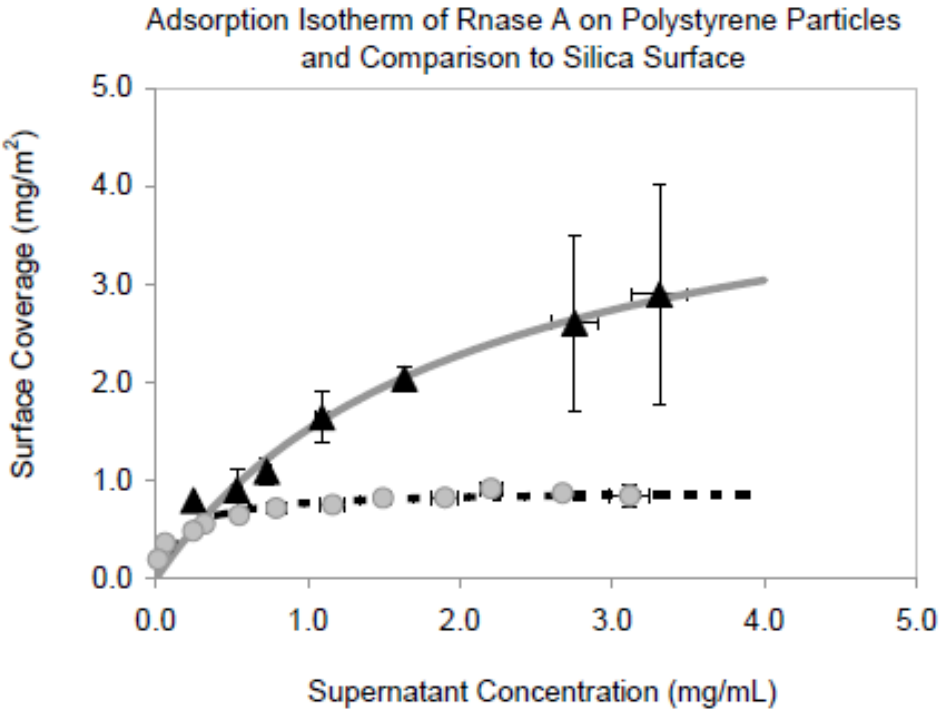

Figure 6-3 Adsorption isotherms of ribonuclease on polystyrene and silica

Adsorption values for HSA 290 nm polystyrene particles (▲) and 290 nm silica particles (●). Error bars represent the average of three separate replicate, and lines represent the Langmuir fit for polystyrene (solid) and silica (dashed).

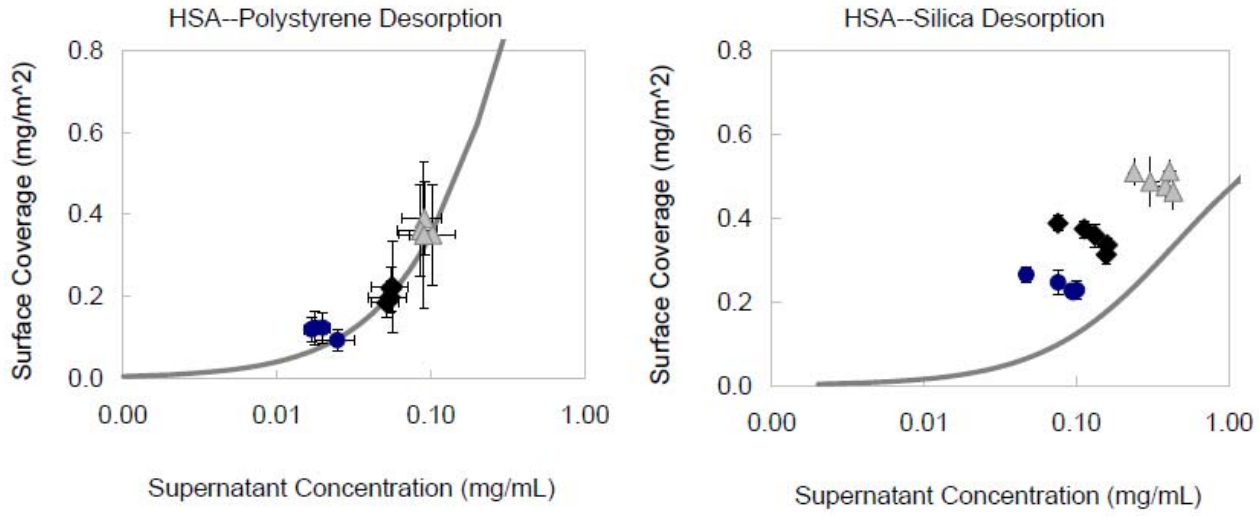

Figure 6-4 Comparison of desorption behavior between polystyrene and silica for albumin

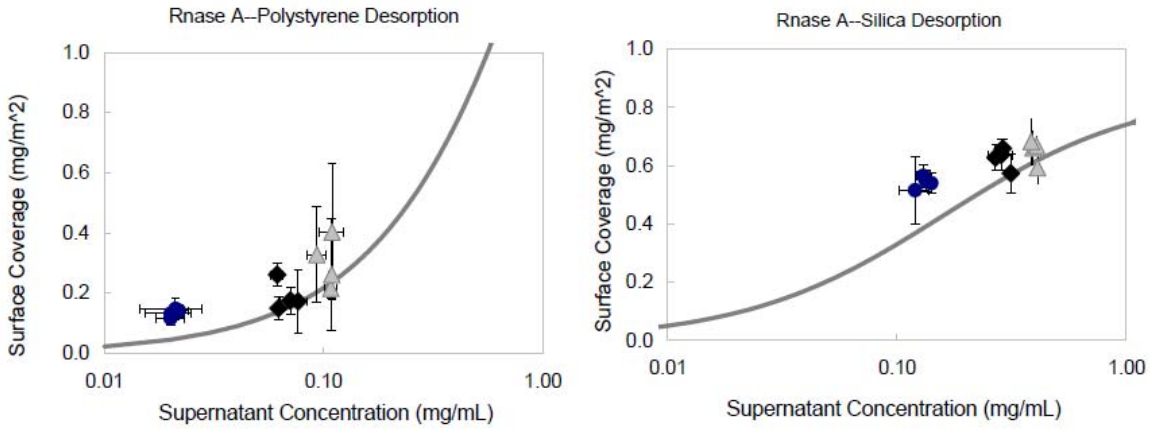

Figure 6-5 Comparison of desorption between polystyrene and silica for ribonuclease

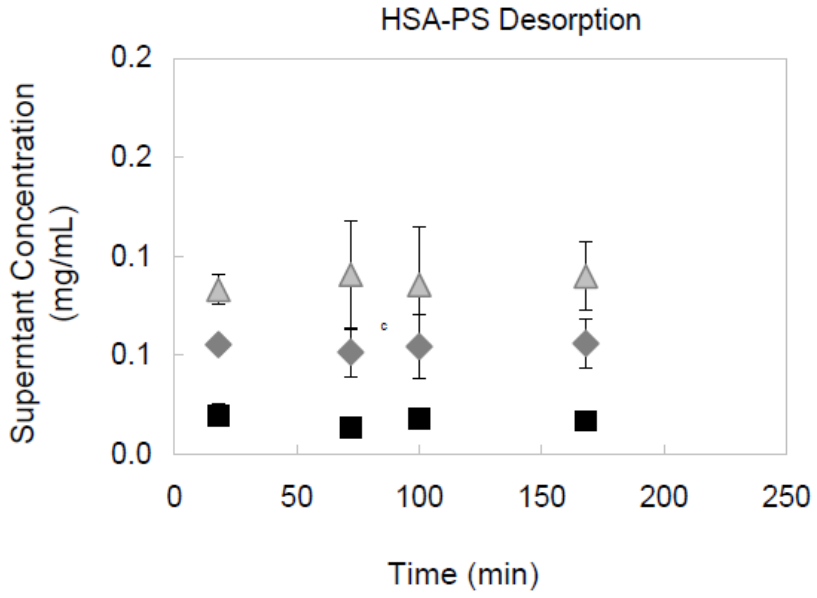

Figure 6-6 Desorption kinetics of albumin from polystyrene

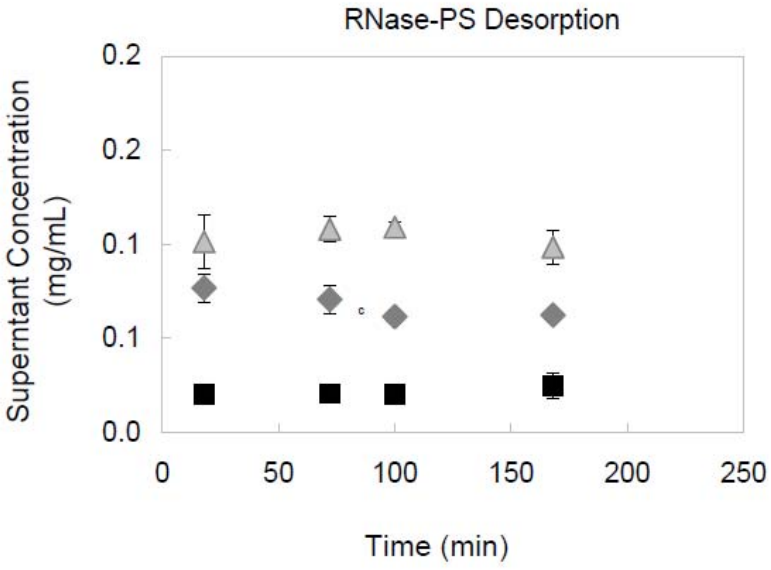

Figure 6-7 Desorption kinetics of ribonuclease from polystyrene

CHAPTER 7. REFERENCES

1. Leader, B., Q.J. Baca, and D.E. Golan, *Protein therapeutics: a summary and pharmacological classification.* 2008. **7**: p. 21-39.

2. Chaubal, M.V. and T.J. Roseman, *Drug delivery trends for parenteral therapeutics.* Drug Delivery System, 2006. **21**(4): p. 388-397.

3. Reichert, J.M., *Trends in development and approval times for new therapeutics in the United States.* Nat Rev Drug Disc, 2003. **2**(9): p. 695-702.

4. Zhou, X.H. and A. Li Wan Po, *Peptide and protein drugs. I, Therapeutic applications, absorption and parenteral administration.* International journal of pharmaceutics, 1991. **75**(2-3): p. 97-115.

5. Tan, J.S. and P.A. Martic, *Protein adsorption and conformational change on small polymer particles.* Journal of Colloid and Interface Science, 1990. **136**(2): p. 415-431.

6. Frokjaer, S. and D.E. Otzen, *Protein drug stability: a formulation challenge.* Nature Reviews Drug Discovery, 2005. **4**(4): p. 298-306.

7. Chi, E.Y., et al., *Physical stability of proteins in aqueous solution: mechanism and driving forces in nonnative protein aggregation.* Pharm Res, 2003. **20**(9): p. 1325-36.

8. Manning, M.C., K. Patel, and R.T. Borchardt, *Stability of protein pharmaceuticals.* Pharm Res, 1989. **6**(11): p. 903-18.

9. Norde, W., *Energy and Entropy of Protein Adsorption* Journal of Dispersion Science and Technology, 1992. **13**(4): p. 363-377.

10. MacRitchie, F. and A.E. Alexander, *Kinetics of adsorption of proteins at interfaces.* J. Colloid Sci, 1963. **18**: p. 453–458.

11. Bentaleb, A., et al., *Kinetics of the homogeneous exchange of lysozyme adsorbed on a titanium oxide surface.* Langmuir, 1997. **13**(4): p. 729-735.

12. Ball, V., P. Schaaf, and J.C. Voegel, *Biopolymers at interfaces.* 1998.

13. Horbett, T.A., et al., *Proteins at interfaces II: fundamentals and applications*. 1995: American Chemical Society Washington, DC.

14. Soderquist, M.E. and A.G. Walton, *Structural changes in proteins adsorbed on polymer surfaces.* J. Colloid Interface Sci, 1980. **75**(2): p. 386–397-386–397.

15. Vermonden, T., C.E. Giacomelli, and W. Norde, *Reversibility of Structural Rearrangements in Bovine Serum Albumin during Homomolecular Exchange from AgI Particles.* Langmuir, 2001. **17**(12): p. 3734-3740.

16. Dillman, W.J. and I.F. Miller, *On the adsorption of serum proteins on polymer membrane surfaces.* J. Colloid Interface Sci., 1973. **44**: p. 221-241.

17. Karlsson, M., et al., *Reduction of irreversible protein adsorption on solid surfaces by protein engineering for increased stability.* J Biol Chem, 2005. **280**(27): p. 25558-25558.

18. Billsten, P., et al., *Adsorption to silica nanoparticles of human carbonic anhydrase II and truncated forms induce a molten-globule-like structure.* Febs Letters, 1997. **402**(1): p. 67-72.

19. Bower, C.K., et al., *Activity losses among T4 lysozyme charge variants after adsorption to colloidal silica.* Biotech and Bioeng, 1999. **64**(3): p. 373-376.

20. Brandes, N., et al., *Adsorption-induced conformational changes of proteins onto ceramic particles: Differential scanning calorimetry and FTIR analysis.* Journal of Colloid and Interface Science, 2006. **299**(1): p. 56-69.

21. Giacomelli, C.E. and W. Norde, *Conformational changes of the amyloid beta-peptide (1-40) adsorbed on solid surfaces.* Macromolecular Bioscience, 2005. **5**(5): p. 401-407.

22. Lundqvist, M., I. Sethson, and B.H. Jonsson, *Protein adsorption onto silica nanoparticles: conformational changes depend on the particles' curvature and the protein stability.* Langmuir, 2004. **20**(24): p. 10639-10647.

23. Norde, W., *Adorption of Proteins at Solid-Liquid Interfaces.* Cells and Materials, 1995. **5**(1): p. 97-112.

24. Castillo, E.J., J.L. Koenig, and J.M. Anderson, *Characterization of Protein Adsorption on Soft Contact-Lenses .1. Conformational-Changes of Adsorbed Human-Serum Albumin.* Biomaterials, 1984. **5**(6): p. 319-325.

25. McMillin, C.R. and A.G. Walton, *A circular dichroism technique for the study of adsorbed protein structure.* J. Colloid Interface Sci., 1974. **48**: p. 345-349.

26. Sethuraman, A., et al., *Protein unfolding at interfaces: slow dynamics of alpha-helix to beta-sheet transition.* Proteins, 2004. **56**(4): p. 669-78.

27. Norde, W., *Adsorption of Proteins from Solution at the Solid-Liquid Interface.* Adv Coll Int Sci 1986. **25**(4): p. 267-340.

28. Norde, W. and J.P. Favier, *Structure or adsorbed and desorbed proteins.* Colloids and Surfaces, 1992. **64**(1): p. 87-93.

29. Kondo, A., et al., *Kinetic and circular dichroism studies of enzymes adsorbed on ultrafine silica particles.* Appl Microbiol Biotechnol, 1993. **39**(6): p. 726-31.

30. Giacomelli, C.E. and W. Norde, *The adsorption-desorption cycle. Reversibility of the BSA-silica system.* Journal of Colloid and Interface Science, 2001. **233**(2): p. 234-240.

31. Billsten, P., et al., *Conformation of human carbonic anhydrase II variants adsorbed to silica nanoparticles.* Langmuir, 1999. **15**(19): p. 6395-6399.

32. Maste, M.C.L., W. Norde, and A. Visser, *Adsorption-induced conformational changes in the serine proteinase savinase: A tryptophan fluorescence and circular dichroism study.* Journal of Colloid and Interface Science, 1997. **196**(2): p. 224-230.

33. Norde, W. and C.E. Giacomelli, *BSA structural changes during homomolecular exchange between the adsorbed and the dissolved states.* J Biotechnol, 2000. **79**(3): p. 259-68.

34. Kondo, A. and H. Fukuda, *Effects of adsorption conditions on kinetics of protein adsorption and conformational changes at ultrafine silica particles.* Journal of Colloid and Interface Science, 1998. **198**(1): p. 34-41.

35. Kondo, A., S. Oku, and K. Higashitani, *Structural changes in protein molecules adsorbed on ultrafine silica particles.* J Coll Int Sci, 1991. **143**(1): p. 214-221.

36. Giacomelli, C.E. and W. Norde, *Influence of hydrophobic Teflon particles on the structure of amyloid beta-peptide.* Biomacromol, 2003. **4**(6): p. 1719-1726.

37. Kondo, A., F. Murakami, and K. Higashitani, *Circular-Dichroism Studies on Conformational-Changes in Protein Molecules Upon Adsorption on Ultrafine Polystyrene Particles.* Biotechnology and Bioengineering, 1992. **40**(8): p. 889-894.

38. Haynes, C.A. and W. Norde, *Structures and Stabilities of Adsorbed Proteins.* J Coll Int Sci, 1995. **169**(2): p. 313-328.

39. Haynes, C.A., et al., *Exploring Adsorbed Protein Conformations and Rotational Mobilities through Microcalorimetry and Raman-Spectroscopy.* Abstracts of Papers of the American Chemical Society, 1994. **207**: p. 161.

40. Vermeer, A.W.P., M. Bremer, and W. Norde, *Structural changes of IgG induced by heat treatment and by adsorption onto a hydrophobic Teflon surface studied by circular dichroism spectroscopy.* Biochimica Et Biophysica Acta-General Subjects, 1998. **1425**(1): p. 1-12.

41. Zoungrana, T., G.H. Findenegg, and W. Norde, *Structure, stability, and activity of adsorbed enzymes.* J Coll Int Sci, 1997. **190**(2): p. 437-448.

42. Morrissey, B.W. and R.R. Stromberg, *The conformation of adsorbed blood proteins by infrared bound fraction measurements.* J. Colloid Interface Sci, 1974. **46**(1): p. 152-1.

43. Koutsoukos, P.G., W. Norde, and J. Lyklema, *Protein adsorption on hematite(a-Fe2O3) surfaces.* Journal of Colloid and Interface Science, 1983. **95**(2): p. 385-397.

44. Ball, A. and R.A.L. Jones, *Conformational changes in adsorbed proteins.* Langmuir, 1995. **11**(9): p. 3542-3548.

45. Lu, D.R. and K. Park, *Effect Of Surface Hydrophobicity On The Conformational Changes Of Adsorbed Fibrinogen.* Journal of Colloid and Interface Science, 1991. **144**(1): p. 271-281.

46. Page, C., et al., *Development of a lyophilization formulation that preserves the biological activity of the platelet-inducing cytokine interleukin-11 at low concentrations.* Journal of Pharmacy and Pharmacology, 2000. **52**(1): p. 19-26.

47. Tzannis, S.T., et al., *Adsorption of a Formulated Protein on a Drug Delivery Device Surface.* Journal of Colloid and Interface Science, 1997. **189**(2): p. 216-228.

48. Douglas, J.F., H.E. Johnson, and S. Granick, *A Simple Kinetic-Model of Polymer Adsorption and Desorption.* Science, 1993. **262**(5142): p. 2010-2012.

49. Johnson, H.E., J.F. Douglas, and S. Granick, *Topological influences on polymer adsorption and desorption dynamics.* Physical review letters, 1993. **70**(21): p. 3267-3267.

50. Lee, S.H. and E. Ruckenstein, *Adsorption of proteins onto polymeric surfaces of different hydrophilicities: a case study with bovine serum albumin.* Journal of Colloid and Interface Science, 1988. **125**(2): p. 365-379.

51. McGuire, J., M.C. Wahlgren, and T. Arnebrant, *The Influence of Net Charge and Charge Location on the Adsorption and Dodecyltrimethylammonium Bromide-Mediated Elutability of Bacteriophage-T4 Lysozyme at Silica Surfaces.* Journal of Colloid and Interface Science, 1995. **170**(1): p. 193-202.

52. Hibbert, D.B., J.J. Gooding, and P. Erokhin, *Kinetics of irreversible adsorption with diffusion: Application to biomolecule immobilization.* Langmuir, 2002. **18**(5): p. 1770-1776.

53. Kozak, D., A. Chen, and M. Trau, *Profiling protein-surface interactions of multicomponent suspensions via flow cytometry.* Langmuir, 2008. **24**(4): p. 1204-11.

54. Nakamura, K. and K. Matsumoto, *Adsorption behavior of BSA in microfiltration with porous glass membrane.* Journal of Membrane Science, 1998. **145**(1): p. 119-128.

55. Bagchi, P. and S.M. Birnbaum, *Effect of pH on the adsorption of immunoglobulin G on anionic poly(vinyltoluene) model latex particles.* Journal of Colloid and Interface Science, 1981. **83**(2): p. 460-478.

56. Ball, V., et al., *Dynamic aspects of protein adsorption onto titanium surfaces: Mechanism of desorption into buffer and release in the presence of proteins in the bulk.* Langmuir, 1996. **12**(6): p. 1614-1621.

57. Baszkin, A. and D.J. Lyman, *The interaction of plasma proteins with polymers. I. Relationship between polymer surface energy and protein adsorption/desorption.* Journal of Biomedical Materials Research, 1980. **14**(4): p. 393-403.

58. Barroug, A., J. Lemaitre, and P.G. Rouxhet, *Lysozyme on apatites: A model of protein adsorption controlled by electrostatic interactions.* Colloids and Surfaces A, 1989. **37**: p. 339-355.

59. Romacker, M., T. Shoenknecht, and R. Forster, *The rise of prefilled syringes from niche product to primary container of choice: a short history.* On Drug Delivery, 2008. **4**: p. 4-5.

60. French, D., *Market trends in Injection Devices for Pharmaceuticals.* Future Trends in Drug Delivery, 2006. **June**: p. 20-24.

61. Overcashier, D., E. Chen, and S. Hsu, *Technical considerations in the development of prefilled syringes for protein products. American Pharmaceutical Review*, 2006. **9**(7): p. 77-83.

62. Treuheit, M.J., A.A. Kosky, and D.N. Brems, *Inverse relationship of protein concentration and aggregation.* Pharm Res, 2002. **19**(4): p. 511-6.

63. Lewis, D. and T. Whatley, *Adsorption of enzymes at the soli-liquid interface I. Trypsin on polystyrene latex.* Biomaterials, 1988. **9**(1): p. 71-75.

64. Griffiths, A.J.F., et al., *Introduction to genetic analysis*. 2005: WH Freeman.

65. Dobson, C.M., *Protein folding and misfolding.* Nature, 2003. **426**(6968): p. 884-890.

66. Andrade, J.D. and V. Hlady, *Protein adsorption and materials biocompatibility: a tutorial review and suggested hypotheses.* Adv. Polym. Sci, 1986. **79**(1): p. 1-63.

67. Bhaduri, A. and K.P. Das, *Proteins at solid water interface - A review.* J Disp Sci Tech, 1999. **20**(4): p. 1097-1123.

68. Gray, J.J., *The interaction of proteins with solid surfaces.* Curr Opin Struct Biol, 2004. **14**(1): p. 110-5.

69. Stuart, M.A.C., et al., *Adsorption of Ions, Polyelectrolytes and Proteins.* Adv Collo Inte Sci, 1991. **34**: p. 477-535.

70. Norde, W., et al., *Protein adsorption at solid-liquid interfaces: reversibility and conformation aspects.* J Coll Int Sci, 1986. **112**(2): p. 447-456.

71. Brash, J., S. Uniyal, and Q. Sarnak, *Exchnage of alnumin adsorbed on polymer surfaces.* Trans - Am Soc Artif Intern Organs, 1974. **20**(69).

72. Adamczyk, Z. and P. Weronski, *Kinetics of Irreversible Adsorption of Nonspherical Particles.* Bulletin of the Polish Academy of Sciences-Chemistry, 1994. **42**(4): p. 543-566.

73. Chan, B.M.C. and J.L. Brash, *Adsorption of fibrinogen on glass: reversibility aspects.* J. Colloid Interface Sci., 1981. **82**: p. 217-225.

74. Engel, M.F.M., C.P.M. van Mierlo, and A.J.W.G. Visser, *Kinetic and Structural Characterization of Adsorption-induced Unfolding of Bovine α-Lactalbumin.* Journal of Biological Chemistry, 2002. **277**(13): p. 10922-10930.

75. Mollmann, S.H., et al., *Interfacial adsorption of insulin conformational changes and reversibility of adsorption.* Eur J Pharm Sci, 2006. **27**(2-3): p. 194-204.

76. Chittur, K.K., *FTIR/ATR for protein adsorption to biomaterial surfaces.* Biomaterials, 1998. **19**(4-5): p. 357-369.

77. Daly, S.M., T.M. Przybycien, and R.D. Tilton, *Aggregation of lysozyme and of*

poly(ethylene glycol)-modified lysozyme after adsorption to silica. Colloids and Surfaces B: Biointerfaces, 2007. **57**(1): p. 81-88.

78. Hlady, V., J. Rickel, and J.D. Andrade, *Fluorescence of Adsorbed Protein Layers .2. Adsorption of Human Lipoproteins Studied by Total Internal-Reflection Intrinsic Fluorescence.* Colloids and Surfaces, 1988. **34**(2): p. 171-183.

79. Elwing, H., et al., *Conformational changes of a model protein(complement factor 3) adsorbed on hydrophilic and hydrophobic solid surfaces.* Journal of Colloid and Interface Science, 1988. **125**(1): p. 139-145.

80. McNay, J.L. and E.J. Fernandez, *How does a protein unfold on a reversed-phase liquid chromatography surface?* Journal of Chromatography A, 1999. **849**(1): p. 135-148.

81. Engel, M.F.M., A. Visser, and C.P.M. van Mierlo, *Conformation and orientation of a protein folding intermediate trapped by adsorption.* Proceedings of the National Academy of Sciences of the United States of America, 2004. **101**(31): p. 11316-11321.

82. Billsten, P., et al., *Structural changes of T4 lysozyme upon adsorption to silica nanoparticles measured by circular dichroism.* Journal of Colloid and Interface Science, 1995. **175**(1): p. 77-82.

83. Imoto, T., et al., *The Enzyme.* 1972: p. 655.

84. Chen, X.J.J., et al., *Detection of the Superoxide Radical Anion Using Various Alkanethiol Monolayers and Immobilized Cytochrome c.* Anal Chem, 2008. **80**(24): p. 9622-9629.

85. Sreerama, N., *Estimation of Protein Secondary Structure from Circular Dichroism Spectra: Comparison of CONTIN, SELCON, and CDSSTR Methods with an Expanded Reference Set.* Analytical Biochemistry, 2000. **287**(2).

86. Jackler, G., et al., *Spherical polyelectrolyte brushes as carrier particles for proteins: An investigation of the structure of adsorbed and desorbed bovine serum albumin.* Spectroscopy-an International Journal, 2004. **18**(2): p. 289-299.

87. Burkett, S.L. and M.J. Read, *Adsorption-induced conformational changes of alpha-*

helical peptides. Langmuir, 2001. **17**(16): p. 5059-5065.

88. Daly, S.M., T.M. Przybycien, and R.D. Tilton, *Adsorption of poly(ethylene glycol)-modified lysozyme to silica.* Langmuir, 2005. **21**(4): p. 1328-1337.

89. Read, M.J., A.M. Mayes, and S.L. Burkett, *Effects of temperature and pH on the helicity of a peptide adsorbed to colloidal silica.* Colloids and Surfaces B-Biointerfaces, 2004. **37**(3-4): p. 113-127.

90. Vertegel, A.A., R.W. Siegel, and J.S. Dordick, *Silica nanoparticle size influences the structure and enzymatic activity of adsorbed lysozyme.* Langmuir, 2004. **20**(16): p. 6800-7.

91. Kelly, S.M. and N.C. Price, *The application of circular dichroism to studies of protein folding and unfolding.* Biochim Biophys Acta, 1997. **1338**(2): p. 161-85.

92. Morrissey, B.W., *Adsorption and conformation of plasma-proteins - Physical Approach.* Annals of the New York Academy of Sciences, 1977. **283**(FEB10): p. 50-64.

93. Ivarsson, B., et al., *Adsorption of Proteins on Metal Surfaces Studied by Ellipsometric and Capacitance Measurements.* Colloids Surf, 1985. **13**: p. 169-192.

94. Schmidt, C.F., R.M. Zimmermann, and H.E. Gaub, *Multilayer Adsorption of Lysozyme on a Hydrophobic Substrate.* BioPhysical Journal, 1990. **57**(3): p. 577-588.

95. Johnson, H. and S. Granick, *Exchange Kinetics between the Adsorbed State and Free Solution: Poly(methyl methacrylate) in Carbon Tetrachloride.* Macromolecules, 1989. **23**(13): p. 3367-3374.

96. Frantz, P. and S. Granick, *Infrared Dichroism, Chain Flattening, and the Bound Fraction Histogram in Adsorbed Poly(methyl methacrylate) Layers.* Macromolecules, 1995. **28**: p. 6915-6925.

97. Thornton, J.M., *Disulfide bridges in globular proteins.* Journal of Molecular Biology, 1981. **151**(2): p. 261-287.

98. Kato, K., S. Sano, and Y. Ikada, *Protein adsorption onto ionic surfaces.* Colloids and Surfaces B: Biointerfaces, 1995. **4**(4): p. 221-230.

99. Malmsten, M., N. Burns, and A. Veide, *Electrostatic and hydrophobic effects of oligopeptide insertions on protein adsorption.* Journal of Colloid and Interface Science, 1998. **204**(1): p. 104-111.

100. Froberg, J.C., et al., *Effect of structural stability on the characteristics of adsorbed layers of T4 lysozyme.* Langmuir, 1998. **14**(2): p. 456-462.

101. Haynes, C. and N. W, *Globular proteins at sold/liquid interfaces.* Colloids and Surfaces B: Biointerfaces, 1994. **2**: p. 517-566.

102. Arai, T. and W. Norde, *The Behavior of Some Model Proteins at Solid Liquid Interfaces. 1. Adsorption from Single Protein Solutions.* Colloids and Surfaces, 1990. **51**: p. 1-15.

103. Andrade, J.D. and V. Hlady, *Plasma-Protein Adsorption - the Big 12.* Ann NY Ac Sci, 1987. **516**: p. 158-172.

104. Wahlgren, M.C., M.A. Paulsson, and T. Arnebrant, *Adsorption of globular model proteins to silica and methylated silica surfaces and their elutability by dodecyltrimethylammonium bromide.* Colloids and Surfaces a-Physicochemical and Engineering Aspects, 1993. **70**(2): p. 139-149.

105. Xu, S.Q. and S. Damodaran, *Comparative adsorption of native and denatured egg-white, human, and T(4)-phage lysozymes at the air-water interface.* Journal of Colloid and Interface Science, 1993. **159**(1): p. 124-133.

106. Tian, M.H., et al., *Structural stability effects on adsorption of bacteriophage T4 lysozyme to colloidal silica.* Journal of Colloid and Interface Science, 1998. **200**(1): p. 146-154.

107. McGuire, J., M.C. Wahlgren, and T. Arnebrant, *Structural Stability Effects on the Adsorption and Dodecyltrimethylammonium Bromide-Mediated Elutability of Bacteriophage-T4 Lysozyme at Silica Surfaces.* Journal of Colloid and Interface Science, 1995. **170**(1): p. 182-192.

108. Singla, B., V. Krisdhasima, and J. McGuire, *Adsorption kinetics of wild type and two synthetic stability mutants of T4 phage lysozyme at silanized silica surfaces.* Journal of Colloid and Interface Science, 1996. **182**(1): p. 292-296.

109. Apte, J.S., et al., *Kinetics of leucine-lysine peptide adsorption and desorption at -CH3 and -COOH terminated alkylthiolate monolayers.* Biointerphases, 2010. **5**(4): p. 97-104.

110. Weidner, T., et al., *Assembly and structure of alpha-helical peptide films on hydrophobic fluorocarbon surfaces.* Biointerphases, 2010. **5**(1): p. 9-16.

111. Elbaum, D., et al., *Surface-activity of hemoglobin-S and other human hemoglobin variants.* Biochimica Et Biophysica Acta, 1976. **427**(1): p. 57-69.

112. Kato, A. and K. Yutani, *Correlation of surface-properties with conformational stabilties of wild-type and 6 mutant tryptophan synthase alpha-subunits substituted in the same position.* Protein Engineering, 1988. **2**(2): p. 153-156.

113. Jez, J.M., et al., *Comparative anatomy of the aldo-keto reductase superfamily.* Biochemical Journal, 1997. **326**: p. 625-636.

114. Campbell, E., I.R. Wheeldon, and S. Banta, *Broadening the Cofactor Specificity of a Thermostable Alcohol Dehydrogenase Using Rational Protein Design Introduces Novel Kinetic Transient Behavior.* Biotechnology and Bioengineering, 2010. **107**(5): p. 763-774.

115. Machielsen, R., et al., *Production and characterization of a thermostable alcohol dehydrogenase that belongs to the aldo-keto reductase superfamily.* Applied and Environmental Microbiology, 2006. **72**(1): p. 233-238.

116. Bohren, K.M., et al., *Expression of human aldose and aldehyde reductases - Site-directed mutagenesis of a critical lysine-262.* J Biol Chem, 1991. **266**(35): p. 24031-24037.

117. Evans, J.W., *Random and cooperative sequential adsorption.* Reviews of Modern Physics, 1993. **65**(4): p. 1281-1329.

118. Bee, J.S., et al., *Monoclonal antibody interactions with micro- and nanoparticles:*

adsorption, aggregation, and accelerated stress studies. J Pharm Sci, 2009. **98**(9): p. 3218-38.

119. Kelly, S.M. and N.C. Price, *Circular dichroism to study protein interactions.* Curr Protoc Protein Sci, 2006. **Chapter 20**: p. Unit 20 10.

120. van Mierlo, C.P.M. and E. Steensma, *Protein folding and stability investigated by fluorescence, circular dichroism (CD), and nuclear magnetic resonance (NMR) spectroscopy: the flavodoxin story.* Journal of Biotechnology, 2000. **79**(3): p. 281-298.

121. Rezwan, K., L.P. Meier, and L.J. Gauckler, *Lysozyme and bovine serum albumin adsorption on uncoated silica and AlOOH-coated silica particles: the influence of positively and negatively charged oxide surface coatings.* BIOMATERIALS, 2005. **26**(21): p. 4351-7.

122. Felsovalyi, F., et al., *The Reversibility of Lysozyme on Silica.* Langmuir, 2011. **27**: p. 11873-11882.

123. Pellenc, D., O. Gallet, and H. Berry, *Adsorption-induced conformational changes in protein diffusion-aggregation surface assemblies.* Phys Rev E Stat Nonlin Soft Matter Phys, 2005. **72**(5 Pt 1): p. 051904.

124. Tilton, R.D., A.P. Gast, and C.R. Robertson, *Surface diffusion of interacting proteins - Effect of concentration on the lateral mobility of adsorbed bovine serum-albumin* Biophysical Journal, 1990. **58**(5): p. 1321-1326.

125. Buijs, J. and V. Hlady, *Adsorption kinetics, conformation, and mobility of the growth hormone and lysozyme on solid surfaces, studied with TIRF.* Journal of Colloid and Interface Science, 1997. **190**(1): p. 171-181.

126. Knotts, T.A., N. Rathore, and J.J. de Pablo, *Structure and stability of a model three-helix-bundle protein on tailored surfaces.* Proteins-Structure Function and Bioinformatics, 2005. **61**(2): p. 385-397.

127. Arnold, K., et al., *The SWISS-MODEL workspace: a web-based environment for protein structure homology modelling.* Bioinformatics, 2006. **22**(2): p. 195-201.

128. Kiefer, F., et al., *The SWISS-MODEL Repository and associated resources.* Nucleic Acids Research, 2009. **37**(suppl 1): p. D387-D392.

129. Peitsch, M.C., *Protein Modeling by E-mail.* Nat Biotech, 1995. **13**(7): p. 658-660.

130. Vander Jagt, D.L., et al., *Reduction of trioses by NADPH-dependent aldo-keto reductases. Aldose reductase, methylglyoxal, and diabetic complications.* J Biol Chem, 1992. **267**(7): p. 4364-9.

131. Arai, T. and W. Norde, *The Behavior of Some Model Proteins at Solid Liquid Interfaces. 2. Sequential and Competitive Adsorption.* Colloids and Surfaces, 1990. **51**: p. 17-28.

132. Cronican, J.J., et al., *Potent Delivery of Functional Proteins into Mammalian Cells in Vitro and in Vivo Using a Supercharged Protein.* Acs Chemical Biology. **5**(8): p. 747-752.

133. McNaughton, B.R., et al., *Mammalian cell penetration, siRNA transfection, and DNA transfection by supercharged proteins.* Proceedings of the National Academy of Sciences of the United States of America, 2009. **106**(15): p. 6111-6116.

134. Hlady, V. and J. Buijs, *Protein adsorption on solid surfaces.* Current Opinion in Biotechnology, 1996. **7**(1): p. 72-77.

135. Manning, M.C., et al., *Stability of protein pharmaceuticals: an update.* Pharm Res, 2010. **27**(4): p. 544-75.

136. Frantz, P. and S. Granick, *Kinetics of Polymer Adsorption and Desorption.* Physical review letters, 1991. **66**(7): p. 899-902.

137. Frantz, P., D.C. Leonhardt, and S. Granick, *Enthalpic effects in competitve polymer adsorption - adsorption isotope effect and chain end effect.* Macromolecules, 1991. **24**(8): p. 1868-1875.

138. Fang, F. and I. Szleifer, *Kinetics and thermodynamics of protein adsorption: A generalized molecular theoretical approach.* Biophysical Journal, 2001. **80**(6): p. 2568-2589.

139. van Gelder, B. and E.C. Slater, *The extinction coefficient of cytochrome c.* Biochim Biophys Acta, 1962. **58**: p. 593-5.

140. Bee, J.S., et al., *Monoclonal antibody interactions with micro- and nanoparticles: adsorption, aggregation, and accelerated stress studies.* Journal of Pharmaceutical Sciences, 2009. **98**(9): p. 3218-38.

141. Sreerama, N., *Estimation of protein secondary structure from circular dichroism spectra: comparison of CONTIN, SELCON, and CDSSTR methods with an expanded reference set.* Anal Biochem, 2000. **287**(2).

142. Cover, T.M. and P.E. Hart, *Nearest neighbor pattern classification.* Ieee Transactions on Information Theory, 1967. **13**(1): p. 21-+.

143. Wallace, B., *Circuar Dichroism Spectroscopy for higher order strcuture: Validation, calibration, analyses, and the Protein Circular Dichroism Data Bank (PCDDB)*, in *1st International Symposium on Higher Order Structure of Protein Therapeutics*. 2011: Rockville, MD.

144. Kella, N.K.D., S.T. Yang, and J.E. Kinsella, *Effect of disulfide bond cleavage on structural and interfacial properties of whey proteins.* Journal of Agricultural and Food Chemistry, 1989. **37**(5): p. 1203-1210.

145. de Gennes, P.G., *Relaxation anomalies in linear polymer melts.* Macromolecules, 2002. **35**(9): p. 3785-3786.

146. Felsovalyi, F., et al., *Adsorption to Silica Using Homologous Aldo-keto Reductases.* Protein Science in press, 2012. **DOI: 10.1002/pro.209**.

147. Wetter, L.R. and H.F. Deutsch, *Immunological studies on egg white proteins. IV. Immunochemical and physical studies of lysozyme.* J Biol Chem, 1951. **192**(1): p. 237-42.

148. Gekko, K. and Y. Hasegawa, *Compressibility Structure Relationship of Globular-Proteins.* Biochemistry, 1986. **25**(21): p. 6563-6571.

149. Norde, W., *Driving Forces for Protein Adsorption at Solid Surfaces*, in *Biopolymers at*

Interfaces, Second Edition. 2003, CRC Press.

150. Gessner, A., et al., *Nanoparticles with decreasing surface hydrophobicities: influence on plasma protein adsorption.* International journal of pharmaceutics, 2000. **196**(2): p. 245-249.

151. Flisk, E., *Handbook of Adhesive Raw Materials*, in *Handbook of paint raw materials*. 1989, William Andrew Publishing/Noyes.

152. Sugio, S., et al., *Crystal structure of human serum albumin at 2.5 Ã… resolution.* Protein Engineering, 1999. **12**(6): p. 439-446.

153. Pinholt, C., et al., *The importance of interfaces in protein drug delivery - why is protein adsorption of interest in pharmaceutical formulations?* Expert Opinion on Drug Delivery. **8**(7): p. 949-964.

154. Mandal, H.S. and H.-B. Kraatz, *Effect of the Surface Curvature on the Secondary Structure of Peptides Adsorbed on Nanoparticles.* Journal of the American Chemical Society, 2007. **129**(20): p. 6356-6357.

155. Roach, P., D. Farrar, and C.C. Perry, *Interpretation of protein adsorption: surface-induced conformational changes.* J Am Chem Soc, 2005. **127**(22): p. 8168-73.

156. Mollmann, S.H., et al., *Interfacial adsorption of insulin - Conformational changes and reversibility of adsorption.* Eur J Pharm Sci, 2006. **27**(2-3): p. 194-204.

157. Elwing, H., *Protein absorption and ellipsometry in biomaterial research.* Biomaterials, 1998. **19**(4-5): p. 397-406.

158. Tantipolphan, R., et al., *Adsorption of,bovine serum albumin (BSA) onto lecithin studied by attenuated total reflectance Fourier transform infrared (ATR-FTIR) spectroscopy.* International Journal of Pharmaceutics, 2007. **337**(1-2): p. 40-47.

159. Green, R.J., I. Hopkinson, and R.A.L. Jones, *Unfolding and Intermolecular Association in Globular Proteins Adsorbed at Interfaces.* Langmuir, 1999. **15**(15): p. 5102-5110.

160. Pinholt, C., et al., *Influence of PEGylation with linear and branched PEG chains on the adsorption of glucagon to hydrophobic surfaces.* Eur J Pharm Biopharm. **77**(1): p. 139-147.

161. Sonesson, A.W., et al., *A comparison between dual polarization interferometry (DPI) and surface plasmon resonance (SPR) for protein adsorption studies.* Colloids and Surfaces B-Biointerfaces, 2007. **54**(2): p. 236-240.

162. Kamilya, T., P. Pal, and G.B. Talapatra, *Interaction of ovalbumin with phospholipids Langmuir-Blodgett film.* Journal of Physical Chemistry B, 2007. **111**(5): p. 1199-1205.

163. Lan, Q., et al., *A modified Langmuir model for the prediction of the effects of ionic strength on the equilibrium characteristics of protein adsorption onto ion exchange/affinity adsorbents.* Chemical Engineering Journal, 2001. **81**(1): p. 179-186.

164. Schwegman, J.J., J.F. Carpenter, and S.L. Nail, *Evidence of Partial Unfolding of Proteins at the Ice/Freeze-Concentrate Interface by Infrared Microscopy.* Journal of Pharmaceutical Sciences, 2009. **98**(9): p. 3239-3246.

165. Ludwig, D.B., et al., *Protein adsorption and excipient effects on kinetic stability of silicone oil emulsions.* Journal of Pharmaceutical Sciences, 2010. **99**: p. 1721-33.

166. Nayak, A., A.K. Dutta, and G. Belfort, *Surface-enhanced nucleation of insulin amyloid fibrillation.* Biochem Biophys Res Commun, 2008. **369**(2): p. 303-7.

167. Anand, G., et al., *Conformational Transitions of Adsorbed Proteins on Surfaces of Varying Polarity.* Langmuir. **26**(13): p. 10803-10811.

168. Koutsopoulos, S., et al., *Adsorption of trypsin on hydrophilic and hydrophobic surfaces.* Langmuir, 2007. **23**(4): p. 2000-2006.

169. McPherson, T., et al., *Prevention of Protein Adsorption by Tethered Poly(ethylene oxide) Layers:â€‰ Experiments and Single-Chain Mean-Field Analysis.* Langmuir, 1998. **14**(1): p. 176-186.

170. Michel, R., et al., *Influence of PEG Architecture on Protein Adsorption and Conformation.* Langmuir, 2005. **21**(26): p. 12327-12332.

171. Simonovsky, F.I., et al., *Poly(ether urethane)s incorporating long alkyl side-chains with terminal carboxyl groups as fatty acid mimics: synthesis, structural characterization and protein adsorption.* J Biomater Sci Polym Ed, 2005. **16**(12): p. 1463-83.

172. Knotts, T.A., N. Rathore, and J.J. de Pabloz, *An entropic perspective of protein stability on surfaces.* Biophysical Journal, 2008. **94**(11): p. 4473-4483.

173. Iyer, S., H. HogenEsch, and S.L. Hem, *Effect of the degree of phosphate substitution in aluminum hydroxide adjuvant on the adsorption of phosphorylated proteins.* Pharmaceutical Development and Technology, 2003. **8**(1): p. 81-86.

174. Pereira Arias-Bouda, L.M., et al., *Enzyme-linked immunosorbent assays using immune complexes for the diagnosis of tuberculosis.* J Immunol Methods, 2003. **283**(1-2): p. 115-24.